8-2002

The Correlation of Pedal Position to Tail Rotor Power Requirement on the OH-58A+

Kan-Wai Tong
University of Tennessee - Knoxville

To the Graduate Council:

I am submitting herewith a thesis written by Kan-Wai Tong entitled "The Correlation of Pedal Position to Tail Rotor Power Requirement on the OH-58A+." I have examined the final electronic copy of this thesis for form and content and recommend that it be accepted in partial fulfillment of the requirements for the degree of Master of Science, with a major in Aviation Systems.

W. Lewis, Major Professor

We have read this thesis and recommend its acceptance:

R. Kimberlin, F. Stellar

Accepted for the Council:
Carolyn R. Hodges

Vice Provost and Dean of the Graduate School

(Original signatures are on file with official student records.)

To the Graduate Council:

I am submitting herewith a thesis written by Kan-Wai Tong entitled "The Correlation of Pedal Position to Tail Rotor Power Requirement on the OH-58A+." I have examined the final electronic copy of this thesis for form and content and recommend that it be accepted in partial fulfillment of the requirements for the degree of Master of Science, with a major in Aviation Systems.

Dr. W. Lewis
Major Professor

We have read this thesis and
recommend its acceptance:

Dr. R. Kimberlin

Mr. F. Stellar

Accepted for the Council:

Anne Mayhew

Vice Provost and Dean of
Graduate Studies

(Original signatures are on file with official student records.)

The Correlation of Pedal Position to Tail Rotor Power Requirement on the OH-58A+

A Thesis

Presented for the

Master of Science

Degree

The University of Tennessee, Knoxville

Kan-Wai Tong

August 2002

DEDICATION

To my family and friends

ACKNOWLEDGMENTS

The author wishes to express sincere appreciation to Doctor William Lewis, Doctor Ralph Kimberlin, and Professor Fred Stellar for their assistance in the preparation of this manuscript. Their patience and guidance played an important role towards the completion of this manuscript. Additionally, other faculty members and staff of the Aviation Systems Department of The University of Tennessee Space Institute also enriched my knowledge in aviation.

ABSTRACT

Every mechanical component has a finite failure life. Excessive usage of a component may cause damage. Therefore, life determination is essential to safe operation. Replacement of mechanical components prior to the end of useful life results in higher costs of maintenance. Monitoring rotating components is not always reliable or cost effective. This thesis attempts to solve this problem for a helicopter tail rotor. The development of an algorithm to calculate the loads on a component using stationary measurements can eliminate the need for rotating measurement equipment.

The purpose is to predict the tail rotor power requirement of a helicopter throughout the mission profile by using the algorithm developed.

The scope of this investigation was limited to representative flight regimes based upon a survey of Bell 206 jet rangers or OH-58A derivatives operators. Flight test data were collected at University of Tennessee Space Institute (UTSI). These data were then used to correlate with the results of the algorithm model.

The model incorporated helicopter blade element theory, momentum theory, fin blockage effects, inertia effects, translational velocity effects, mechanical losses and altitude density correction. The model was executed using Microsoft Excel. The model required input data including helicopter characteristics, altitude, engine shaft horsepower, velocity. Based upon these data, the tail rotor power and pedal position were calculated.

The calculation results of pedal position were compared with the flight test data. The accuracy of the tail rotor power was presented in the percentage of the maximum tail rotor power. It was found that the pedal position alone was a poor indicator of tail rotor

power. The modeled elements mentioned above were included and resulted in significant improvement. Based on the calculated results, this model and measured pedal positions can provide at least 90-% confidence of the tail rotor power, except at large sideslip angles. Additionally, due to the tail rotor power sensitivity to the pedal position variations, the measurement of pedal positions should be performed precisely.

Based on the results of this investigation, utilizing the algorithm model for predicting tail rotor power from pedal position will result in a 90-% confidence of the tail rotor power being applied.

Recommend an alternative fuselage yaw moment due to sideslip chart be used to improve sideslip data. Recommend instrumented tail rotor for tail rotor power measurements.

TABLE OF CONTENTS

LIST OF FIGURES

LIST OF FIGURES (continued)

LIST OF FIGURES (continued)

LIST OF TABLES

Chapter 1

INTRODUCTION

Background

Historically, rotating component lives were determined through component testing applied to an anticipated mission usage spectrum. This process had multiple layers of conservatism embedded for safety. This conservatism was necessary due to unknowns in both material characteristics and the actual usage spectrum.

Modern sensors and prognostic tools have eliminated some of the uncertainty inherent in the component usage. Consequently, the component replacement criteria are evolving from an hourly requirement to one based upon a usage spectrum. In the aerospace industries, Goodrich Aerospace has been conducting research and development on the Health and Usage Management Systems (HUMS) in the past ten years. By implementing the HUMS, systems evaluators can tailor necessary maintenance schedules based on the collected data from the on-board data acquisition systems. The goal of HUMS is to reduce downtime, increase readiness, reduce maintenance costs and enhance safety. To date, various helicopters, e.g. H-60, H-53, S-76, S-92, have been equipped and benefit from an installed HUMS.

However, instrumenting certain components for monitoring is not a simple process. Many helicopter components involve rotating machinery. Monitoring these require

complex, unreliable slipring assemblies or more expensive RF sensor transmitters. An alternative to active monitoring of these components is the development of an algorithm derived from an associated system. The tail rotor is such a system. It has been hypothesized that tail rotor power can be inferred from the pedal position during steady state conditions and inferred as a difference in engine torque during transient conditions.

Purpose

The purpose of this investigation was to develop a predictive algorithm for correlation of tail rotor power to antitorque pedal position. This predictive method requires the knowledge of the vertical tail and tail rotor configuration and operating conditions. The design of the algorithm incorporates simplified theoretical methodologies.

Process

This investigation of the helicopter tail rotor power was based on aerodynamic theories and representative operational conditions. The aerodynamic theories are readily available in various references, e.g. textbooks, manufacturer supplied materials and technical reports. These aerodynamic theories were applied in developing a specially designed calculation model. Due to the familiarization to the software program, the author selected the Microsoft Excel as a calculation tool for the prediction of the tail rotor power requirements. A variable input page was assigned for all flight data entries, and it provided convenience to the users. In addition, user changes to equations for calculation is not required. By using the iteration option, users can determine the corresponding pedal

position, as well as the required tail rotor power at the end of each test. Therefore, a basic understanding of Microsoft Excel operation is required for operation of this model.

In order to evaluate this calculation model, the University of Tennessee Space Institute (UTSI) collected more than two hundred surveys from various Bell 206 jet rangers or OH-58A derivative operators. The representative flight conditions were simulated at the UTSI flight research facilities with a fully instrumented OH-58A+ helicopter. The collected data were used in the analytical model and its results to compare with the flight test results.

Chapter 2

EQUIPMENT

Description of the OH-58A+

The OH-58A+ helicopter is a single-engine, single main rotor, observation-type helicopter with the capability to carry four people with a maximum gross weight of 3200 pounds. The aircraft is equipped with an Allison T63-A-720 gas turbine engine rated at 420 shaft horsepower (uninstalled sea level, standard day conditions). The main transmission is rated at 317 shaft horsepower maximum. The tailboom is a monocoque structure that supports the horizontal stabilizer, vertical stabilizer, and tail rotor assembly. The main rotor assembly is a two-bladed, semi-rigid rotor mounted on an under-slung feathering axis hub. The main rotor is 35 feet, 4 inches in diameter and rotates at 354 RPM (100%). The main rotor airfoil section is an 11.2% modified symmetrical airfoil with a drooped leading edge, an average drag coefficient (c_{md_o}) of 0.00123, and an average chord (c) of 13.0 inches. The equivalent flat plate drag area of the OH-58 helicopter is 12.0 square feet. The test aircraft was tested with the doors installed, instrumentation boom installed, and bleed air off. Cockpit instruments included: an engine oil pressure driven torquemeter gauge (%Q), a self-generating, electrically-driven Turbine Outlet Temperature (TOT) gauge (°C), a gas producer (N_1) tachometer (%RPM), and an engine (N_2) and rotor (N_R) dual-tachometer gauge (%RPM). In addition to the cockpit instruments, flight data can be also collected

through the instrumentation boom and transferred to the on-board data acquisition system. The test aircraft is depicted in figure 2.1 and a detailed description can be found in appendices F.1 & F.2.

Main Rotor Hub and Blade Assembly

The main rotor assembly is a tow-bladed, semi-rigid, seesaw type rotor with under slung mounting (Fig 2.2). The blades are mounted in the hub assembly grips with through bolts, which have hollow shanks for installation of weights to balance the hub. After balancing, the bolts must be kept with their respective rotor hub grips. Blade alignment is accomplished by adjustment of blade latches, which engage the root end of the blade. The blade grips are retained on the hub yoke by means of tension-torsion strap assemblies. Changes in blade pitch angle are made by rotating the grips on the yoke journals; each grip has two pitch change bearings.

Figure 2.1. OH-58A+ (Test Aircraft - N88UT)

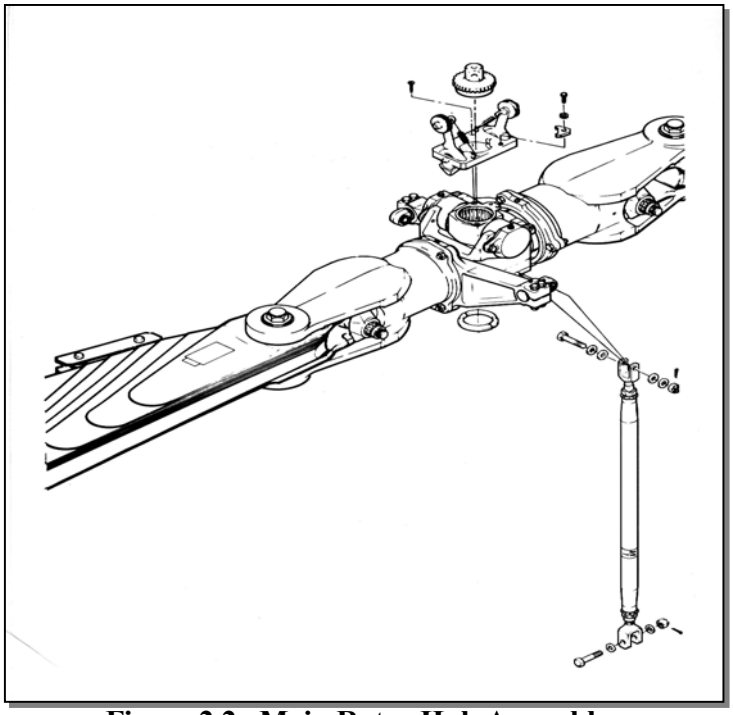

Figure 2.2. Main Rotor Hub Assembly.

Oil reservoirs, with sight gages, are provided for pitch change bearing in the tow grips and for the tow pillow block bearing utilized with the flapping axis trunnion. The rotor blades are all metal, five piece assemblies consisting of an extruded aluminum alloy nose block, aluminum alloy trailing edge, and aluminum honeycomb filler. A flap restraint mechanism is installed on the main rotor hub. The flap restrain assembly serves to prevent excessive flapping of the main rotor during starting and shut down.

Tail Rotor Hub and Blade Assembly

The tail rotor hub and blade assembly consists of an aluminum alloy forged yoke with stainless steel blades (Fig 2.3).

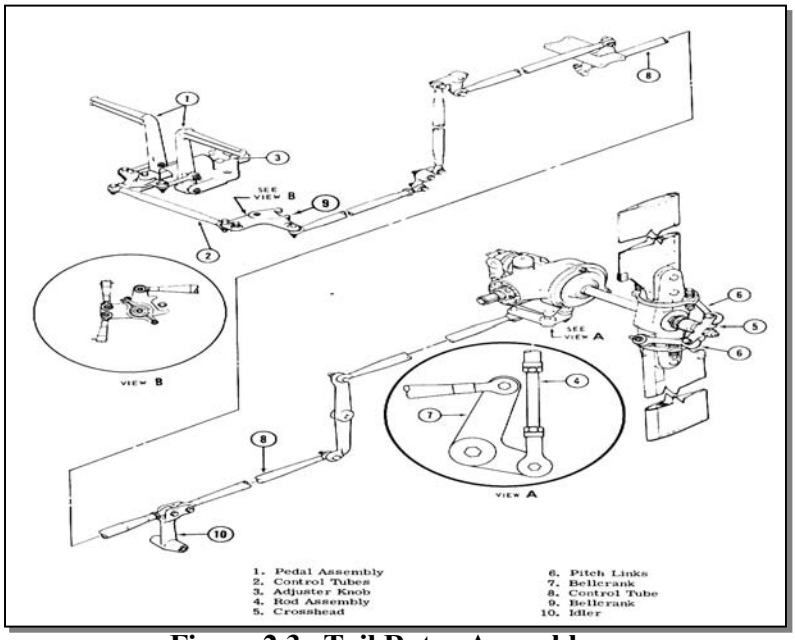

Figure 2.3. Tail Rotor Assembly

The blades are mounted in the yoke by means of spherical bearing, which are mounted in the grip plates on the pitch change axis. The spherical bearings provide for pitch change of the blades. The yoke and blade assembly is mounted on the 90-degree gearbox shaft by means of a splined trunnion, mounted in bearings in the yoke, to provide a flapping axis for the assembly. At time of assembly, spanwise balance is accomplished by use of washers on the blade retention bolts at the yoke, and chordwise balance is attained by washers and/or weights on the trunnion bearing housing retention bolts

Flight Control Hydraulic System

The primary unit of the hydraulic system is a combined pump and reservoir assembly located on the left forward side of the transmission (Fig 2.4).

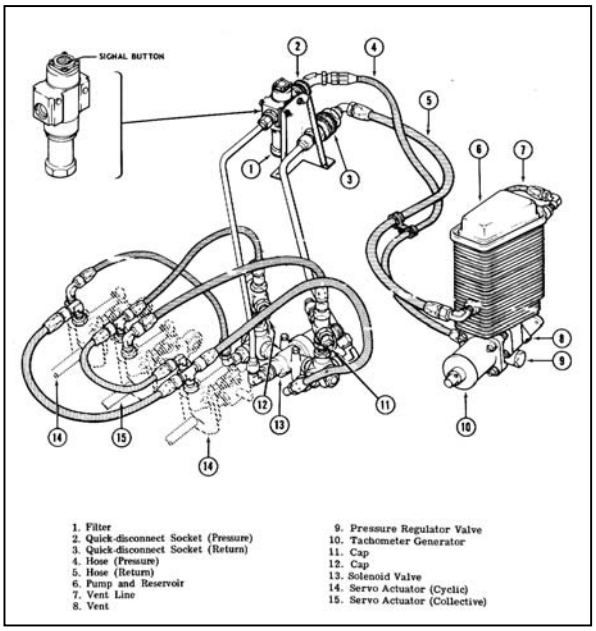

Figure 2.4. OH-58A+ Hydraulic System.

The reservoir filler opening is located on the top of the reservoir. Fluid level may be observed through a transparent plastic sight glass in the side of the reservoir. A valve assembly, located on the right-hand side of the system just above the work deck incorporated a solenoid by-pass valve and filter element assembly, which incorporates a filter condition red button. The hydraulic system is serviced with oil, Specification MIL-H-6506. Reservoir capacity is one pint. The main hydraulic system contains one power pack, three servo actuators with three irreversible valves. The system operates at 600 PSI and adjustment is provided at the relief valve and pressure regulator. The power pack is a self-contained unit located on the forward face of the transmission and driven by the transmission oil pump shaft. The transmission driven hydraulic pump provides for fully boosted flight controls being available during autorotative flight. The complete unit is removable from the pylon without disrupting the hydraulic system. The irreversible valves

isolate the servo system from the flight controls in the case of hydraulic malfunction and permit extended periods of flying without excessive feedback from the controls.

Flight Control Mechanical System

The flight control system consists of push-pull control tubes and bellcranks actuated by conventional helicopter cyclic, collective, and directional controls (Fig 2.5). The controls are routed beneath the pilot's seats aft of the center of the helicopter and up to the cabin roof through the control column, which also serves as a primary cabin structure.

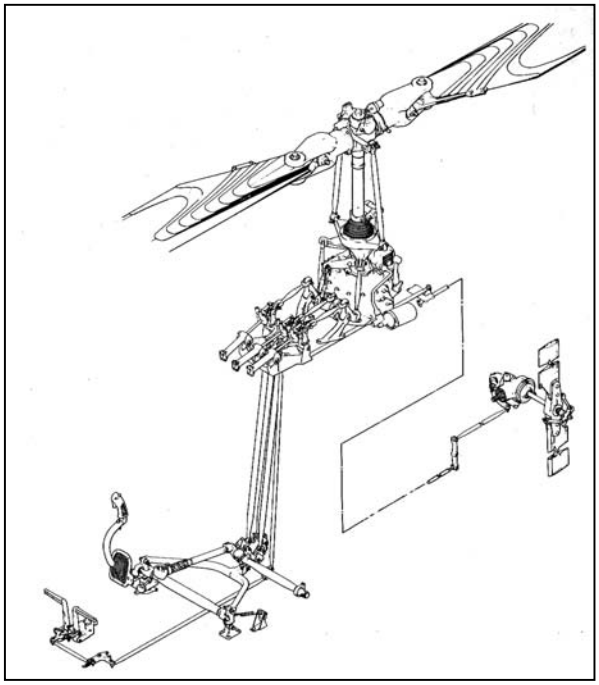

Figure 2.5. OH-58A+ Flight Control System.

Access doors located on the aft side of the control column and removable seats are provided for control inspection and maintenance accessibility. Cyclic and collective controls are routed to the main rotor blades through the swashplate. The directional controls are routed through the tail boom to the tail rotor. Fixed length control tubes and a minimum of adjustable tubes simplify rigging. All self-aligning bearings and rod ends are spherical bearings and require no lubrication. The cyclic and collective control systems incorporate hydraulic servo actuators that utilize irreversible valves to minimize control force feedback.

Description of Test Instrumentation

In addition to the standard ship instrumentation (Ref 9), this test helicopter is equipped with an independent data acquisition instrumentation system. This onboard data acquisition system weighs approximately 70-lbs and is located in the aft avionics compartment. This UTSI designed system allows easy data recording and calibration through a Daqbook mounted on the rack containing power supply, gyros, and accelerometers. When the system is activated, flight data are recorded on the Daqbook or selectively displayed at one of three engineer stations. Storage of flight test data may be accomplished by connecting a laptop computer to the Daqbook terminals. After selecting the necessary parameters, each run can be initiated by pressing the start button. According to the preset sampling points and frequency, the data acquisition process stops automatically and is ready for the next run. Data from each run are stored as a text file

and can be transferred to Microsoft Excel file. As such, one can perform the data reductions and generate some data plots, as necessary.

The capability of this data acquisition system is recorded in the table 2.1 and the package is controlled from the cockpit control (Fig 2.6). The data acquisition system is located at the baggage storage area of the aircraft (Fig. 2.7) while the nose boom (Fig. 2.9) collects the aerodynamic pressure. The system assembly is shown in figure 2.8.

Engine Torque Measurement

The engine torque is measured via a measurement of oil pressure developed within the engine and transmitted through a wet line to gauge (Fig 2.10). 74-psi represents 100-% on the indicator. Also, according to the operating limits, the 10-second limit for the T63-A-720 engine, used on the test aircraft, represents 109-psi at the gauge, which would indicate 146-% of the rated torque (if it could be read).

Figure 2.6. Data Acquisition Control Panel

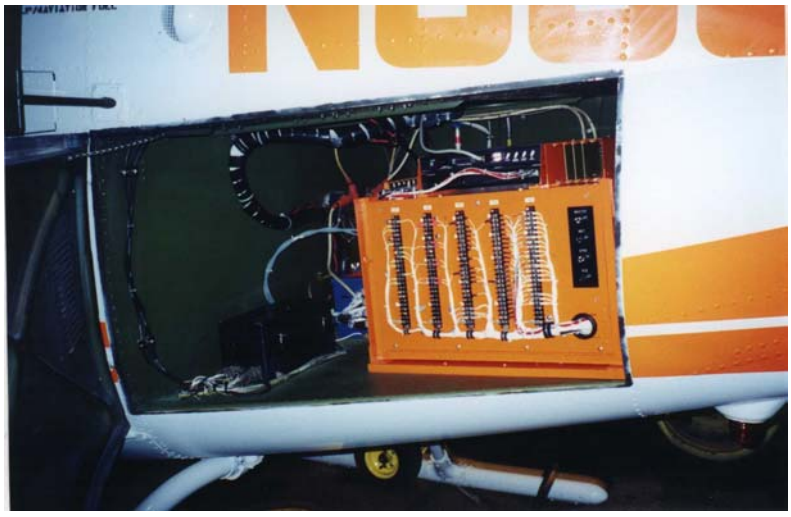

Figure 2.7. Location of the Data Acquisition Instrumentation

Table 2.1. Data Acquisition System Capability

Parameter	Range	Units	Comments
Ambient Pressure	0 to 20	Inch Hg	Boom Static Port
Pitot Pressure	0 to 12	Inch H_{2O}	Boom Static Port
Outside Air Temperature	0 to 100	Degree C	
Sideslip Angle	+/- 40	Degree	Boom Value
Rotor Speed	0 to 80	Hz	Pulse Train
Gas Generate Speed	0 to 80	Hz	Pulse Train
Power Turbine Speed	0 to 80	Hz	Pulse Train
Turbine Outlet Temperature	0 to 1000	Degree C	
Engine Torque Pressure	0 to 100	PSIG	
Pitch Attitude	+/- 40	Degree	Gravity Erection
Roll Attitude	+/- 60	Degree	Gravity Erection
Pitch Rate	+/- 30	Deg./Sec.	
Roll Rate	+/- 30	Deg./Sec.	
Yaw Rate	+/- 30	Deg./Sec.	
Normal Acceleration, Nz	+/- 3	g	
Longitudinal Acceleration, Nx	+/- 3	g	
Lateral Acceleration, Ny	+/- 3	g	
Longitudinal Stick Position	-20 to +15	Degree	
Lateral Stick Position	-15 to +15	Degree	
Collective Stick Position	0 to 35	Degree	
Pedal Position	+/- 30	Degree	

*Negative values represent the left or downward motions, and vice versa.

Figure 2.8. Data Acquisition Instrumentation Assembly

Figure 2.9. OH-58A+ Pitot/Static Boom with Sideslip Vane

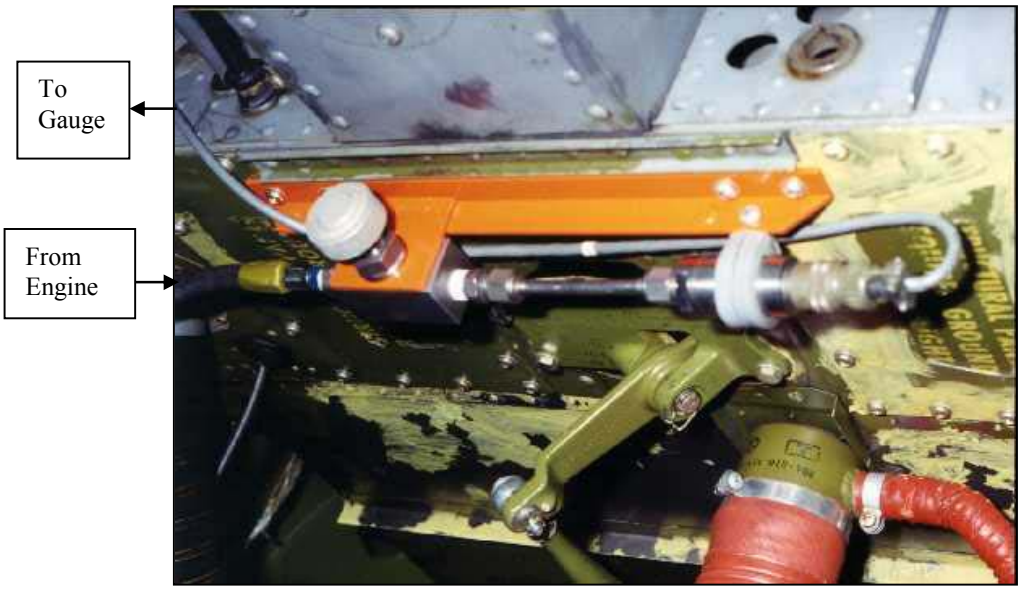

Figure 2.10. Main Engine Torque Measurement Assembly

Chapter 3

ANALYTICAL MODEL

Introduction

An analytical model was developed using rotary wing performance theory. Testing was performed to validate the analytical model. By comparing the test data with the analytical model, accuracy of the analytical model was determined.

Since it was desired to create as simple an analytical model as possible while creating accurate results, some assumptions were made at the design stage. The errors caused by these assumptions were believed to be insignificant to the tail rotor power requirement. The design input section was created and used to record all the necessary aircraft parameters for the calculation. With the established assumptions and design input data, the analytical model could be tested. This analytical model consists of some conceptual approaches and methodologies, which encompass different elements in hover and forward flight, respectively. These elements include profile power, induced power, fin blockage effects, inertia effects, axial velocity effects, altitude density correction, fuselage moment contribution and power losses. The logic of the analytical model is presented in appendix B. At the end of each run, a required tail rotor power was derived from a calculated pedal position, which was compared with the flight-tested pedal position. All these elements are explained in

the remainder of this chapter. A sample run of this analytical model is included in appendix E.

Assumptions

1. The dimensions of the helicopter are described in figure F.1 (Ref. 9).
2. All mechanical linkages are within approved maintenance tolerances.
3. Power losses from the tail shaft bearings and the cooling fan are insignificant, and ignored in the calculations.
4. The blade element profile drag coefficient varies little over the normal operating range of angles of attack and Mach number, and is therefore considered a constant.
5. Main rotor downwash effect does not affect tail rotor.

Design Input

1. For the hover case, the forward velocity (v_F) is 0-ft/s.
2. The tail rotor of the OH-58A+ is a pusher which means that the rotor generates a pushing thrust to the right to cause the tail boom to rotate in a counterclockwise direction to oppose the torque reaction of the main rotor.
3. Total directional control (pedal) travel between mechanical stops was measured to be 6.7-in.
4. Based on measurement, the vertical fin has a 7-deg. offset right of centerline.

5. Total tail rotor blade deflection is 30-deg (23-deg left with full left pedal and 7-deg right with full right pedal, respectively) ref 3, p. 11-42.
6. The torque gage reading of 100% corresponds to 317-shp.
7. Based on measurement, the ratio of the vertical fin area to the tail rotor disk area is 0.8. (OH-58A+)
8. See figure F.1 (Ref. 9) for more OH-58A+ dimensional information.

Overall Approach and Methodology

A single rotor helicopter with the rotor blades propelled by the rotation of a central mast develops a reaction torque on the fuselage. It is this reactive torque that must be countered by tail rotor thrust to provide controlled flight.

The power of the tail rotor can be determined by measuring the twist of the tail rotor mast. This method requires a complex and unreliable slip ring assembly as part of an instrumentation system due to the nature of the rotating components.

A more simplistic and reliable approach to determine tail rotor power is to infer the tail rotor power by measuring the antitorque pedal position. This approach necessitates the determination of the separate power contributions from the main rotor and tail rotor, (assuming all other power consumptions are much less than tail rotor power)

$$P_A = P_M + P \tag{1}$$

where: P_A = Applied Power

P_M = Main Rotor Power

P = Tail Rotor Power

The power applied is measured using the standard torquemeter system of the helicopter. Solving for the tail rotor component, equation (1) becomes,

$$P = P_A - P_M \tag{2}$$

The counterbalancing torque on a single rotor helicopter, e.g. OH-58A+, is provided by an antitorque tail rotor which is driven directly by the main accessory gearbox so that the output of the tail rotor is determined by the antitorque pedal position in a hover condition.

The antitorque tail rotor is located at a fixed distance from the helicopter center of gravity. The torque developed by the antitorque tail rotor thrust is equal to the product of the thrust and tail length defined as the distance from the center of tail rotor thrust to the aircraft center of gravity,

$$Q = Tl_T = -Q_M = \frac{P_M * 550}{\Omega_M} \tag{3}$$

where: T = Tail Rotor Thrust

l_T = Tail length

Q = Counter Torque

Ω = Rotor RPM

The subscript M refers to the Main rotor.

The thrust required to balance the main rotor torque is a function of the applied torque,

$$T = \frac{550 * P_M / \Omega_M}{l_T} = \frac{Q_M}{l_T} \tag{4}$$

Antitorque Power in Hover

During the hover condition, the tail rotor, like the main rotor, requires power to overcome the profile and induced drag. Analysis of the power required is handled more easily if the induced power term is predicted by use of the momentum theory, and the blade element theory is used to predict the profile power term.

In addition to the profile power and induced power, mechanical losses, inertial effects, and the aerodynamic losses must be considered when determining the tail rotor power requirement. Aerodynamic losses include Vertical Fin Blockage Effect and Rotor Blade Tip losses. Engine oil cooler blower and tail gearbox are examples of contributions to mechanical losses.

Variable Inputs

Development of a generic algorithm must allow variable inputs to accommodate design and operational differences between helicopters. The design inputs reflect the actual dimensions, configurations, and operating conditions. All variables are for the tail rotor unless otherwise specified.

Profile Power (P_o)

Profile power is the friction drag that the rotor blades must overcome during rotation. It is primarily determined by the rotating speed of the rotor blades. In addition, the size and the surface roughness of the rotor blades also impact the profile power. This relationship can be presented in the following equation,

$$P_o = \frac{1}{550 * 8}(\Omega R)^3 \rho_a A \sigma_R c_d \tag{5}$$

where: ΩR = blade tip speed

ρ_a = ambient air density

A = Disc Area

σ_R = Rotor Solidity

c_d = Profile Drag Coefficient

The disc area (A) is the total area scribed by the path of the rotor without coning,

$$A = \pi R^2 \tag{6}$$

where: R = Radius of the Tail Rotor Blade

The Profile Drag Coefficient (c_d) varies little over the normal operating range of angles of attack and Mach number, and is considered to be a constant (minimum profile drag and standard roughness).

Rotor Solidity (σ_R) is defined as the ratio of the total blade area to this disc area. For the number of blades (b) of a constant chord (c) and a radius (R), the total blade area is bcR, and the solidity is,

$$\sigma_R = \frac{bc}{\pi R} \tag{7}$$

This equation applies only to the test aircraft and the rectangular rotor blades.

Induced Power (P_i)

Induced Power is the power required to accelerate the air through the tail rotor and it is a function of the tail rotor thrust. The induced power of a thrusting rotor is altered by forward and lateral relative velocities of the helicopter and the rotor tip losses.

$$P_i = \frac{1}{550} T v_i \tag{9}$$

where: P_i = Induced Power

v_i = Induced Velocity

The tail rotor thrust was determined using the moment balance relationship established by equation 4. The induced velocity is a function of the tail rotor thrust. The following parameters are used as inputs to a non-dimensional induced velocity approximation chart (Fig F.3) to determine v_i,

$$\frac{Bv_i}{v_o}, \frac{BV_V}{v_o}, \frac{BV_F}{v_o} \tag{10}$$

where: B = Tip Loss Factor

V_v = Kinematic Velocity of the Tail Section

V_F = Horizontal Velocity

In the hover case, horizontal velocity is zero and the tail rotor is assumed unaffected by the main rotor downwash and therefore the vertical velocity is also zero.

To use the chart to determine the induced velocity, the tip loss factor and the inflow velocity must first be calculated.

The tip loss accounts for the diminishing thrust near the rotor blade tip. In order to produce lift, an airfoil (rotor) must have a difference in pressure between the upper and lower surfaces. At the tip of the rotor blade, air tends to flow from the high-pressure region (lower surface) to the low-pressure region (upper surface). This flow, which creates the tip vortices, tends to diminish the pressure difference at the tips and thereby reduces the lift in the general area of the tips. Because of the flow over the top surface of the rotor, this tip flow is not spanwise, but creates a resultant flow at an angle aft of the span line. Not only does this motion produce the tip vortices, but this diverts the normal chord-wise component of the flow and adds to the reduction of the generated lift. The amount of the tip loss is dependent on the total thrust of the blades, increasing as the coefficient of thrust increases and decreases with the number of blades. Both of these effects are included in an empirical equation for tip loss that was first derived by Prandtl and gives satisfactory correlation with the Goldstein-Lock calculations for lightly loaded rotors.

$$B = 1 - \frac{\sqrt{2C_T}}{b} \tag{11}$$

where: C_T = Tail Rotor Thrust Coefficient

b = Number of blades. The OH-58A+ has a 2-bladed tail rotor.

The value for no tip loss is 1.0 and the expected range for typical rotors is from 0.90 to 0.97.

The tail rotor thrust coefficient is given by the following expression,

$$C_T = \frac{T}{\rho_a (\Omega R)^2 \pi R^2} \tag{12}$$

where: C_T = Tail Rotor Thrust Coefficient

ρ_a = Ambient density

ΩR = Tip Speed

πR^2 = Disc Area

The hover inflow velocity (v_o) of the rotating rotor is a function of thrust (T), density (ρ_a), area of the disk (A) and tip loss (B),

$$v_o = \sqrt{T \big/ 2\rho_a A B^2} \tag{13}$$

With the above calculation results, $\frac{Bv_i}{v_o}$ can be determined. Since induced velocity, v_i, is the only remaining unknown, the solution of this equation can be used to determine v_i. Using this value of v_i, the analytical tail rotor induced power can be determined. This value is compared to the original assumed value and an iterative solution for the tail rotor power determined with a zero convergence.

Fin Blockage Effects (fn)

The tail rotor is mounted on the left side of the helicopter tail boom. Air is pulled by the rotating tail rotor blades and rejected to the left side of the helicopter. Since a vertical fin is installed in the airflow path, it reduces the net thrust that can be developed for antitorque purposes. Consequently, isolated tail rotor performance must be adjusted for the blockage effect by increasing total tail rotor thrust as shown in figure F.4 (Ref. 2). The ratio of the tail rotor thrust to net thrust is a function of the fin/rotor separation (s/R), where (s) is the distance between the tail rotor and the vertical fin, and the blocked fin area to rotor disc area ratio ($S_v/\pi R^2$). Utilizing the thrust ratio from figure F.4 (Ref. 2), the magnitude of the increased tail rotor thrust and, consequently, power can be determined.

Inertia Effects (IE)

The Inertia Effects do not apply when the helicopter is in trimmed flight with no kinematic body acceleration. However, once the trimmed condition is disturbed by unbalanced forces, e.g. transient force, the tail boom will tend to rotate about the helicopter center of gravity. The rotation rate, in part, depends on the moment of inertia of the helicopter, and is inversely proportional to the moment of inertia.

In addition, due to the moment change, the required tail rotor power is changed. If the moment is in the same direction as the tail rotor thrust, the moment will assist countering torque and the required tail rotor power is reduced. On the other hand, if

the moment is in the opposite direction, the tail boom will contribute additional moment in the direction of the torque reaction and more tail rotor power is needed. This relationship is presented in the following equation:

$$\Delta N = l_T * T_{IE} = I_{zz}\alpha \tag{14}$$

where: ΔN = Change of Fuselage Moment about the vertical axis (z-axis)

l_T = Length of the Tail

T_{IE} = Tail Rotor Thrust due to inertia effects

I_{zz} = Moment of Inertia about Z-axis

α = Angular Acceleration

Rearrange equation 14 as follows, so that the change of thrust due to the angular acceleration imposed on the helicopter can be determined,

$$T_{IE} = \frac{I_{ZZ}\alpha}{l_T} \tag{15}$$

The tail rotor thrust corresponding to the inertial acceleration for a specific helicopter can be determined. Since this thrust affects the tail rotor power requirement during different flight regimes, it is included in the total tail thrust calculation.

Axial Velocity Effects

The axial velocity effects will appear when the tail rotor encounters a directional component of airflow perpendicular to the rotor blades. For example: a pusher tail rotor is installed on the left side of OH-58A+. A gust of wind from the left increases

the angle of attack thereby, increases tail rotor thrust. To maintain balanced, antitorque requires a reduction of tail rotor power in this situation. The axial velocity effects may cause tail rotor power requirements to increase or decrease. Knowledge of local blade axial velocity due to winds, lateral translation and yaw rate are required to quantify the axial velocity effects on tail rotor power. For winds and lateral helicopter translation, the velocity is applied directly to analyze the yaw effects that require a kinematic solution. The yaw rate multiplied by the length of the tail calculates the axial velocity at the helicopter tail rotor. Including the axial velocity, the total inflow speed of the tail rotor can be determined in the following equation,

$$V_v = r * l_T + V_L \tag{16}$$

where: V_v = Total Kinematic Velocity of the Tail Section

r = Yaw Rate of the Tail Section

V_L = Lateral Velocity

This velocity is used to calculate the tail rotor power. Therefore, it needs to be converted in terms of power. A variation in axial velocity modifies the inflow velocity of the tail rotor. This requires the recalculation of the parameters of the $\frac{BV_v}{v_o}$. From this relationship, the induced velocity (v_i) can be determined from the chart (Ref. 9.7). Based on this v_i, the axial velocity effects are incorporated and the resultant effect on induced power can be calculated with the following equation,

$$P_i = \frac{1}{550} T v_i \tag{17}$$

Altitude Density Correction

Helicopter missions may be flown from sea level to mountainous conditions. As the altitude increases, the air density decreases and rotors must increase angle of attack to generate the same required thrust for antitorque. To obtain a more accurate result, the density altitude correction is included in the tail rotor power calculations.

The equation for this correction is as follows:

$$P_D = \frac{P}{\sigma_D} \tag{18}$$

where: σ_D = Density Ratio, $\sqrt{\frac{\rho_D}{\rho_a}}$

Antitorque Power in Forward Flight

Profile Power

The same theory applies to the forward flight condition with few modifications. Rotor H-Forces and torque effects are included in this profile power calculation for a more accurate result.

The dissymmetry of the local velocity on the rotor in forward flight produces a variation in local drag forces. The effects of this local drag variation are examined by looking, at the effects of the chordwise and spanwise components of velocity.

The H_1 force is a result of the chordwise velocity components and is a summation of the element profile drag forces parallel to the chord of the rotor blade. In hover, the H_1 force is zero, but in forward flight, difference in the advancing (high velocity, moving into the forward flight ëwindí) and the retreating (low velocity, moving ëdownwindí) blade chordwise forces. This variation of the chordwise profile drag force in forward flight produces two effects:

1. An increase in tail rotor torque requirement, which causes the power requirement of $P_o(\mu^2)$.
2. The generation of a rotor hub shear force, H_1, which has a power requirement of $P_o(2\mu^2)$.

The H_2 force is a result of the viscous drag due to the spanwise, i.e., radial, flow and was neglected in the previous determination of profile power requirements. This flow produces a rotor shear force in the downstream direction with an associated increase in the power required in forward flight of approximately 55 percent (Ref. 2). The H_2 forces can be calculated by increasing the profile power required values by $1.65\mu^2$. Summing these components modifies the hover profile power and accounts for the relative increase in forward flights.

$$(1 + 4.65\mu^2)$$

where: μ = Tip Speed Ratio

The Tip Speed Ratio (μ) is the ratio between the forward flight velocity (V_F) and the Tip Velocity (ΩR).

$$\mu = \frac{V_F}{\Omega R} \tag{19}$$

The equation for the forward flight profile power should be modified as follows,

$$P_o = \frac{1}{550 * 8} * (\Omega R)^3 * \rho_a * A * \sigma_R * c_d * (1 + 4.65 * \mu^2) \tag{20}$$

where: ΩR = blade tip speed

ρ_a = Ambient density

A = Disc Area

σ_R = Rotor Solidity

c_d = Profile Drag Coefficient

Induced Power (P_i)

The equation for the hovering induced power can be applied in the forward flight condition.

$$P_i = \frac{1}{550} T v_i \tag{9}$$

where: P_i = Induced Power

v_i = Induced Velocity

While the equation is the same as before, the induced velocity is a variable and is decreased in magnitude significantly from the hover condition.

Using the chart (Fig F.3) to find the new values for the following parameters:

$$\frac{Bv_i}{v_o}, \frac{BV_v}{v_o}, \frac{BV_F}{v_o} \tag{10}$$

where: B = Tip Loss Factor

V_v = Total Kinematic Velocity of the Tail Section

V_F = Horizontal Velocity

In the forward flight case, the vertical velocity remains zero while the horizontal velocity is a variable.

In order to use the chart to find the induced velocity, the tip loss factor and the hover induced velocity have to be determined first.

$$\frac{BV_F}{v_o}$$

Fuselage Moment Contribution (N)

The OH-58A+ is equipped with a vertical fin mounted on the right side of the tail boom. The fin contributes to directional stability in the forward flight condition. In addition, since it has approximately a 7-degree incidence angle right of the centerline, the vertical fin generates a right side force. This right side force reduces the tail rotor antitorque thrust requirement in forward flight conditions. This favorable contribution increases with increased forward flight speed.

The body axis yawing moment is used to obtain the moment for the fuselage. From figure F.5 (Ref. 6), even though no direct information for the fin lift is provided, the fin lift can be calculated with the selected curve.

For given helicopter characteristics, yawing moment factors include forward flight velocity and sideslip angle. The other parameters, e.g. the dimensional and inertial terms, are constant. Therefore, either changing the forward flight velocity or sideslip will result in changing the yawing moment. For example: increasing the forward flight velocity or sideslip angle will increase the yawing moment for given inertial and dimensional conditions.

To determine the incremental effect on tail rotor power, the fuselage moment needs to be calculated and the reduction in tail rotor thrust determined by dividing the yawing moment by the length of the tail as,

$$T_{fn} = \frac{N}{l_T} \tag{21}$$

where: T_{fn} = Vertical Fin Lift

N = Fuselage Moment

l_T = Length of the Tail

Since only the values for the N/q can be obtained directly from the chart provided (Fig F.5, Ref 6), more calculations are required to determine the fuselage yawing moment (N). The simplest approach is to calculate the dynamic pressure (q) and multiply it by the fuselage yawing moment (N). As discussed in this section, the fin of the OH-58A+ is mounted at the end of the tail boom with a 7-degree right incident

angle. When the helicopter is in translational flight, the fin will experience the dynamic pressure caused by the resultant relative wind. The resultant dynamic pressure acting on the area of the fin generates a force and causes the tail boom to rotate about the aircraft center of gravity. Therefore, the local velocity is required for the calculation of the dynamic pressure (q). The resultant velocity of the air in vicinity of vertical fin can be calculatedd from the following equation ignoring rotor downwash effects,

$$V_N = \sqrt{V_F{}^2 + V_v{}^2} \tag{22}$$

Where: V_N = Fuselage Velocity

V_F = Forward Flight Velocity

V_v = Total Kinematic Velocity of the Tail Section

This calculated total kinematic velocity of the tail section can be used in the dynamic pressure (q) calculation.

By multiplying q with N/q, the fuselage moment (N) can be determined.

$$q = \frac{1}{2}\rho_D V_v{}^2 \tag{23}$$

Since the N and l_T are both known now, the T_{fn} can be calculated in the equation 21.

The calculated vertical fin lift reduces the tail rotor thrust requirements and results in reducing the tail rotor power requirement in forward flight. This reduction is included in the iteration loop for the total tail rotor power calculation.

Power Losses

Mechanical losses associated with the tail rotor system occur downstream of the accessory gearbox where the torque is measured. These losses are additive to the power required by the tail rotor. Source of these losses include,

- Tail Rotor Gearbox
- Cooling Fan driven from the drive system
- Tail Shaft Bearings

Gearbox losses are produced by friction between the gear teeth and in the bearings and by aerodynamic drag, or ìwindage.î The losses are a function of the size of the gearbox as well as the power being transmitted at any given time. The losses in the gearbox can be calculated from the following equation,

Power loss per stage = K [Design max. power + Actual power] (Ref. 1, p. 277) (14)

where: K = 0.0025 for spur or bevel gears (OH-58A+)

K = 0.00375 for planetary gears.

Due to the insignificant power consumptions, both the cooling fan and the tail shaft bearings are assumed to have no effect on power required calculations.

This calculated gear box loss is compared with the total power applied from the tail drive shaft. Power losses due to the mechanical components of the tail rotor are calculated using a constant efficiency factor. This efficiency factor is typically less than 1.0 to account for imperfect transmission of power to the tail rotor. The efficiency of the tail rotor system is presented by,

$$\eta = 1 - \frac{P_G}{P_A} \tag{24}$$

where: η = Efficiency of the Tail Rotor system

P_G = Power loss from the Tail Rotor Gear

P_A = Power Applied

Tail Rotor Power Requirement

From the results of the previous sections, the tail rotor power equation is determined as follows:

$$P = (P_i * F + P_o) / \eta \tag{25}$$

where: F = Vertical Fin Blockage Factor

This calculation for the required power from the tail rotor must agree with the calculated value. If not in agreement, an iterative solution using tail rotor power is performed to eliminate the error,

$$Error = P_{ME} - P_M = 0 \tag{26}$$

$$P_{ME} = P_A - P \tag{27}$$

Once again, the applied power is a function of the torque and the rotational speed of the main rotor. These are known parameters and can be obtained from standard cockpit instruments. In order to distinguish the initial assumed main rotor power and the calculated main rotor power, subscript M and ME are used, respectively.

Pedal Position Determination

Correlating the pedal position and the tail rotor power, the lift coefficient (C_L) for the specific tail rotor blade needs to be first determined. Using the blade NACA airfoil chart (Fig F.6, Ref 4) to find the corresponding angle of attack. Since pedals are mechanically linked to tail rotor blades, the movement of the pedal and the tail rotor blade angle should correspond in a linear relationship. Once this relationship is applied, the pedal position can be determined. On OH-58A+ the tail rotor pedal travel is 6.7-in from one extreme to the other while the tail rotor blade travel is 23 to -7 degrees, for full left to full right pedal positions, respectively.

Once the required tail rotor power is determined, the tail rotor thrust and the thrust coefficient (C_T) can be determined by the previously described relationships. The thrust and lift are equal. Change in thrust is given by,

$$\Delta T = \Delta L \cos\varphi + \Delta D \sin\varphi \tag{28}$$

where: T = Thrust

L = Lift

D = Drag

φ = Angle between thrust and lift

As assumed, the angle between blade thrust and lift is small. Using the small angle assumption, the equation can be simplified as follows:

$$T = L \tag{29}$$

Since the value of the tail rotor thrust has been determined in the previous sections, the calculated tail rotor thrust can be used to determine the coefficient of lift as follows,

$$C_L = \frac{2 * T}{\rho_a U^2 A} \tag{30}$$

where: C_L = Lift Coefficient

U = Effective Freestream Velocity

A = Blade Disk Area

The effective freestream velocity (U) is assumed to be a function of the rotor tip speed and the induced velocity. With these two values calculated from the previous sections, the freestream velocity can be determined with the following relationship,

$$U^2 = (\Omega R)^2 + v_i^2 \tag{31}$$

The lift coefficient can be calculated from equation (30). In addition, the coefficient of lift can determine the angle of attack from the known lift curve slope. Normally, the lift curve slope can be found in a NACA chart for a particular airfoil section. As long as the blade airfoil is known, it will be relatively easy to determine the lift curve slope by measurement or data analysis.

After determining the lift curve slope for the specific helicopter, OH-58A+ in this case, it is necessary to determine the angle of attack of the blades. If there is no induced air flowing through the rotating blades, the angle of attack is equal solely to the tail rotor blade angle. However, since the induced flow of air is constantly

passing through the rotating disk area and results in decreasing the effective angle of attack of the rotating blades, the induced flow angle needs to be subtracted from the blade pitch angle. Therefore, the effective angle of attack is always smaller than the blade collective angle of attack. Pedal position is directly correlated to the blade pitch angle of attack. Determination of pedal position is as follows:

$$C_L = a\alpha_r = a(\theta - \varphi_i) \tag{32}$$

where: a = Lift curve slope per radian

θ = Tail Rotor Blade Angle (rad)

φ_i = Inflow Angle (rad)

After rearranging this equation in the following form, the tail rotor pitch blade angle can be determined,

$$\theta = \frac{C_L}{a} + \varphi_i \tag{33}$$

Even though the inflow angle is an unknown in the above equation, it is assumed that this angle can be approximated by the relationship of the induced flow velocity to the rotational velocity. From this approximation, the induced flow angle can be determined with the following equation,

$$\phi_i = ATAN\left(\frac{v_i}{\Omega R}\right) \tag{34}$$

where: v_i = Induced Velocity

ΩR = Rotor Blade Tip Speed

From these series of calculations, the pedal position for any flight regime can be determined. A chart for the relationship between pedal positions vs. tail rotor collective blade angles is included in figure F.7.

Model Fidelity

Based on the analytical model, the calculation for the tail rotor power required consists of various components, which include induced power, density altitude correction, profile power, gearbox loss, vertical fin blockage effects, fuselage moment contribution, and inertia effects. The consideration of all these components minimizes the errors between the actual and the analytical results. Each individual component contributes different values to the total tail rotor power required. These values vary according to the helicopter flight regimes. For example: compared to the level flight performance, hover performance is calculated on primarily from induced power. Additionally, fuselage moment contribution becomes an important factor while a helicopter is in sideslip motion. After the investigation of the various flight regimes, a boundary condition for the possible errors was determined. This condition encompasses the following conditions:

- 60 to 100-% main engine torque
- 0 to 10000-ft altitude
- 40 to 100-kts airspeed
- 0.25-in left and right step inputs
- 25-deg/sec left and right both accelerations and deceleration recovery

- 14-deg left and right sideslip
- 20-kts left and right sideward flights

Table 3.1 presents the breakdown of the error contribution from each contributor in different flight regimes. If only the induced power is considered, the accuracy may decrease to as low as 59.1-% in hover performance, 17.67-% in level flight performance. The parameters listed below induced power indicate the maximum possible errors that could be expected if any one of them is ignored. The significance of each parameter is quantified and presented in the same table. For example: if the profile power is ignored in the level flight performance, it is possible to cause as high as 80.84-% tail rotor power error. Therefore, in order to obtain the highest accuracy, induced power and the other contributors to tail rotor power must be considered.

Table 3.1. Maximum Potential Algorithm Elemental Contributions (%)

	Hover	Level Flight	SideSlip	Sideward	Step Inputs	Rotations	Rotation Recovery
Induced Power	59.1	17.7	35.1	52.2	58.8	63.4	56.9
Profile Power	36.3	80.8	83.0	43.8	36.7	32.3	38.7
Altitude Density Correction	4.40	4.90	11.8	6.30	5.50	5.50	4.70
Gear Box Loss	4.21	8.78	8.95	5.00	4.25	3.80	4.50
Blockage Effects	0.610	0.380	0.330	0.650	0.640	0.600	0.600
Fuselage Moment Contribution	0	62.5	59.3	3.70	0	0.300	0
Inertia Effects	0	0	0	0	15.9	0	24.1

Chapter 4

FLIGHT TEST PROGRAM

Purpose

The objective of this flight test was to validate an analytical model created for the tail rotor power required analysis.

Scope

Two flight tests were performed. These tests consisted of different flight tasks, including Ground Operation, Hover, Take-Off & Climb, Forward Flight, Cruise, Loiter, Descent and Approach and Landing. An OH-58A+ helicopter was used in both tests. Tests were conducted in the vicinity of the Tullahoma Regional Airport (elevation 1082-ft).

The weather for both days was moderate with temperature between 20-C and 24-C. Wind speeds were less than 4-kts wind on both days.

The test details and helicopter configuration were maintained as stated in table 4.1 and flight test plan (App C). The weights were 3022-lbs with c.g. of 109.4-in (aft) and 2797-lbs with c.g. of 110.0-in (aft), respectively. Testing was conducted in 2.5 hours and 109 data sets were recorded. All these flight configurations reflected the general usage of this type of aircraft according to the surveys (App A) provided by various Bell 206 Jet Ranger or OH-58A derivatives pilots. The rationale for collecting more data points on the second day was because of the desire of

constructing a fully populated data set for the level flight airspeed range. As such, the range of the airspeeds from 30-kts to 100-kts, with increments, were flown. All the data were collected by the onboard instrumentation and stored on laptop computer.

Table 4.1. Test and Test Conditions

Type of Test	Average Gross Weight (lbs)	Average Fuselage Station (in)	Pressure Altitude (ft)	Outside Air Temperature (deg C)	Trim Calibrated Airspeed (kts)	Remarks
Hover Performance	2926	109.8	892	24	0	2 to 10-ft skid height
	2720	109.2	985	20		
Low Speed	2944	109.8	1010	24	5, 10 & 20	Same airspeeds for both left, right & forward.
	2770	109.3	901	20		
Level Flight Performance	2881	109.6	4250	22	106	
	2959	109.8	3255	18	33 to 104	
Sideslip	2840	109.5	3715	22	70 & 100	15-deg left to 14-deg right sideslip angles
	2914	109.7	3708	18		
Yaw Acceleration	2818	109.4	885	24	0	Between 40-deg/sec left & right
	2722	109.2	950	20		24-deg/sec left to 37-deg/sec right
Deceleration Recovery	2816	109.4	885	24	0	Between 40-deg/sec left & right
	2720	109.2	950	20		24-deg/sec left to 37-deg/sec right
Step Input	2830	109.4	880	24	0	0.25-in left to 0.25-in right
	2709	109.1	945	20		0.25-in left to 0.32-in right
Ground Operation	3020	110.0	900	24	0	
	2797	109.4	900	20		
Takeoff & Climb	2897	109.6	980 to 2000	24	20 to 55	70 to 80-% main engine torque applied
	2591	108.9	840 to 1650	20	14 to 67	
Loiter	2884	109.6	3620	24	76 to 93	
	2896	109.6	3980	20	69 to 83	
Descent	2918	109.7	1530 to 1400	24	69	
	2654	109.0	2800 to 2130	20	63 to 81	
Approach & Landing	2793	109.3	1008 to 970	24	43 to 0	
	2654	109.0	1600 to 920	20	60 to 0	

Method of Test

All test techniques were performed as described in IAW FTM-106 (Ref 10). Test and test conditions are listed in table 4.1. The following descriptions provide some additional information for this test.

Hover Performance

The hover performance tests were conducted at approximately 1000-ft pressure altitude and at various power settings, 75 to 100-% main engine torque. The selected parameters were collected and stored on laptop computer.

Low Speed

Left, right sideward, and forward flights were conducted In-Ground-Effect (IGE). The helicopter was flown at approximately 20-ft above the ground. In order to maintain the low ground speeds, a pace car calibrated with Global Positioning System (GPS) was used. The tests were conducted from 5-kts to 20-kts ground speed.

Forward Flight

Trimmed Flight and Steady Heading Sideslip were evaluated in this section.

Trimmed Forward Flight

The airspeeds from 35-kts to 100-kts were selected as mission representative for this test. These airspeeds provided representative values of normal cruise conditions as per the surveys attached in appendix A.

Steady Heading Sideslip

In the Sideslip tests, angles from 15-degrees left to 15-degrees right were evaluated on the test helicopter. Two different airspeeds, 70-kts and 100-kts, were used for this test. In each run, the helicopter was maintained at 3700-ft pressure altitude.

Controllability

This test consisted of various step inputs, which included yaw accelerations and rotational recovery.

Yaw accelerations

A range of yaw rates between 40-deg/sec left and right was performed. Pedal inputs were used to initiate and maintain the desired rotation rates. The OH-58A+ accelerated about the Z-axis and resulted in a rotational wind-up, which was controlled by the pilot. Open loop tasks, therefore, did not produce a steady yaw rate.

Deceleration Recovery

The pilot stopped the yaw rate by applying opposite pedal. Pedal inputs and yaw rates were recorded. Also, the deceleration rates were determined by evaluating the slope of yaw rate curves.

Step Inputs

These tests were performed in In-ground-effect. The inputs were measured by the co-pilot. In order to simulate the step input, a fixture (Fig 4.1 & 4.2) was located at the desired distance from the pedal and used to stop the pedal movement.

Figures 4.1. Pedal Fixture

Figure 4.2. Pedal Fixture Function Demonstration

Due to the heavy weight (3022-lbs and 109.4-c.g., with 3200-lbs and 111.4-in c.g. limits), the first tests were limited by the application of 0.5-in left pedal input. At a take off weight (2797-lbs and 110.0-in c.g.), a wider range of pedal inputs were performed without the risk of transient over-torque.

Other Tests

Not all the tests performed on the test days were simulated in the analytical model, some tests, e.g. ground operation, takeoff and climb, loiter, descent, approach & landing, were included in the tests only for the qualitative purposes. The remainder of the chapter is dedicated for those unmodeled activities.

Takeoff and Climb

Normal takeoffs from the ground were utilized. Upon takeoff, the collective was adjusted to the desired torque, the aircraft was then accelerated to approximately 60-kts climb. The aircraft was maintained in trim throughout the maneuver.

Loiter, Descent and Approach and Landing

Loiter was performed by establishing the required loiter airspeed in level flight. Descent and approach were conducted by establishing a rate of descent with a collective reduction that was representative of surveyed information. A 60-kts airspeed was maintained in the resultant descent. The aircraft was maintained in trim until the landing phase was initiated. Landings were accomplished to the ground.

Chapter 5

FLIGHT TEST AND ALGORITHM COMPARISON

Introduction

Data contain measured flight test pedal positions to compare with the analytical results. The percentage errors of the pedal positions between analytical predictions and flight test values were plotted for various flight regimes. These pedal position errors were determined by comparing the measured and calculated values. The ratio of these differences to the maximum pedal travel, 6.7-in, was used to calculate the percentage errors of the pedal positions. The calculated tail rotor power errors were determined in a similar manner. However, since the measured values of the tail rotor power were not available, the calculated values were used. From the analytical model, figure F.8 shows the maximum calculated tail rotor power is 67.9-hp. Since there is a corresponding calculated tail rotor power value for each pedal position, the percentage error of each pedal position generates a corresponding percentage error on tail rotor power. By knowing the pedal position errors, the tail power errors can be determined. The pedal position and tail rotor power errors are normalized by maximum pedal travel, 6.7-in, and tail rotor power, 67.9-hp, at maximum available engine torque, respectively.

Hover Performance

The hover performance tests were conducted as listed in table 4.1. As the main engine torque was increased, the pilot compensated the increased torque by applying left pedal. The pedal positions and the power coefficients are nearly linear (Fig D.1). The agreement between the pedal position and the calculated pedal position contributed to the smallest errors among all tests. All the errors appeared on the negative side of the graph which meant the calculated tail rotor power was always less than the actual flight test results. This agreement resulted in only ñ1.6-% errors and was within the limit recorded in the maximum potential algorithm elemental contributions (Table 3.1). Figure D.2 contains the errors in detail. Varying gradients in the pedal positions vs. c_p graph indicate the power error is not correctable by additional profile or mechanical losses. The incorporation of all components in this analytical model resulted in significantly better results than using only induced power.

Low Speed

The left and right sideward flights were evaluated and compared to the analytical model. The pilot needed to apply more left pedal while in right sideward flight. In the range of 20-kts left to 20-kts right, the required pedal travel was approximately 0.8-in (Fig D.3). The analytical model matched the trend of the test results (Ref 6). The error at each data point is shown in figure D.4. The errors ranged from ñ5.1 to 2.5-% while most of the errors were less than 4-%. Since all the components described in elemental contribution table (Table 3.1) were considered in this

calculation, the errors were smaller than considering the pedal positions in isolation. The model results matched the trends of flight test, but were always lower.

Forward Flight

Two different categories, Trimmed Forward Flight and Sideslip, were evaluated in this section.

Trimmed Forward Flight

Trimmed Forward Flight tests were performed in level unaccelerated trimmed level flight. The trimmed airspeeds, altitudes, and other flight characteristics are presented in the table 4.1. A nearly neutral pedal position at 69-kts is shown in figure D.5. The greatest left pedal inputs were required with the maximum at 104-kts, 3.3-in from the full left position. The vertical fin provided a portion of counter torque thrust. As the minimum left pedal airspeed, 69-kts in this case, was increased, the greater left pedal inputs were required for the increasing main engine torque. Therefore, for all tested forward flight airspeeds, the tail rotor consumed the least power at 69-kts. At this airspeed, the vertical fin could generate 63-% (Table 3.1) of the required anti-torque. The analytical model generated tail rotor power errors of less than 6.7-% (Fig D.6). Figure D.5 also shows that the analytical model and the flight test have the same slopes. This would result in increasing tail rotor power and left pedal required. The new curve would shift closer to the flight test results. The analytical model results in significantly better results than using only induced power.

Steady Heading Sideslip

Sideslips were performed at two thrust settings with collective fixed as described in table 4.1. The test results showed the errors ranged from ñ8.9 to 8.2-% of maximum tail rotor power. The greatest errors appeared at the right sideslip. As shown in figure D.7, the 70-kts test curve had a better agreement with the calculation model on the left sideslip while right sideslip results were better for the 100-kts case. Bank angles were increased linearly as the sideslip angle increased (Fig D.8). There are some scattered data points, especially at 100-kts, located at the left sideslip, but no trend was correlated. The model used contractor (Ref. 8) provided data set for moment due to sideslip. The flight test conditions were not the same as the available wind tunnel data. Additionally, the fuselage model (Fig F.5, Ref 8) used in this algorithm analysis might not include all aerodynamic effects.

Controllability

This part consists of yaw rates, step inputs and rotational recovery tests.

Yaw Rates

Yaw rates were performed as presented in table 4.1. During the tests, accelerations on the helicopter required the pilot to stop the rotations shortly after the initial rotation was commenced. In order to standardize the analysis, the yaw rate at the initiation of every recovery was used to evaluate the characteristics of this

helicopter. Data are presented in figures D.11 to D.22, which describe the time history of the pedal positions and the yaw rates at different rotational rates. Figures D.23 and D.24 present the errors between the flight test and the analytical model. The errors ranged from 1.0 to 4.4-%. The errors scattered widely in the entire range. No discoverable trend is evident. These errors could be caused by the inertia, or inflow changes. However, these errors are still less than considering the induced power (pedal positions) alone.

Deceleration Recovery

Constant rates were difficult to establish by the pilot. The pilot stopped the rotation with an opposite pedal input. The pedal input and yaw rates were collected. With the collected information and calculated yaw rates, the model determined the required tail rotor power accordingly. The errors of the calculation model were within 2.4-% of the calculated tail rotor power (Figs D.25 & D.26). The analytical model results in significantly better results than pedal position alone.

Step Inputs

In order to simulate the step input, a fixture was used as described in test methodology section of chapter 4. The applied main engine torques were between 70 to 80%. Yaw rates and the pedal positions corresponding to the motions were collected and evaluated (Figs D.27 to D.33). After the yaw rates were determined, the calculation model evaluated the data. The errors are presented in figures D.34 and

D.35. The analytical model correlated with pedal position for the flight test results. Generally, the errors were within 3-%, with one exception of 5.7-% in a 0.25-in right test. The analytical model assumes static rates for induced tail rotor performance. The aircraft tail rotor experiences a dynamic acceleration, which is not modeled. Left yaw rates were consistently lower than right to prevent any over torque conditions. The analytical model results in significantly better results than pedal position in isolation.

Other Tests

Ground Operation

For ground operation, the engine torques were between 10-% to 30-% engine torque. There was no need for the tail rotor variations to counter the main rotor torque. The pedal positions did not vary significantly in response to the changing engine torque. Figures D.36 shows the time history of the pedal positions.

Take-Off & Climb

Different engine torques, 73-% to 86-%, were used to document the helicopterís climb performance based on the operational flight profiles (Figs D.37 to D.40). The results from these different engine torques generated a pattern as follows: In correspondence to the sudden increase of the engine torque at the beginning of a climb, the pilot applied the left pedal to counter this high torque. Once the climb was initiated, the left pedal could be decreased slightly to almost neutral position. Within

the 60 seconds periods, the test helicopter could accelerate from 0-kts to approximately 60-kts.

Loiter, Descent and Approach & Landing

There was no calculation model for the either Loiter, Descent or Approach & Landing. Data were collected and plotted only for the reference purpose in figures D.41 to D.43. In the Loiter test, it was necessary to apply more left pedal when the helicopter was operating at higher main engine torque and higher airspeed.

Summary

Two flight tests were successfully performed and the test data were compared with the analytical model. The results from each flight regime revealed various errors when compared to the model. None of the errors exceeded 10-%, except the errors in the steady heading slip regime. Therefore, this analytical model is considered to be 90-% accurate for determining tail rotor power from pedal position within the entire hover and forward flight envelope with sideslip limitations of +4.2-% to ñ7.1-%.

Chapter 6

CONCLUSIONS

Utilizing pedal position in simplified momentum theory as a sole indicator of tail rotor power is a poor metric. Even in the simplest case, a stationary hover, the pedal position has a direct correlation with a profile tail rotor power. In order to get a reasonable approximation for hover tail rotor power, it is necessary to correct for additional profile power effects and mechanical losses. The uncompensated tail rotor power assumption using only the induced power with constant inflow is in error by 27.3-% at full power and increased to 42.7-% at 60% main engine torque.

An accurate estimation for tail rotor power can be made by including parameters which compensate for rotor RPM, altitude density correction, axial velocity, kinematic velocity and forward flight velocity. A model was constructed based on the presented theories. Correlation with the model and flight test results were within ñ 1.6-% in hover and 6.7-% in forward flight. However, the model did not match well with the sideslip flight conditions. Compared to the range of engine power values, the pedal had a very narrow travel range. Therefore, poor pedal position measurements could result in large tail rotor power errors. The ratio of tail rotor power error to pedal position error is approximately 1.1. These errors in table 6.1 were derived from the maximum tail rotor power (67.9-hp) and the maximum pedal position travel (6.7-in), respectively.

Table 6.1. Summary of the Flight Test Results

Type of the Test	Tail Rotor Power Error (%)
Hover Performance	-0.1 to -1.6
Low Speed	Average 4 (with range ñ5.1 to 2.5)
Trimmed Forward Flight	1.9 to 6.7
Sideslip	-8.9 to 8.2
Yaw Rates	0.9 to 4.4
Deceleration Recovery	0.6 to 2.4
Step Inputs	-0.2 to 3.0 (except 5.7% at 0.25-in right)

Different components have different effects on the final calculated tail rotor power required. In general, blockage effect has the least effect, less than 5-%.

Some of the unmodeled errors are due to the transient effects of flight and profile drag. Based upon the mission profiles generated from a recent market survey, these transients are encountered less than 9.7-% of the flight time. By using the pedal positions, this model provides at least 90-% confidence in tail rotor power at all flight regimes evaluated in this report, except any sideslip angle exceeding 7.1-deg (nose right) and 4.2-deg (nose left), respectively. This model can be used on any conventional single rotor helicopter.

Chapter 7

RECOMMENDATIONS

1. An enhanced fuselage yaw moment due to sideslip chart should be used to minimize errors in forward flight sideslip.
2. Use model for predicting tail rotor power required.
3. Instrument the tail rotor to measure tail rotor power applied.

WORK CONSULTED

REFERENCES

1. Prouty, Raymond W. ì Helicopter Performance, Stability, and Control,î Malabar, FL: Krieger, 1990.

2. Donald M. Layton, ì Helicopter Performance,î Matrix Publishers, Inc., Beaverton, Oregon, 1984.

3. OH-58A Maintenance Manual, TM 55-1520-228-23.

4. Ira H. Abbott and Albert E. Von Doenhoff, ì Theory of Wing Sections,î NACA-0012, p. 463.

5. W.Z. Stepniewski and C.N. Keys, ì Rotary-Wing Aerodynamics Vol. 2,î Dover Publications, Inc., New York, 1984.

6. USAAEFA Project No. 76-11-2 ì Airworthiness and Flight Characteristics Evaluation OH-58C Interim Scout Helicopter,î April 1979.

7. Chart: Induced velocity Approximation

8. Bell Helicopter Company Report No. 206-099-188, ì A Qualitative Analysis of The Data from a Wind-Tunnel Test of a 0.25-Scale Model 206î, Jan 15, 1970.

9. OH-58A Operatorsí Manual, TM 55-1520-228-10.

10. Flight Test Manual, ì *Rotary Wing Performance*î Naval Air Test Center, USNTPS-FTM-No. 106, 31 December 1996.

11. Flight Test Manual, ì *Rotary Wing Stability and Control*.î Naval Air Test Center, USNTPS-FTM-No. 107, 31 December 1995.

APPENDICES

APPENDIX A.

USAGE SPECTRUMS ñ RESULTS FROM SURVEY

INTRODUCTION

A survey was conducted to describe and quantify in terms of torque applied and time, the typical usage spectrum for different mission types. The survey was conducted by e-mail (152 surveys sent by e-mail), fax, regular mail (50 surveys) and at the AHS Convention on Washington D.C., May 9-11.

NOTES:

The following results, for each mission category, correspond to the most-repeated intervals (mode) in the case of the torque values and to the arithmetic mean (average) in the case of times and airspeeds.

CHARTER/ PART 133/135

Ground operations
Torque applied = 0-20%
Time = 3 minutes

Hover
Torque applied = 86-100%
Avg. time = 3 minutes

Take-off & climb
Torque applied = 86-100%
Time = 3 minutes

Cruise
Torque applied = 80-85%
Time = 55 minutes
Cruise speed = 96 kts

Loiter
Torque applied = 60-70%
Time = 25 minutes

Descent
Torque applied = 30-39%
Time = 3 minutes

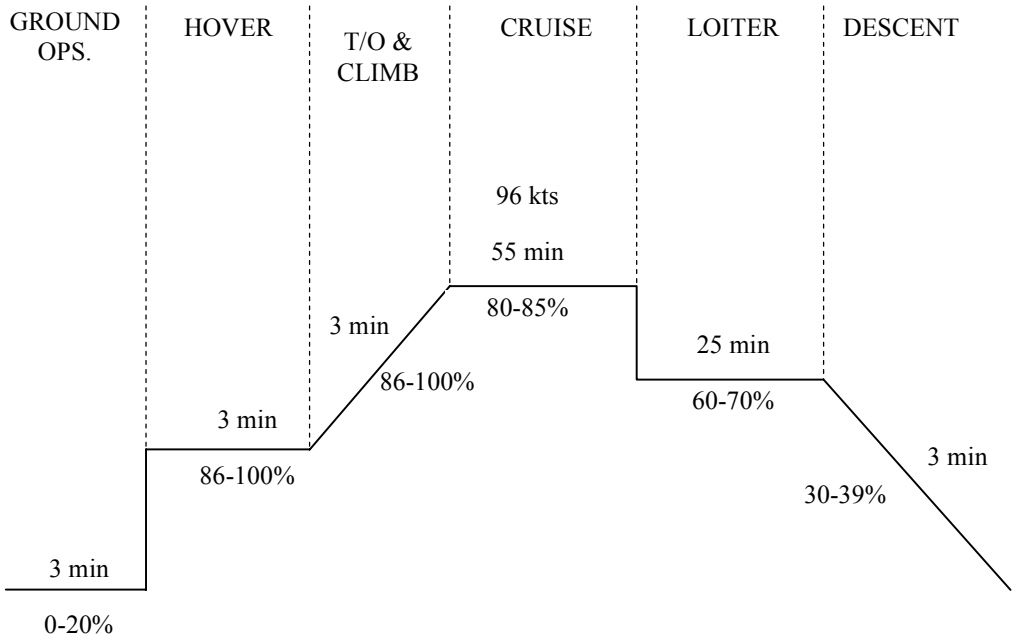

EXECUTIVE TRANSPORT

Ground operations		
Torque applied	=	21-25%
Time	=	4 minutes
Hover		
Torque applied	=	80-85%
Time	=	3 minutes
Take-off & climb		
Torque applied	=	80-85%
Time	=	4 minutes
Cruise		
Torque applied	=	80-85%
Time	=	55 minutes
Cruise speed	=	96 kts
Loiter		
Torque applied	=	
Time	=	
Descent		
Torque applied	=	40-49%
Time	=	3 minutes

Note: No loiter for executive transport missions

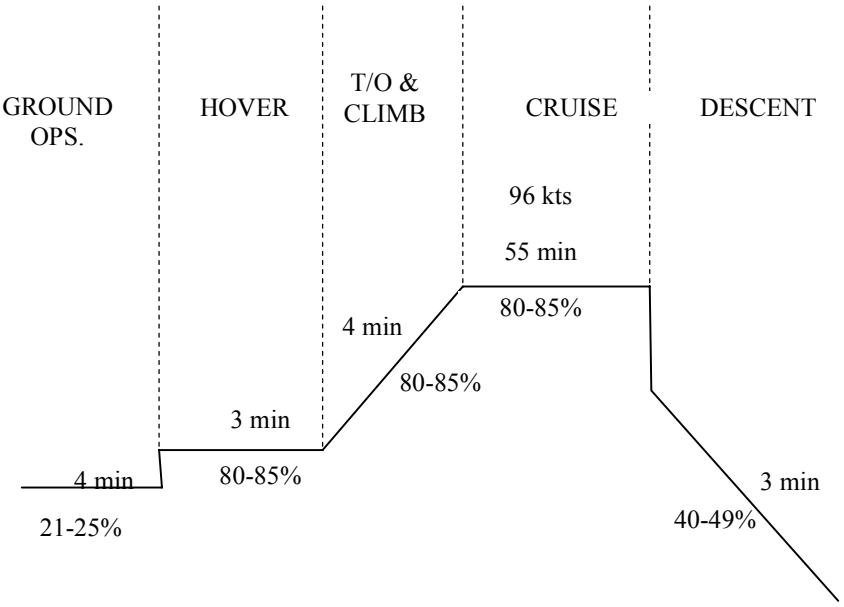

TRAINING

Ground operations
Torque applied = 21-25%
Time = 4 minutes

Hover
Torque applied = 80-85%
Time = 3 minutes

Take-off & climb
Torque applied = 80-85%
Time = 3 minutes

Cruise
Torque applied = 80-85%
Time = 45 minutes
Cruise speed = 96 kts

Loiter
Torque applied = 50-59%
Time = 15 minutes

Descent
Torque applied = 40-49%
Time = 3 minutes

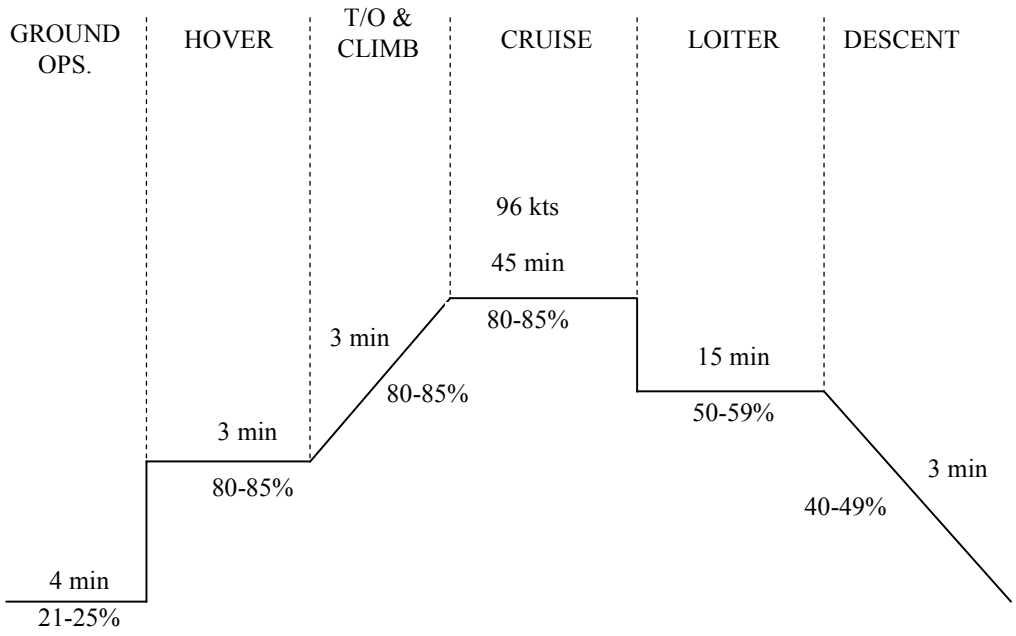

POLICE

Ground operations
Torque applied = 0-20%
Time = 3 minutes

Hover
Torque applied = 75-79%
Time = 3 minutes

Take-off & climb
Torque applied = 75-79%
Time = 3 minutes

Cruise
Torque applied = 70-74%
Time = 90 minutes
Cruise speed = 65 kts

Loiter
Torque applied = 70-74%
Time = 90 minutes

Descent
Torque applied = 30-39%%
Time = 3 minutes

Note: For police patrols over metropolitan areas cruise is equivalent to loiter; and they average 2-2.5 hours per flight

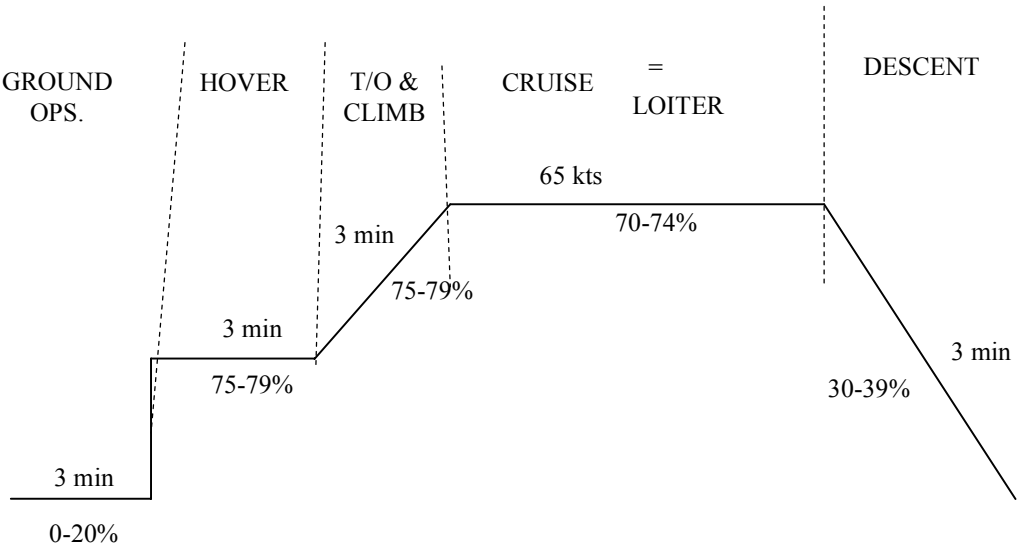

FIRE PATROL

Ground operations
Torque applied = 0-20%
Time = 3 minutes

Hover
Torque applied = 86-100%
Time = 3 minutes

Take-off & climb
Torque applied = 80-85%
Time = 3 minutes

Cruise
Torque applied = 80-85%
Time = 50 minutes
Cruise speed = 96 kts

Loiter
Torque applied = 60-70%
Time = 23 minutes

Descent
Torque applied = 30-39%
Time = 4 minutes

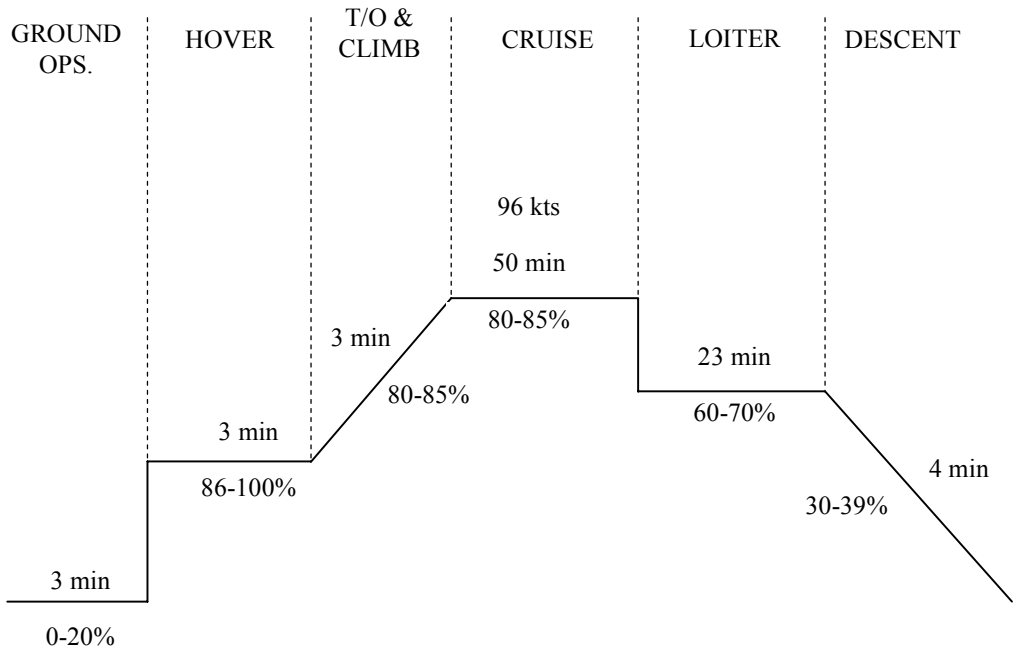

PIPELINE/ELECTRIC/OIL PATROL

Ground operations
Torque applied = 21-25%
Time = 4 minutes

Hover
Torque applied = 80-85%
Time = 3 minutes

Take-off & climb
Torque applied = 80-85%
Time = 3 minutes

Cruise
Torque applied = 80-85%
Time = 45 minutes
Cruise speed = 96 kts

Loiter
Torque applied = 50-59%
Time = 15 minutes

Descent
Torque applied = 30-39%
Time = 3 minutes

Note:
For offshore oil support the operators average 50-100 landings per day

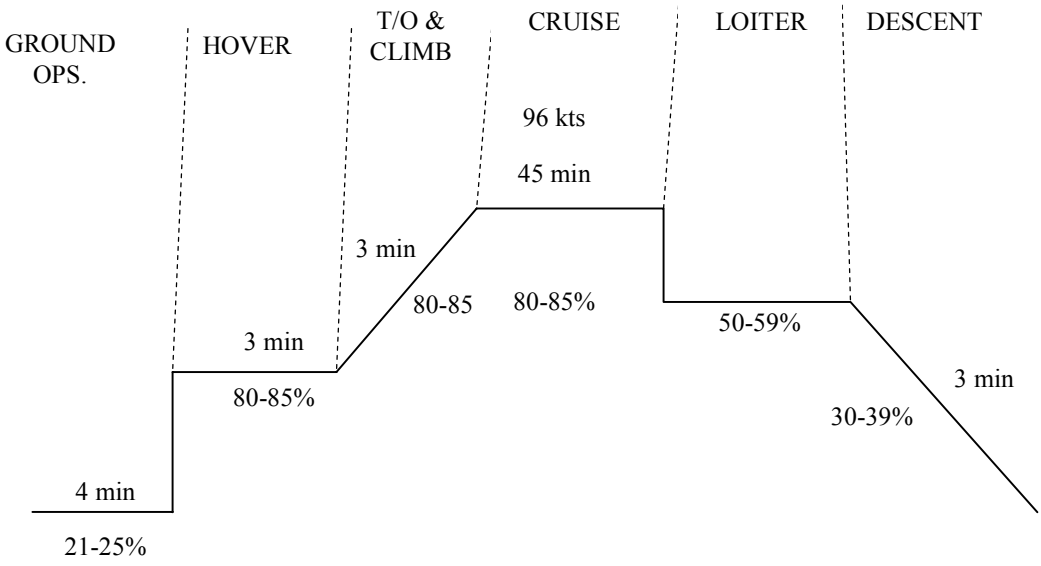

TV/AERIAL PHOTOGRAPHY/LAND SURVEY/ENVIRONMENTAL CONTROL

Ground operations
Torque applied = 21-25%
Time = 4 minutes

Hover
Torque applied = 80-85%
Time = 3 minutes

Take-off & climb
Torque applied = 80-85%
Time = 3 minutes

Cruise
Torque applied = 80-85%
Time = 45 minutes
Cruise speed = 96 kts

Loiter
Torque applied = 50-59%
Time = 30 minutes

Descent
Torque applied = 30-39%
Time = 3 minutes

Note:
For environmental control missions the cruise speed is often between 20 and 50 kts

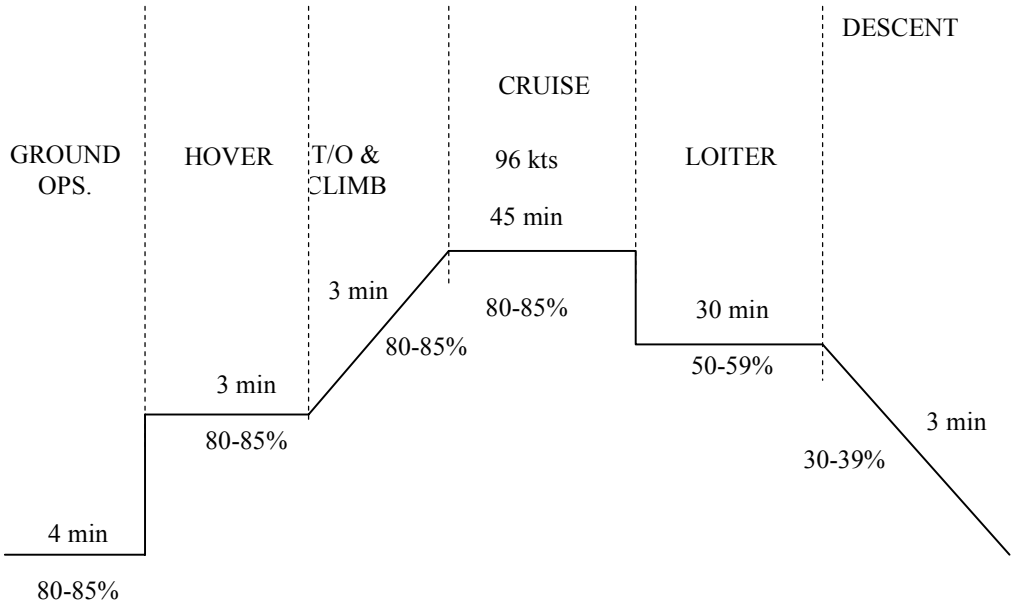

APPENDIX B

ANALYTIC MODEL FLOW CHART

ANALYTIC MODEL FLOW CHART

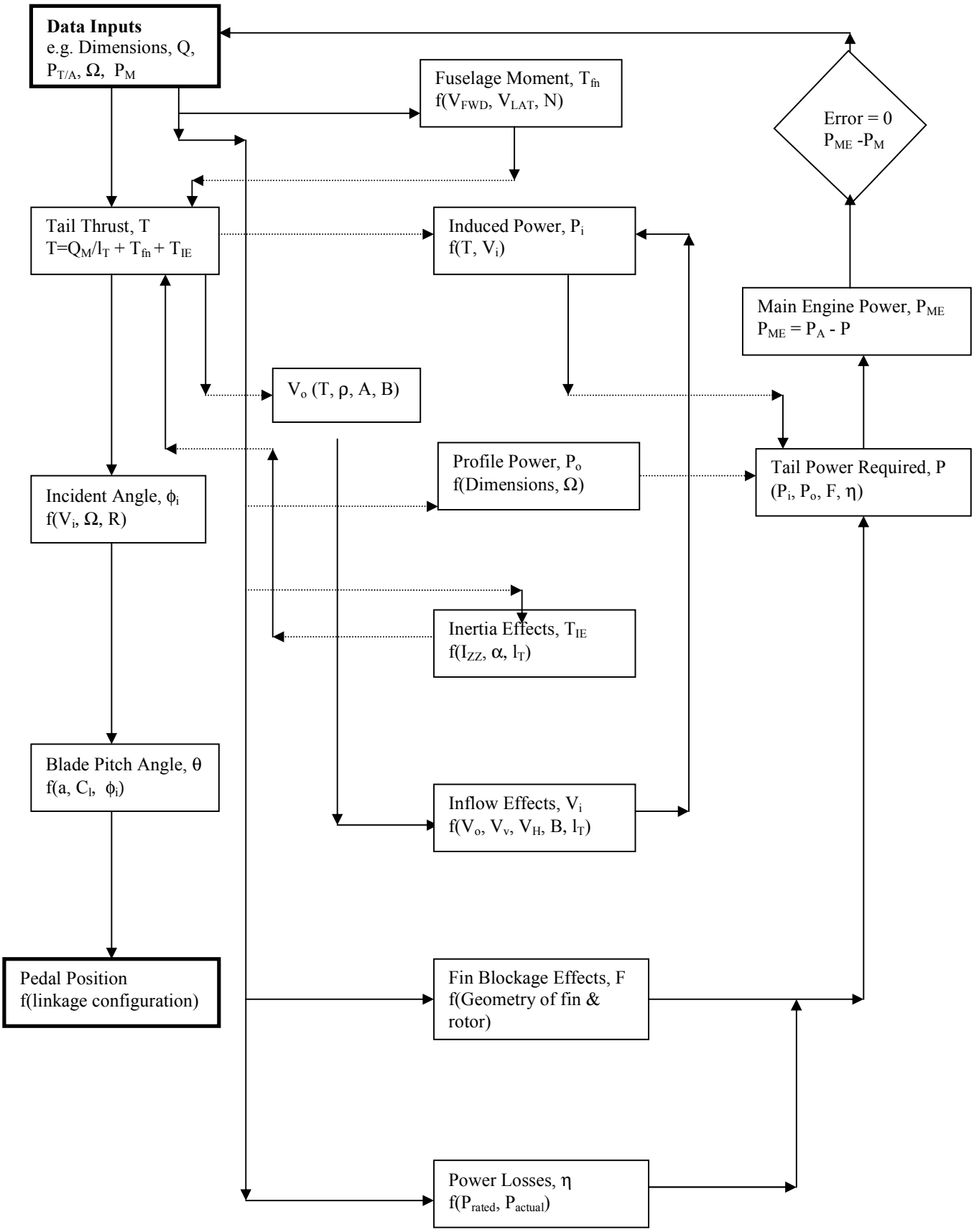

APPENDIX C

FLIGHT TEST PLAN

FLIGHT TEST PLAN

Purpose

The purpose of this test is to validate an analytical model created for the tail rotor power required analysis.

Scope of Tests

Tests and Test Conditions

The tests will be conducted in two flights for a maximum of 4.0 flight hours. All flights will be conducted under daylight visual meteorological conditions (VMC) at Tullahoma Regional Airport, Tullahoma, Tennessee. The tests and test conditions matrix is presented as Table 4.1.

Test Envelope

The test will be conducted within the limits of the Operator's Manual (Ref 9). The maximum altitude for the purpose of this test is 5,000 feet pressure altitude. Minimum test altitude will be ground level. The V_{NE} limits will be 100 KIAS with the doors installed.

Test Loadings

Test loading will be varied only by the number of personnel aboard the aircraft and the amount of fuel used during the tests. The actual aircraft test gross weight will vary from

3109 to 2827 pounds, while the center of gravity (CG) varies from 109.0 to 110.5 inches. Test loading is included in Table 4.1.

Test Configurations

The aircraft configuration for all tests will be: Flight test pitot static system (Boom) installed, doors installed and all engine bleed air systems off.

Method of Tests

Test Methods and Procedures

Engineering tests will be conducted in accordance with USNTPS FTM-106. USNTPS FTM-107, and this test plan as described in the Tests and Test Conditions Table (Table 4.1.) in order to assess the aircraftís performance and handling characteristics.

Hover Performance

Hover performance will be evaluated at 100-% rotor RPM. The hover performance test will be evaluated during a single flight of approximately 2.0 hour. The pressure altitude will be approximately 1000 feet. The main engine torque will be maintained at to to 100%. Helicopter loading will be two pilots on the front seats, and one observer in the passenger compartment. The center of gravity (CG) will be 109.5 inches, at the take-off

gross weight (GW) of 3000 pounds. The observer in the passenger compartment will collect data with the laptop computer.

Low Speed

Low Speed test will be evaluated during a single flight of approximately 2.0 hour. A chase car calibrated with GPS will be used to show various ground speeds (5 to 20-kts) to the pilots. This test will include left and right sideward flight. The helicopter will maintain In-Ground-Effect. The crew in the chase car will use portable radio to communicate with the pilots. Helicopter loading will be two pilots on the front seats, and one observer in the passenger compartment. The center of gravity (CG) will be 109.5 inches, at the take-off gross weight (GW) of 3000 pounds. The observer in the passenger compartment will collect data with the laptop computer.

Level Flight Performance

Level flight performance will be evaluated at 100% rotor RPM. The Level Flight Test will be evaluated during a single flight of approximately 2.0 hour. The pressure altitude will be 4000 feet. The tested airspeeds will start from 30-kts and increase to 100-kts. Helicopter loading will be two pilots on the front seats, and one observer in the passenger compartment. The center of gravity (CG) will be 109.5 inches, at the take-off gross weight (GW) of 3000 pounds. The observer in the passenger compartment will collect data with the laptop computer.

Steady Heading Sideslip

Steady Heading Sideslip test will be conducted during a 2.0 flight hours. The pressure altitude will be 4000 feet. Left and right sideslip angles, 20 degrees each side, will be evaluated. Helicopter loading will be two pilots on the front seats, and one observer in the passenger compartment. The center of gravity (CG) will be 109.5 inches, at the take-off gross weight (GW) of 3000 pounds. The observer in the passenger compartment will collect data with the laptop computer.

Yaw Acceleration and Deceleration Recovery

Yaw Acceleration and Deceleration Recovery test will be conducted at 100% rotor RPM. The Yaw Acceleration and Deceleration Recovery test will be evaluated during a single flight of approximately 2.0 hour. The pressure altitude will be 1000 feet. The indicated airspeeds will be maintained at zero. The information at the end of the Yaw Acceleration will be used to analyze the characteristics of the Deceleration Recovery. The pilots will perform various rotational rates about the helicopter vertical axis. Helicopter loading will be two pilots on the front seats, and one observer in the passenger compartment. The center of gravity (CG) will be 109.5 inches, at the take-off gross weight (GW) of 3000 pounds. The observer in the passenger compartment will collect data with the laptop computer.

Step Input

Step Input test will be conducted at 100% rotor RPM. The Step Input test will be evaluated during a single flight of approximately 2.0 hour. The pressure altitude will be 1000 feet. The indicated airspeeds will be maintained at zero. A removable fixture will be installed and used for the incremental movements of the pedals. The fixture will be moved 0.5-in each time. The pilots will step the pedals onto the fixture and let the helicopter rotate about its vertical axis. Test is considered completed when the helicopter starts to become unstable. Helicopter loading will be two pilots on the front seats, and one observer in the passenger compartment. The center of gravity (CG) will be 109.5 inches, at the take-off gross weight (GW) of 3000 pounds. The observer in the passenger compartment will collect data with the laptop computer.

Ground Operation

Ground Operation test will be conducted at 100% rotor RPM. The Ground Operation test will be evaluated during a single flight of approximately 2.0 hour. The helicopter will remain on the ground. The indicated airspeed will be maintained at zero. Helicopter loading will be two pilots on the front seats, and one observer in the passenger compartment. The center of gravity (CG) will be 109.5 inches, at the take-off gross weight (GW) of 3000 pounds. The observer in the passenger compartment will collect data with the laptop computer.

Takeoff and Climb

Takeoff and Climb test will be conducted at 100% rotor RPM. The Takeoff and Climb test will be evaluated during a single flight of approximately 2.0 hour. The initial pressure altitude will be from the ground. The pilots will perform this test with 75 to 100-% main engine torque. Helicopter loading will be two pilots on the front seats, and one observer in the passenger compartment. The center of gravity (CG) will be 109.5 inches, at the take-off gross weight (GW) of 3000 pounds. The observer in the passenger compartment will collect data with the laptop computer.

Loiter

Loiter test will be conducted at 100-% rotor RPM. The Loiter test will be evaluated during a single flight of approximately 2.0 hour. The pressure altitude will be at 3500 feet. The pilots will perform this test with 50 to 75-% main engine torque. Helicopter loading will be two pilots on the front seats, and one observer in the passenger compartment. The center of gravity (CG) will be 109.5 inches, at the take-off gross weight (GW) of 3000 pounds. The observer in the passenger compartment will collect data with the laptop computer.

Descent

Descent test will be conducted at 100-% rotor RPM. The Descent test will be evaluated during a single flight of approximately 2.0 hour. The initial pressure altitude will be at 2000 feet. The pilots will perform this test with 30 to 50-% main engine torque.

Helicopter loading will be two pilots on the front seats, and one observer in the passenger compartment. The center of gravity (CG) will be 109.5 inches, at the take-off gross weight (GW) of 3000 pounds. The observer in the passenger compartment will collect data with the laptop computer.

Approach and Landing

Approach and Landing test will be conducted at 100-% rotor RPM. The Approach and Landing test will be evaluated during a single flight of approximately 2.0 hour. The initial pressure altitude will be at 1500 feet. The pilots will perform this test with 30 to 50-% main engine torque. Helicopter loading will be two pilots on the front seats, and one observer in the passenger compartment. The center of gravity (CG) will be 109.5 inches, at the take-off gross weight (GW) of 3000 pounds. The observer in the passenger compartment will collect data with the laptop computer.

INSTRUMENTATION AND DATA EXTRACTION/PROCESSING

Sensitive instrumentation and data recording equipment is installed onboard the test aircraft. Daqbook will be used to acquire engine and flying parameters. Fuel flow data will be extracted from the Operatorís Manual. The external equipment required to collect the desired test data are: A laptop computer, Stopwatch, GPS, tape measurement and a chase car. Data will be recorded on the laptop computer. The data will be evaluated on the analytical model. All the equations are stated in appendix E.

The following will be taken at each data point:

1. Heading;
2. OAT;
3. Altitude;
4. Airspeed;
5. % of Torque;
6. RPM;
7. Pedal Positions;
8. Side Slip Angle;
9. Yaw Rate;

.

The following is a list of data requirements:

V_o - ± 1 knot.

H_P - ± 20 feet.

N_R - ± 0.5%.

Special Precautions

Safety Considerations

The test crew must have a thorough knowledge of aircraft limitations. All level flight-testing shall be conducted within the established flight envelope and normal operating limitations contained in the Aircraft Operator's Manual. A chase car will be required for the Low Speed Tests. The crew will terminate the test in the event of any unusual handling characteristics or vibrations. A thorough review of smoke and fume elimination and fuselage fire in flight emergency procedures will be conducted during the flight briefings. During all tests the crew must remain vigilant to air traffic and obstacle avoidance.

Risk Management

The flight shall be conducted in VFR conditions during daylight. Emergency actions will be developed and briefed by the aircrew prior to the installation of experimental (non-standard) equipment. Consideration will be given to a formation training flight prior to the Low Speed tests. The overall risk associated with the conduct of this test is assessed to be low. However, with the exception of formation flight which is assessed as a medium risk.

Management

Schedule/Milestones

Coordination meeting for the Tail Rotor Power Requirement Project is scheduled on 25 July 2002 (1530 hours) at the UTSI hangar facility for all personnel concerned in the flight test. The first flight test is scheduled to be conducted on 26 August 2002 pending approval of the test plan by the project advisor.

Test Plan approval	25 July 2002
Flight Brief	26 August 2002
Flight Tests	26 and 31 August 2002

Personnel Assignment

Dr. Lewis is assigned as the aircraft pilot-in-command of the test aircraft and project advisor. Professor Stellar is assigned as a project advisor. Kan-Wai Tong is assigned as the test director and FTE for each of the tests. Mr. Leigh is designated as the technical advisor for all instrumentation. Mr. Heatherly is designated chief of maintenance.

Reports

An individual Report of Test Results will be completed as soon as practicable after the successful completion of the flight tests. The report will:

- Determine the tail rotor power required through the calculations of the corresponding pedal positions to the applied main engine torques.
- Summarize the differences between the analytical model and flight test data.
- Suggest improvements should be made for better results.

REVELANT OH-58A/C EMERGENCY PROCEDURES

Engine Failure-Hover
Autorotate

Eng Fail-Low Alt/Low Airspd or Cruise
1. Autorotate
2. EMER SHUTDOWN

Engine Restart-During Flight
1. Throttle-Close
2. Attempt Start
3. Land ASAP

Engine Compressor Stall
1. Collective-Reduce
2. ENG DEICE and HTR-OFF
3. Land ASAP

Engine Overspeed
1. Collective-Increase
2. Throttle-Adjust
3. Land ASAP

If RPM cannot be controlled manually:
4. Autorotate
5. EMER SHUTDOWN

Engine Underspeed
a. If powered flight w/ rotor in green
Land ASAP
b. Engine underspeed below 94% N2
1. Autorotate
2. EMER SHUTDOWN

Engine Surges
1. GOV RPM switch-INCR
landing
2. Throttle-Adjust to 98% N2
3. Land ASAP

If engine surges are not controlled:
4. Autorotate
ON
5. EMER SHUTDOWN

Flight Control Malfunctions
1. Land ASAP
2. EMER SHUTDOWN after landing

Loss of Tail Rotor Effectiveness
1. Pedal-Full Left
2. Cyclic-Forward

Main Driveshaft Failure
1. Autorotate-maintain power
2. EMER SHUTDOWN-after landing

Clutch Fails to Disengage
1. Throttle-Open
2. Land ASAP

Mast Bumping
Land ASAP

Hot Start
1. STARTER switch-Press
2. Throttle-Close

Engine/Fuselage/Elec. Fire-Ground
EMER SHUTDOWN

Engine/Fuselage Fire-In Flight
If Power-On landing:
1. Land ASAP
2. EMER SHUTDOWN after landing

If Power-Off landing:
1. Autorotate
2. EMER SHUTDOWN

Electrical Fire-In Flight
1. BAT and GEN switches-OFF
2. Land ASAP
3. EMER SHUTDOWN after

Smoke and Fume Elimination
1. Vents-Open
2. DEFOG & VENT switches-

Overheated Battery
1. BAT switch-OFF
2. Land ASAP
3. EMER SHUTDOWN after landing

APPENDIX D

FLIGHT TEST DATA

Aircraft Model: OH-58A+ Pilot: Bill Lewis Gross Weight: 2926-lbs OAT: 24-C
Serial No.: N88UT Co-Pilot: Fred Stellar C.G.: 109.8-in Skid Height: 2 to 10-ft Configuration:
Doors on, Bleed Air off Flight Test Engineer: Kan-Wai Tong Pressure Altitude: 985-ft RPM: 354

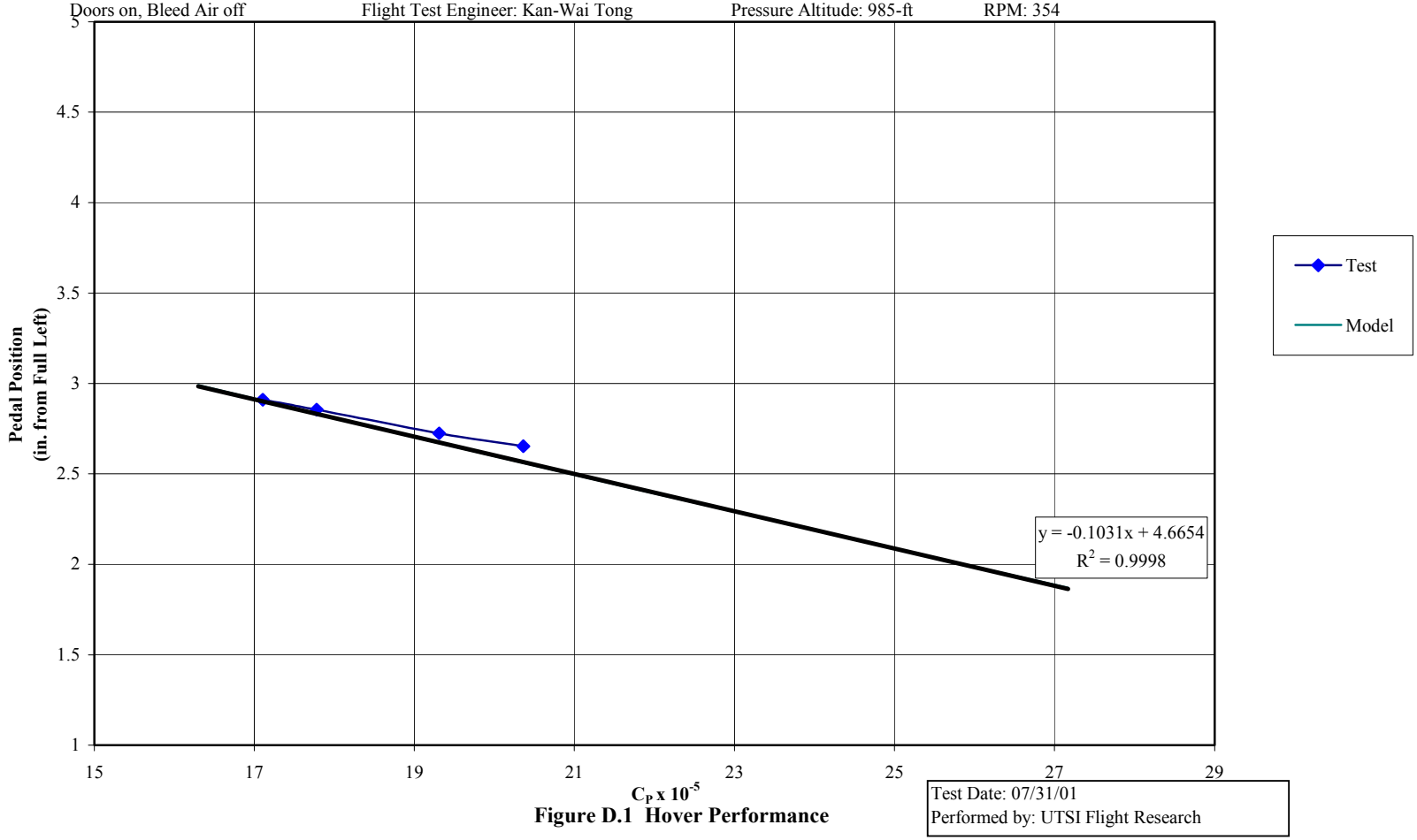

Figure D.1 Hover Performance

Aircraft Model: OH-58A+
Serial No.: N88UT
Configuration: Doors on, Bleed Air off

Pilot: Bill Lewis
Co-Pilot: Fred Stellar
Flight Test Engineer: Kan-Wai Tong

Gross Weight: 2720 & 2926-lbs
C.G.: 109.2 & 109.8-in
Pressure Altitude: 892 & 985-ft

OAT: 20 & 24-C
Skid Height: 2 to 10-ft
RPM: 354

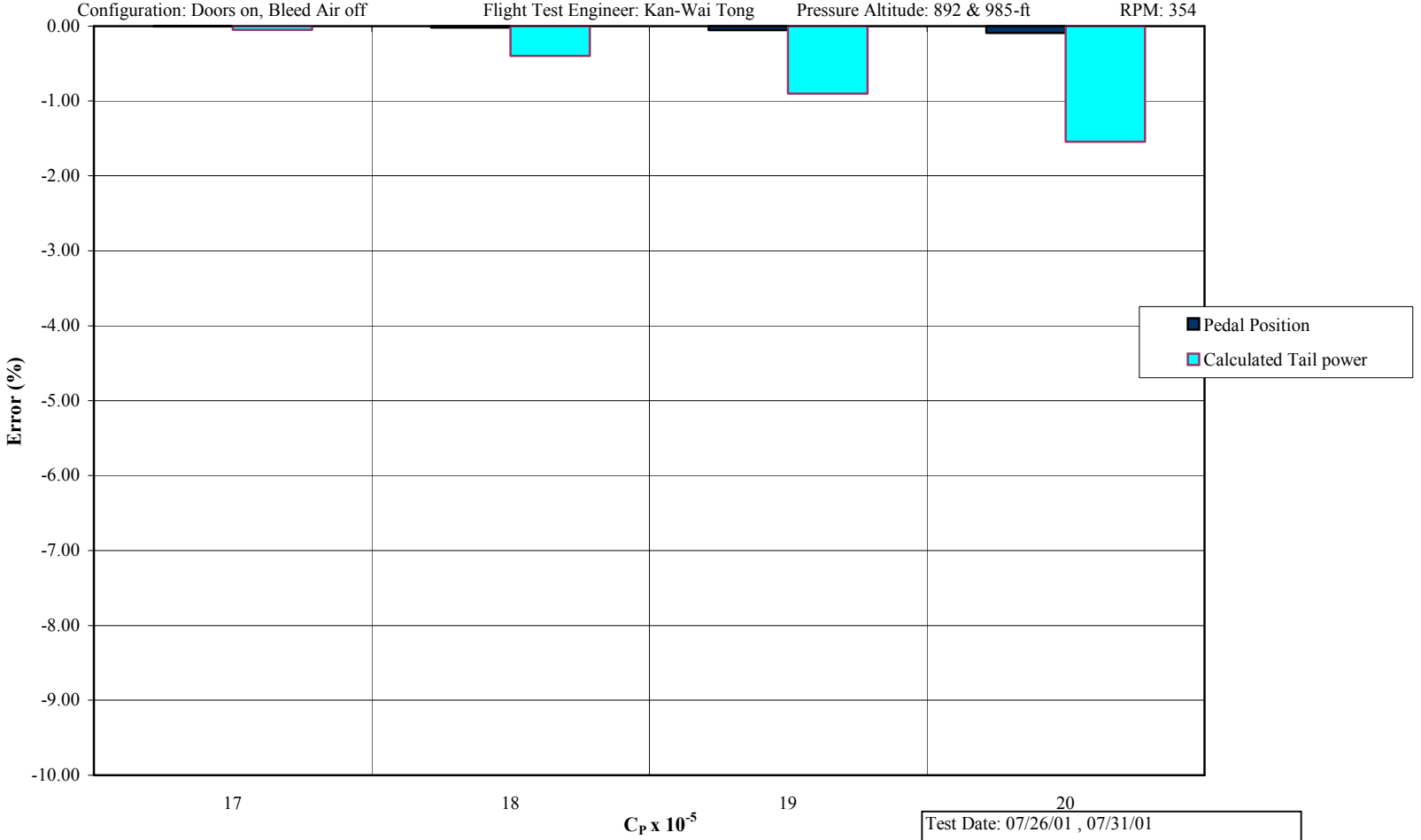

Test Date: 07/26/01 , 07/31/01
Performed by: UTSI Flight Research

Figure D.2 Hover Performance Error

Aircraft Model: OH-58A+
Serial No.: N88UT
Configuration: Doors on, Bleed Air off

Pilot: Bill Lewis
Co-Pilot: Fred Stellar
Flight Test Engineer: Kan-Wai Tong

Gross Weight: 2770 & 2944-lbs
C.G.: 109.3 & 109.8-in
Pressure Altitude: 901 & 1010-ft

OAT: 20 & 24-C
RPM: 354
Skid Height: 10 to 20-ft

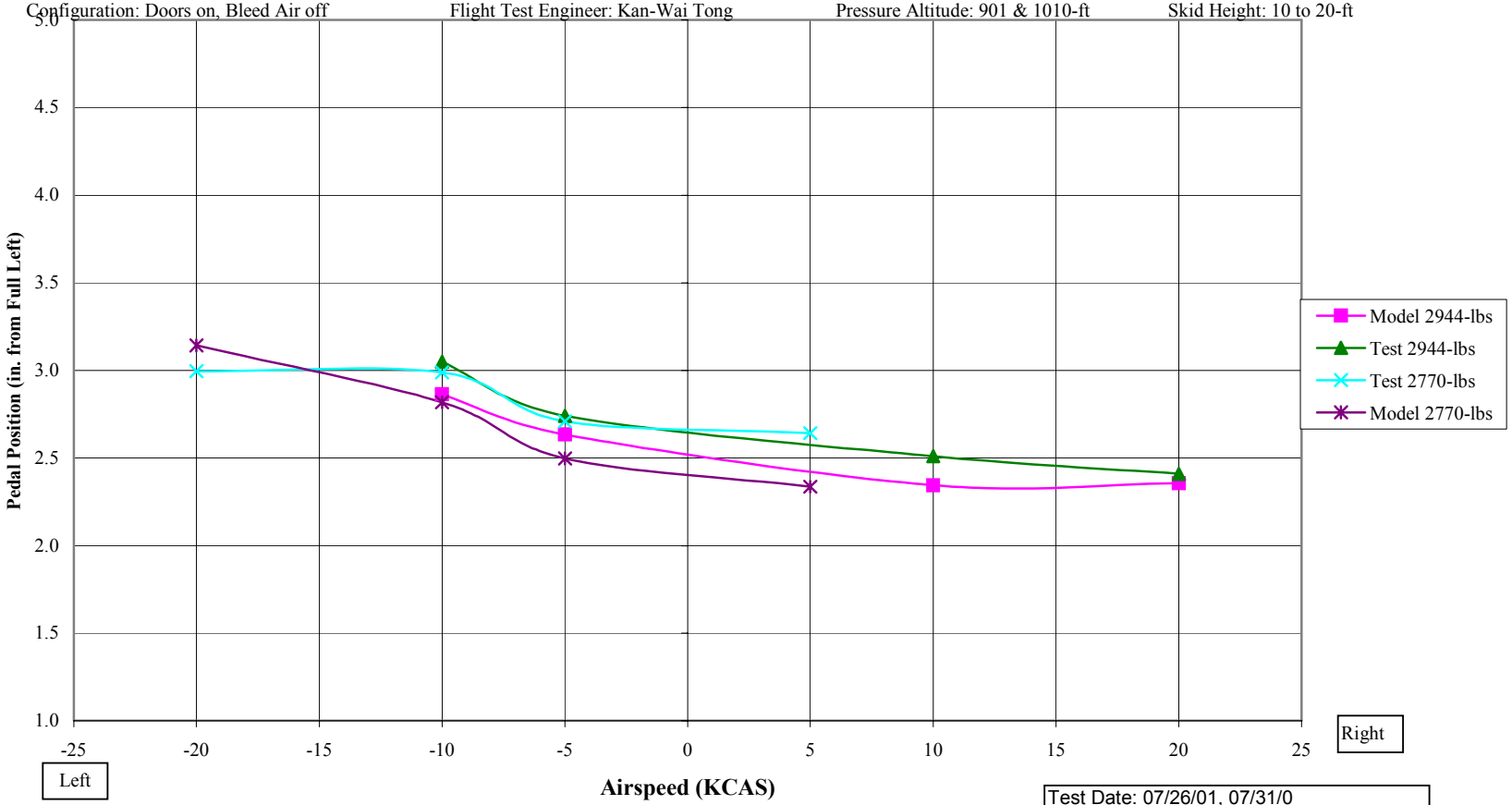

Figure D.3 Sideward Flight

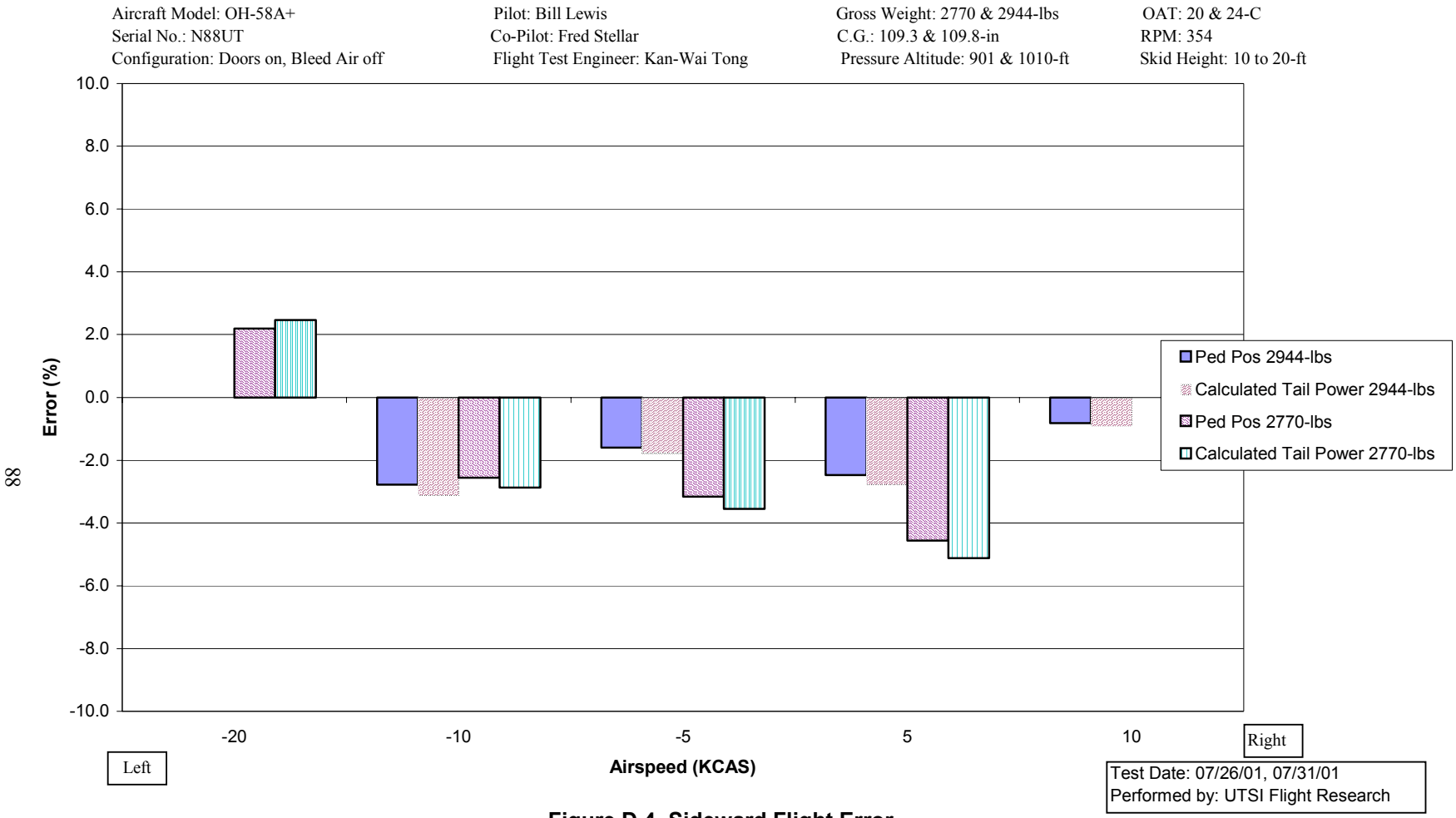

Figure D.4. Sideward Flight Error

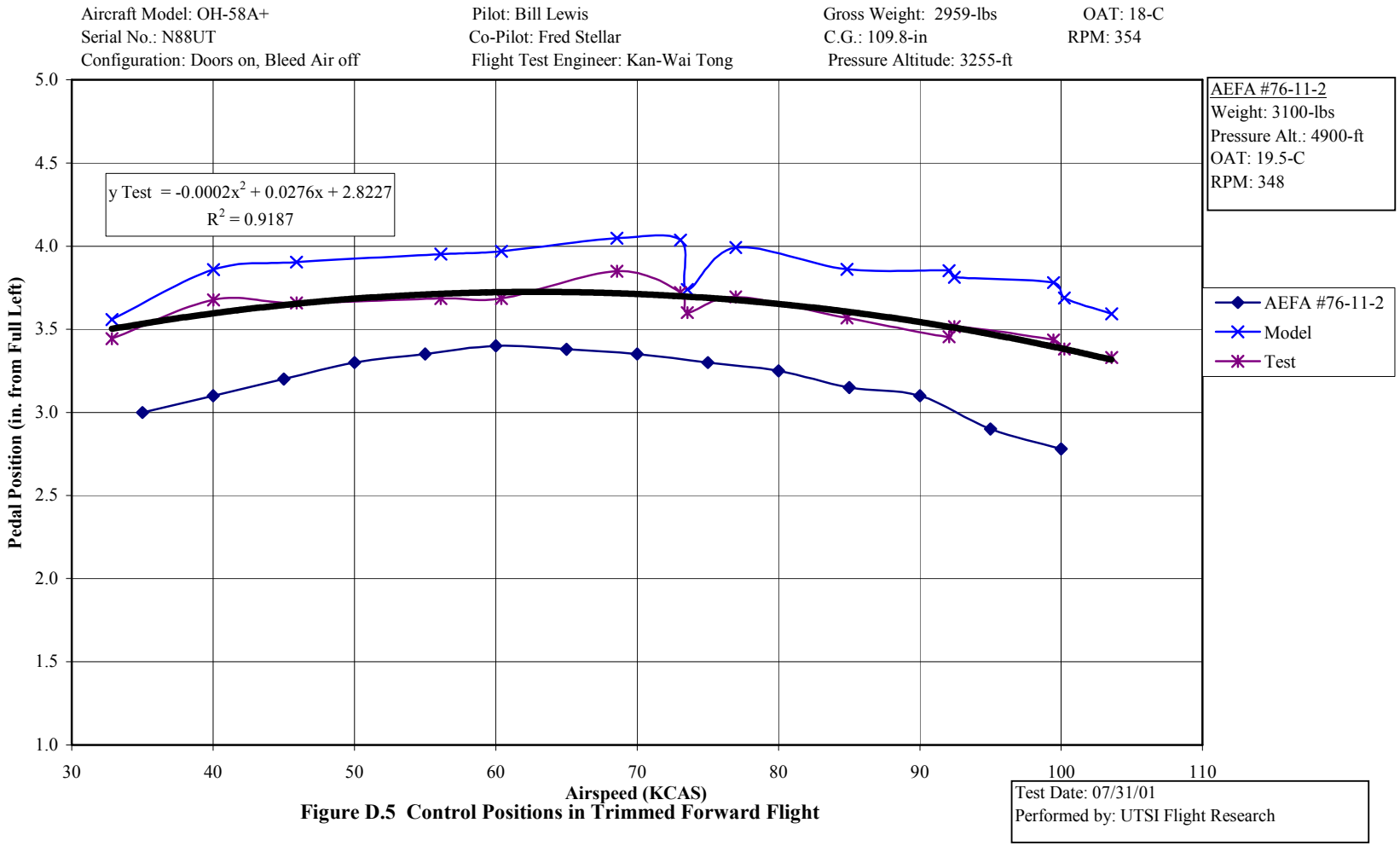

Figure D.5 Control Positions in Trimmed Forward Flight

Aircraft Model: OH-58A+ | Pilot: Bill Lewis | Gross Weight: 2959-lbs | OAT: 18-C
Serial No.: N88UT | Co-Pilot: Fred Stellar | C.G.: 109.8-in | RPM: 354
Configuration: Doors on, Bleed Air off | Flight Test Engineer: Kan-Wai Tong | Pressure Altitude: 3255-ft

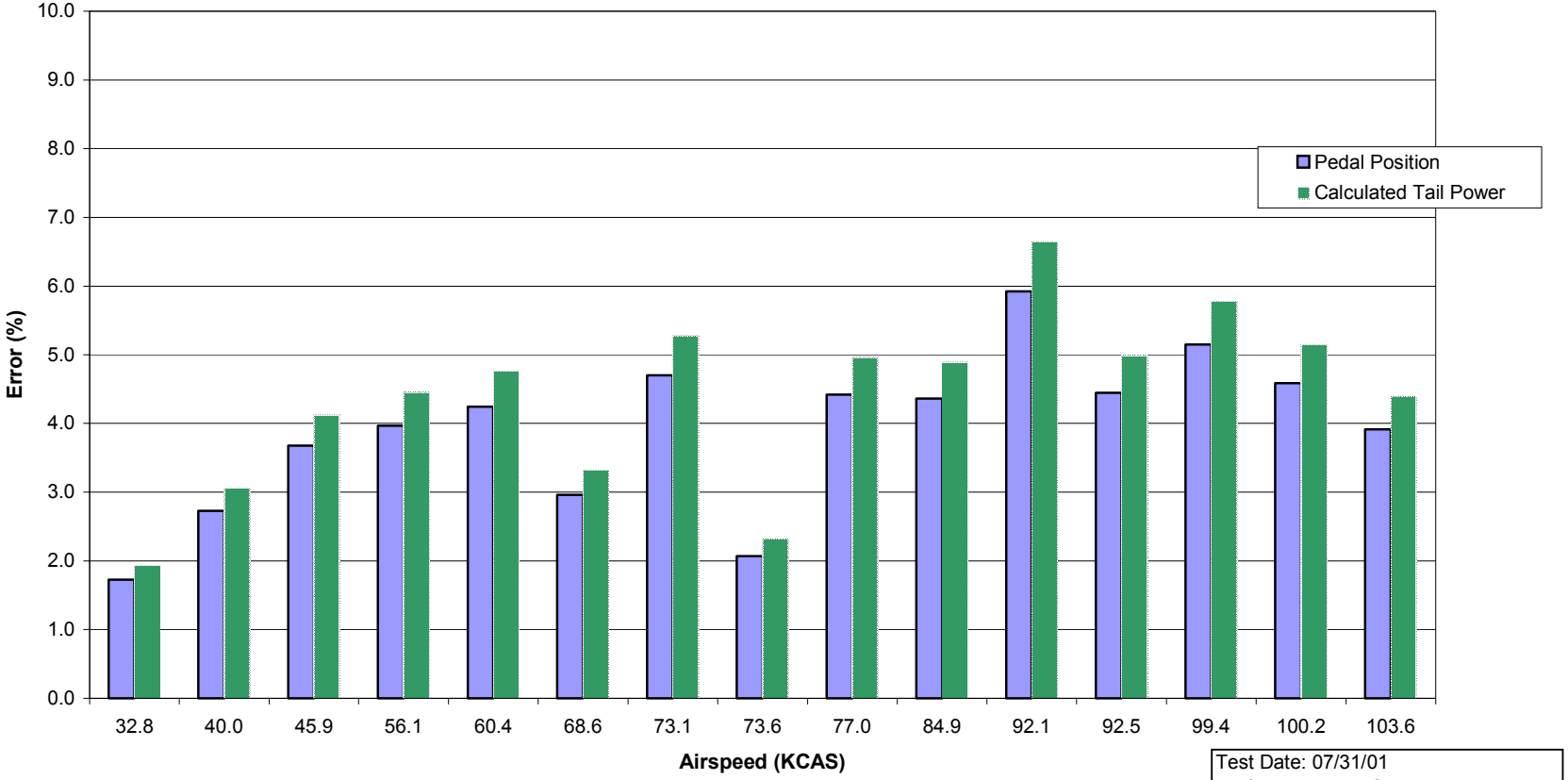

Figure D.6. Control Positions in Trimmed Forward Flight

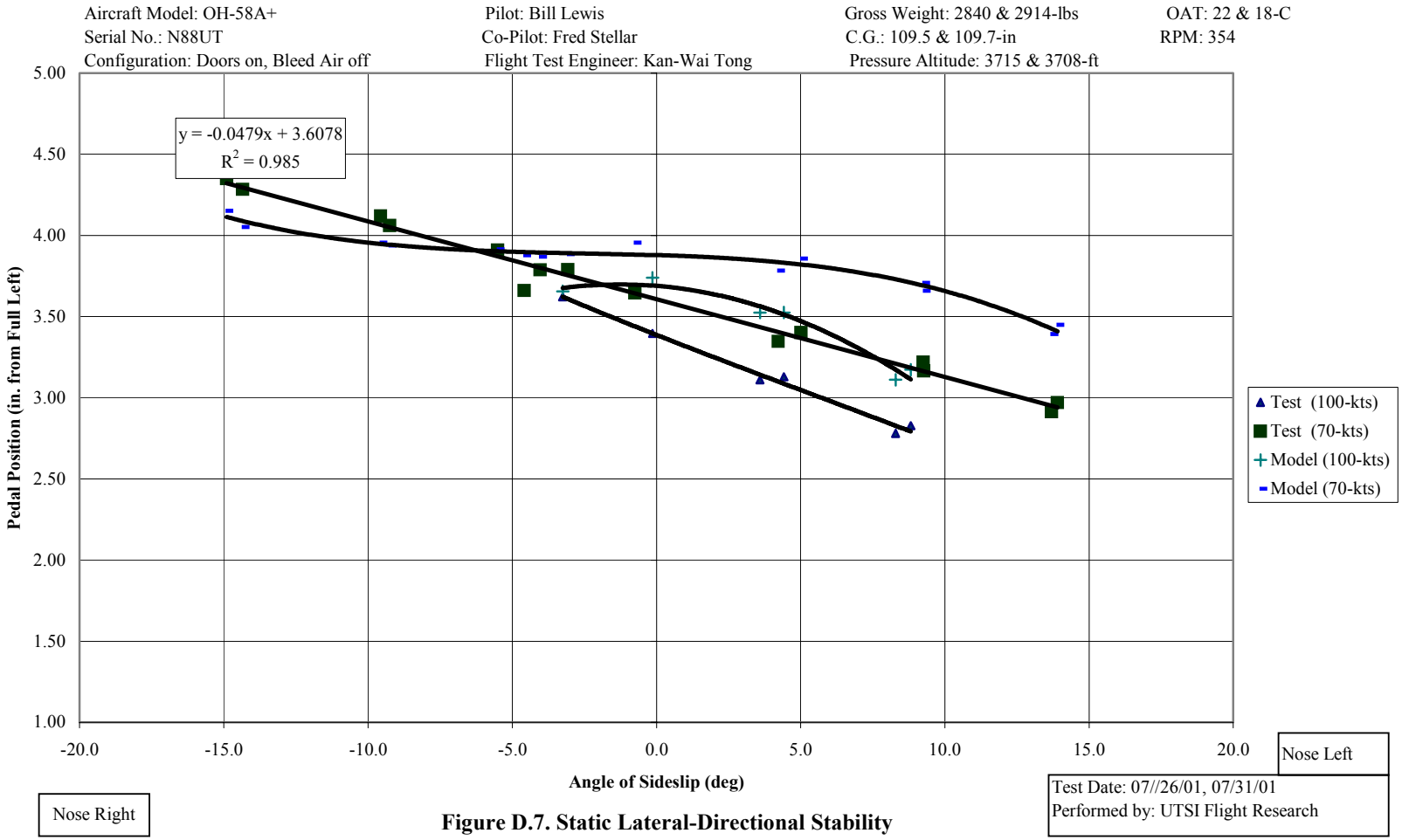

Figure D.7. Static Lateral-Directional Stability

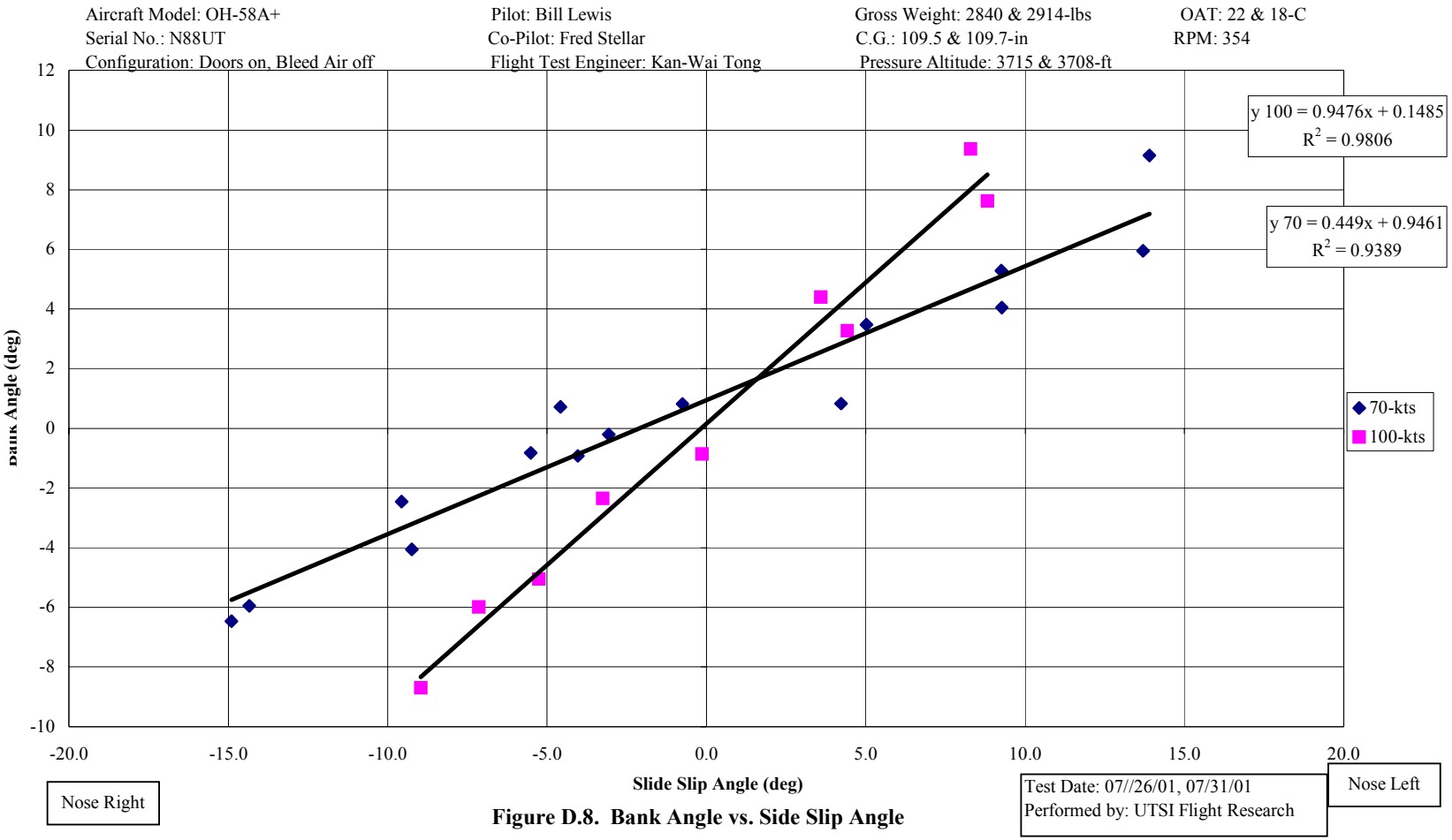

Figure D.8. Bank Angle vs. Side Slip Angle

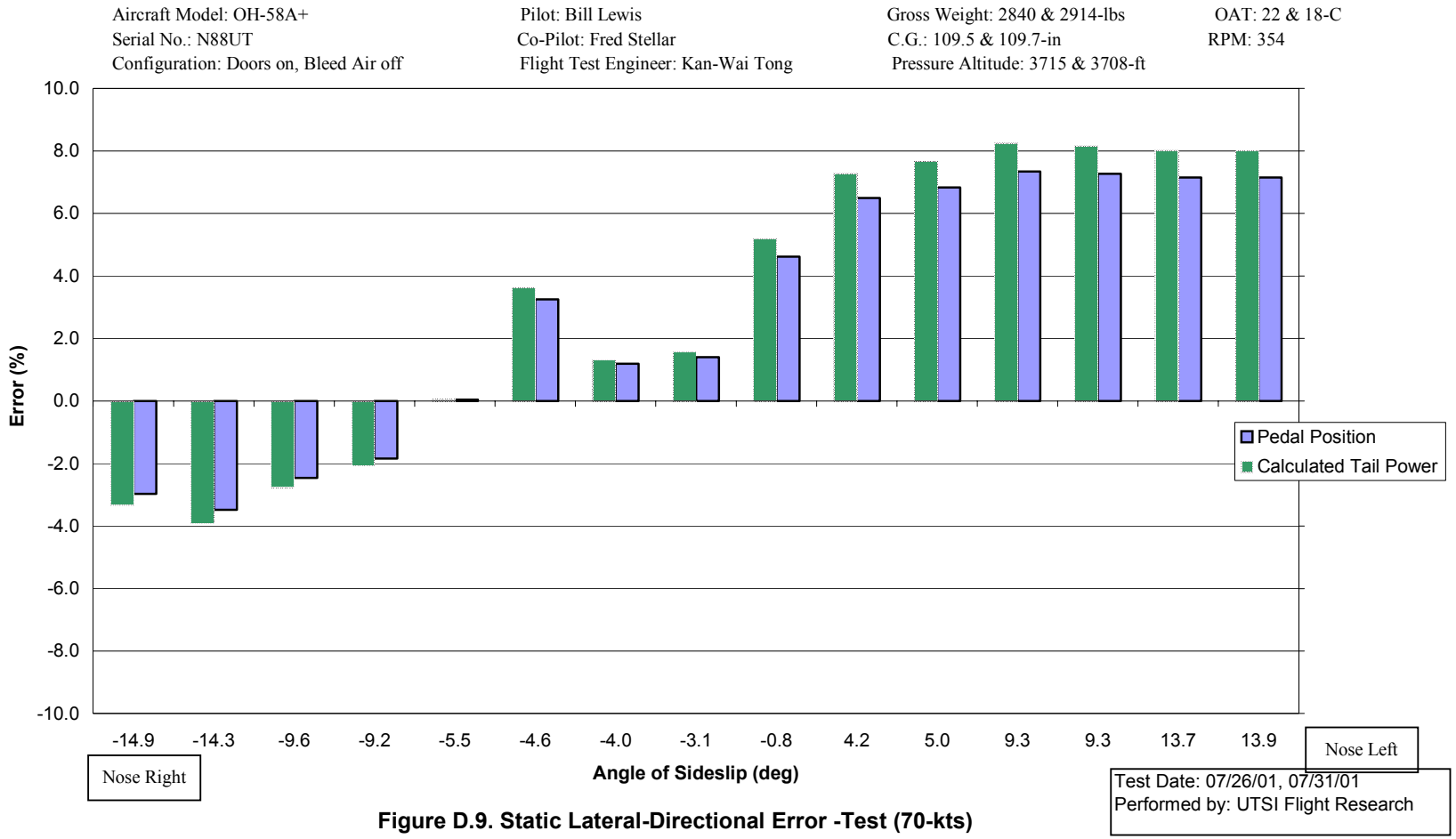

Figure D.9. Static Lateral-Directional Error -Test (70-kts)

Aircraft Model: OH-58A+ | Pilot: Bill Lewis | Gross Weight: 2840 & 2914-lbs | OAT: 22 & 18-C
Serial No.: N88UT | Co-Pilot: Fred Stellar | C.G.: 109.5 & 109.7-in | RPM: 354
Configuration: Doors on, Bleed Air off | Flight Test Engineer: Kan-Wai Tong | Pressure Altitude: 3715 & 3708-ft

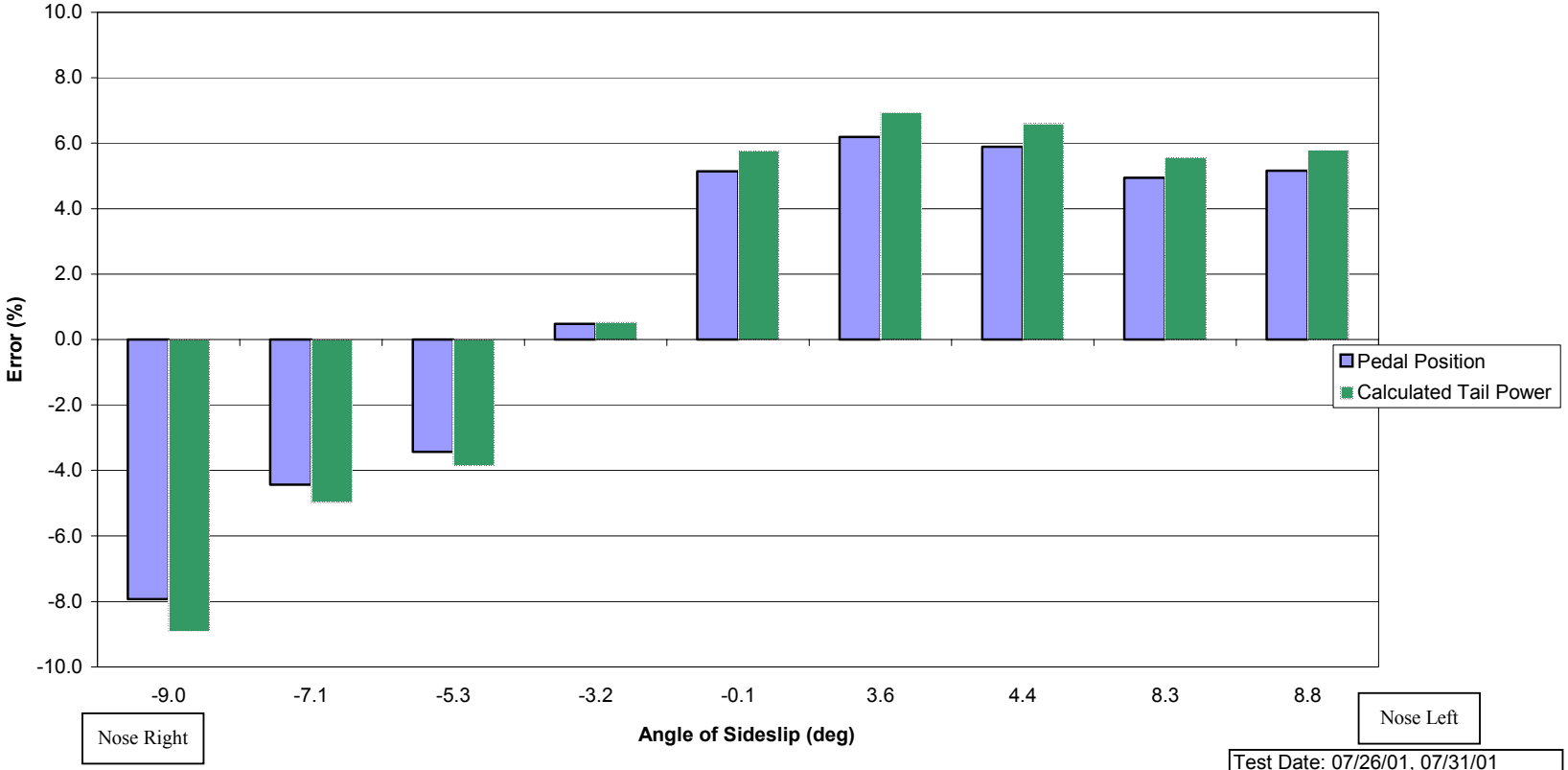

Figure D.10 Static Lateral-Directional Error - 100-kts

Test Date: 07/26/01, 07/31/01
Performed by: UTSI Flight Research

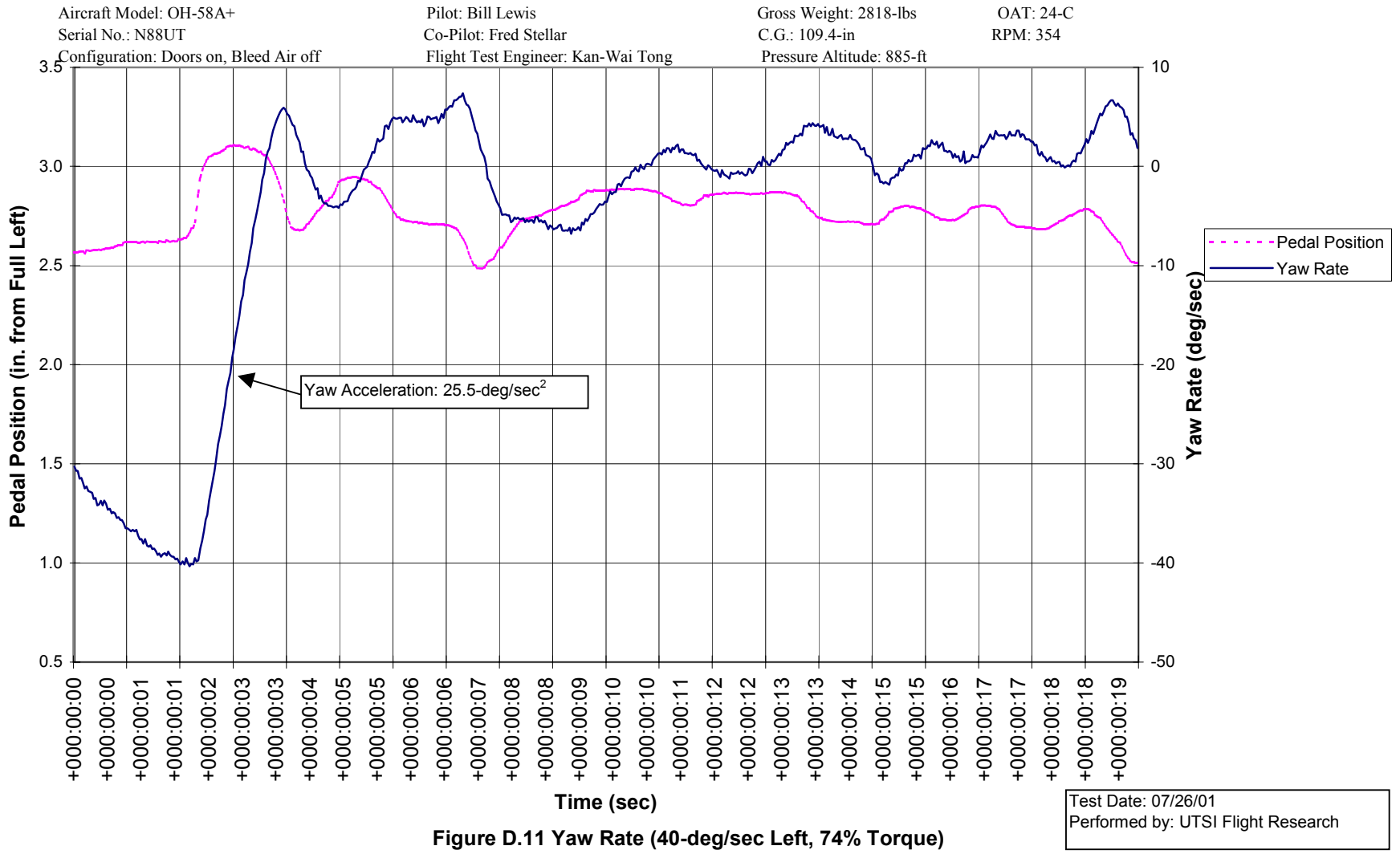

Figure D.11 Yaw Rate (40-deg/sec Left, 74% Torque)

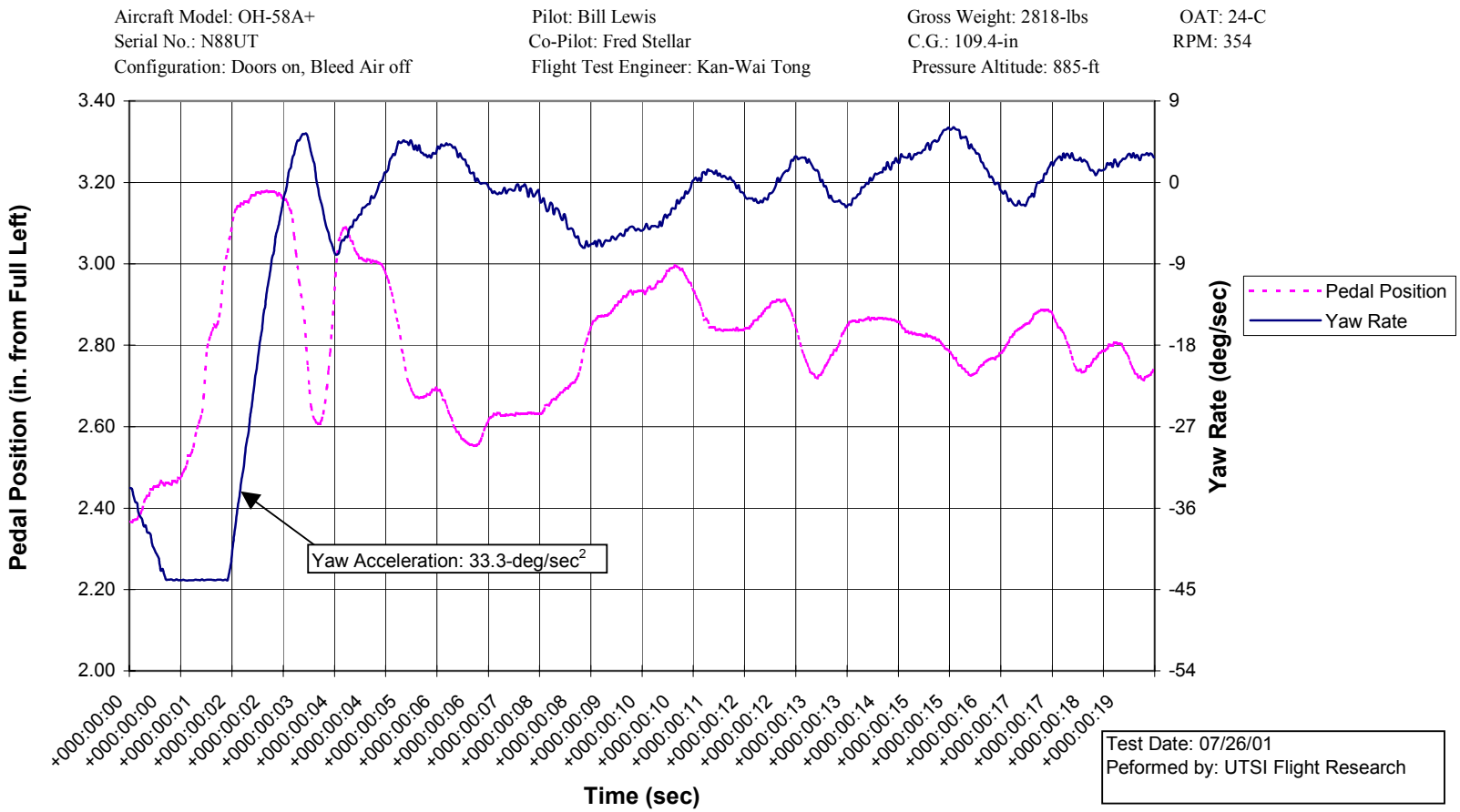

Figure D.12. Yaw Rate (44-deg/sec Left, 72.8% Engine Torque)

Aircraft Model: OH-58A+ | Pilot: Bill Lewis | Gross Weight: 2818-lbs | OAT: 24-C
Serial No.: N88UT | Co-Pilot: Fred Stellar | C.G.: 109.4-in | RPM: 354
Configuration: Doors on, Bleed Air off | Flight Test Engineer: Kan-Wai Tong | Pressure Altitude: 885-ft

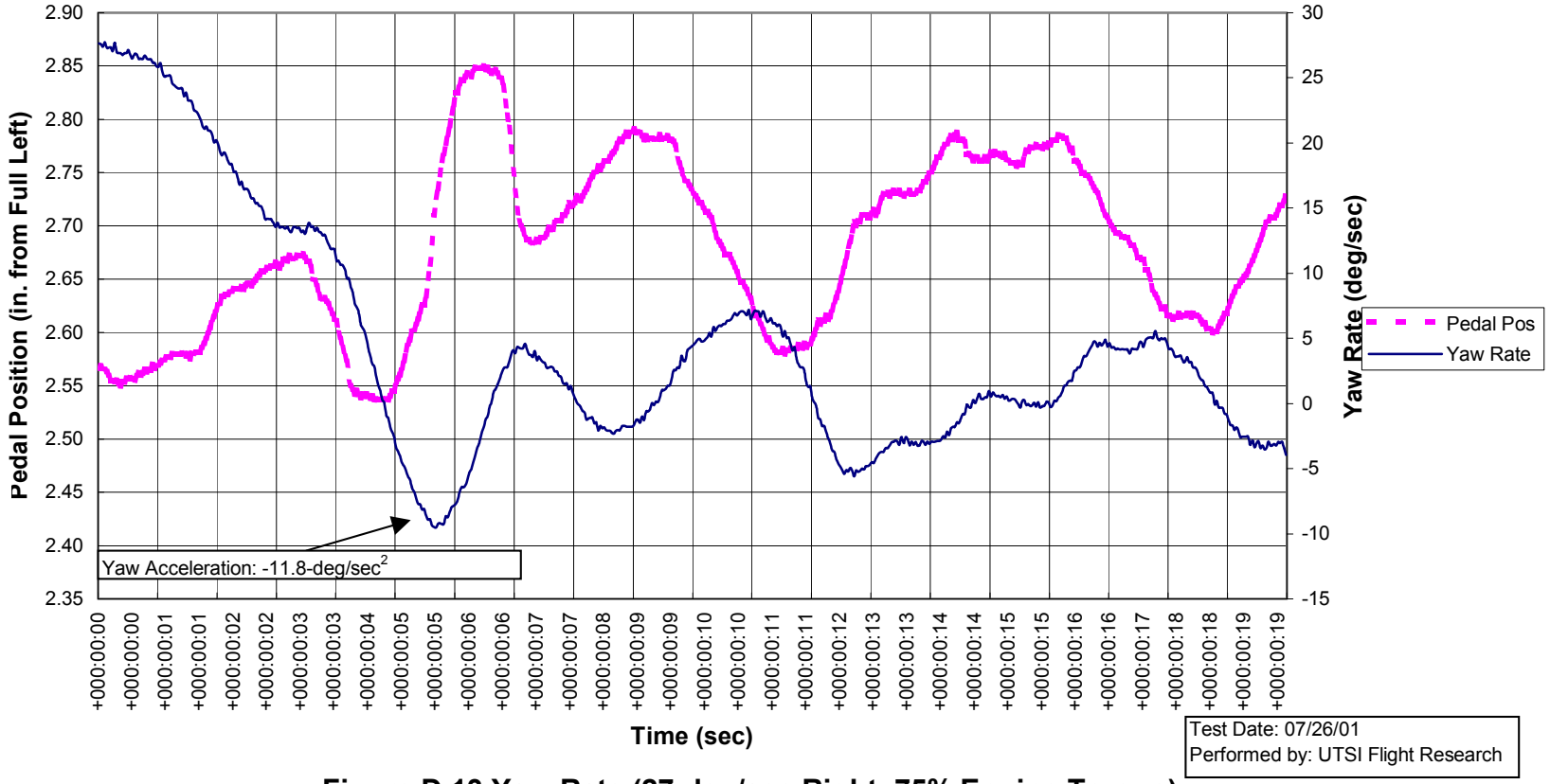

Figure D.13 Yaw Rate (27-deg/sec Right, 75% Engine Torque)

Aircraft Model: OH-58A+ | Pilot: Bill Lewis | Gross Weight: 2818-lbs | OAT: 24-C
Serial No.: N88UT | Co-Pilot: Fred Stellar | C.G.: 109.4-in | RPM: 354
Configuration: Doors on, Bleed Air off | Flight Test Engineer: Kan-Wai Tong | Pressure Altitude: 885-ft

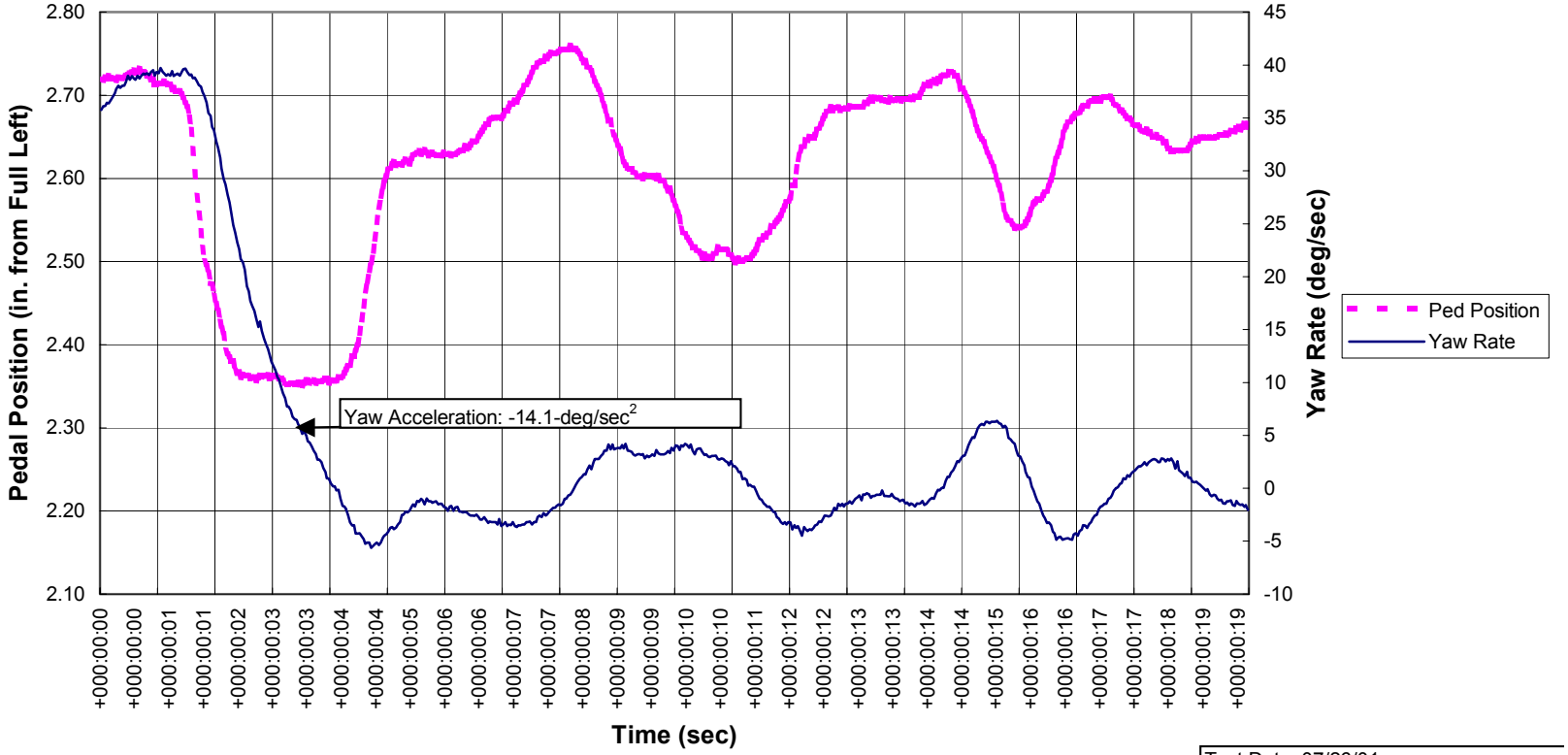

Figure D.14. Yaw Rate (38-deg/sec Right, 78% Engine Torque)

Test Date: 07/26/01
Performed by: UTSI Flight Research

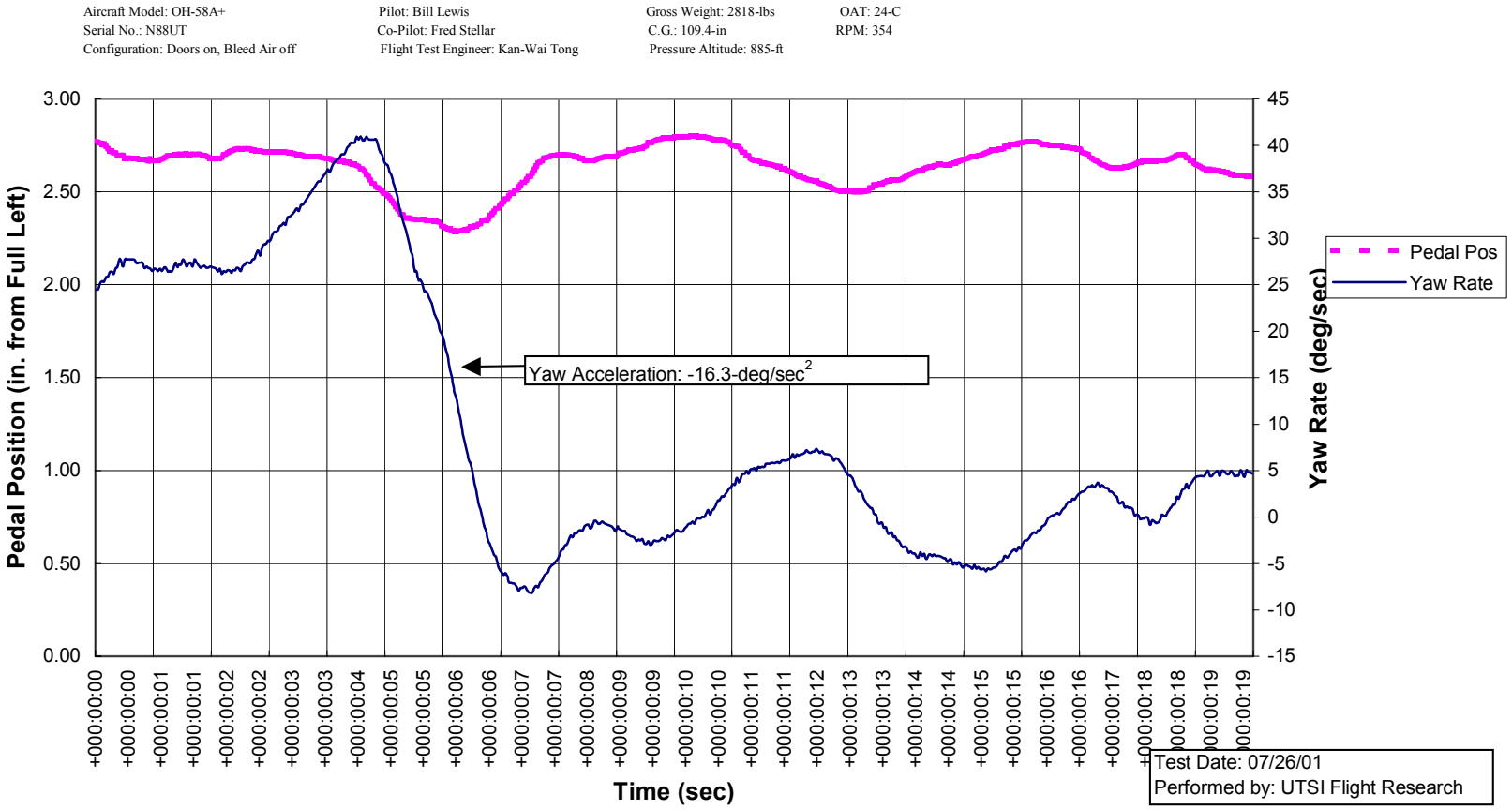

Figure D.15. Yaw Rate (40-deg/sec Right, 77% Engine Torque)

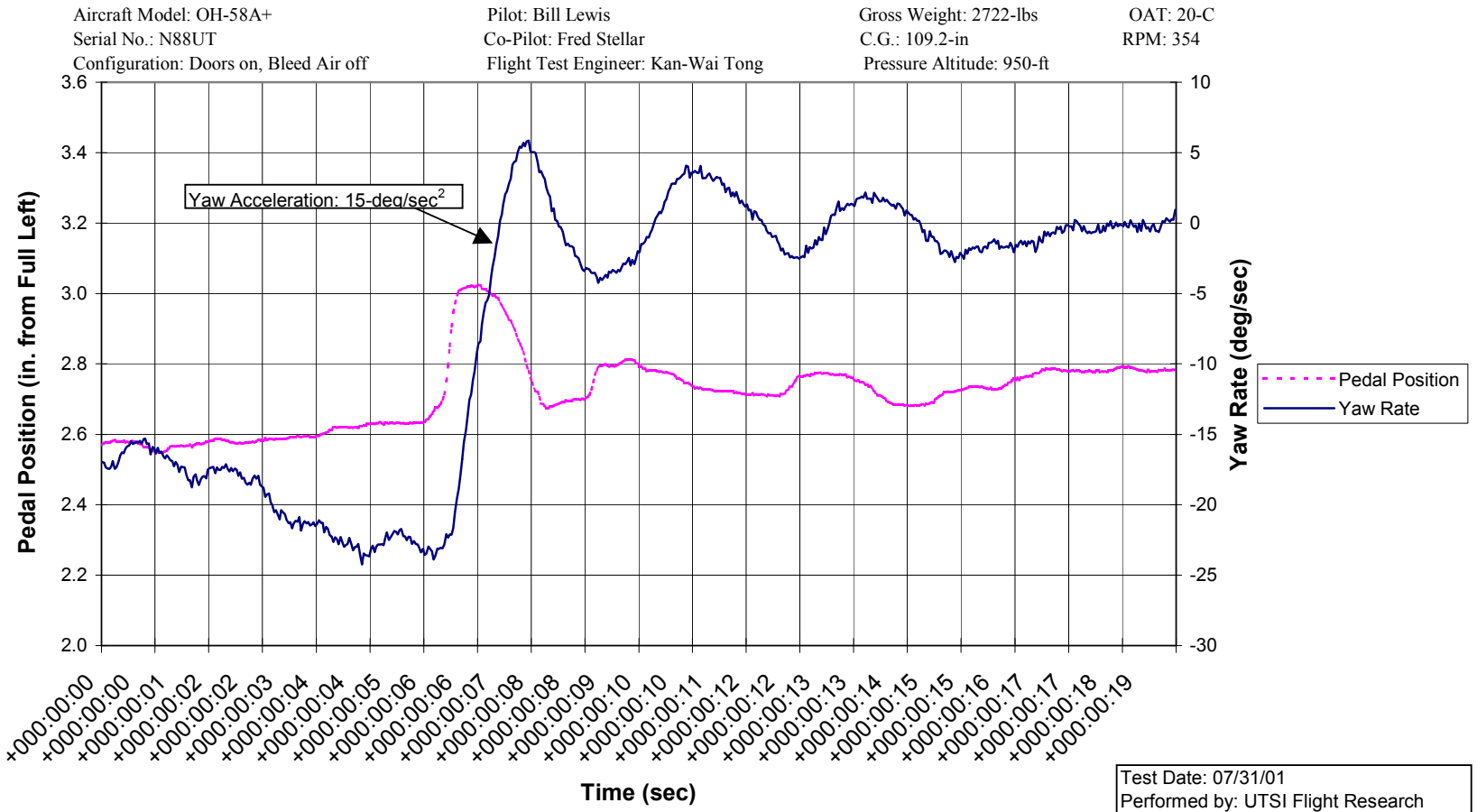

Figure D.16. Yaw Rate (24-deg/sec Left, 72% Engine Torque)

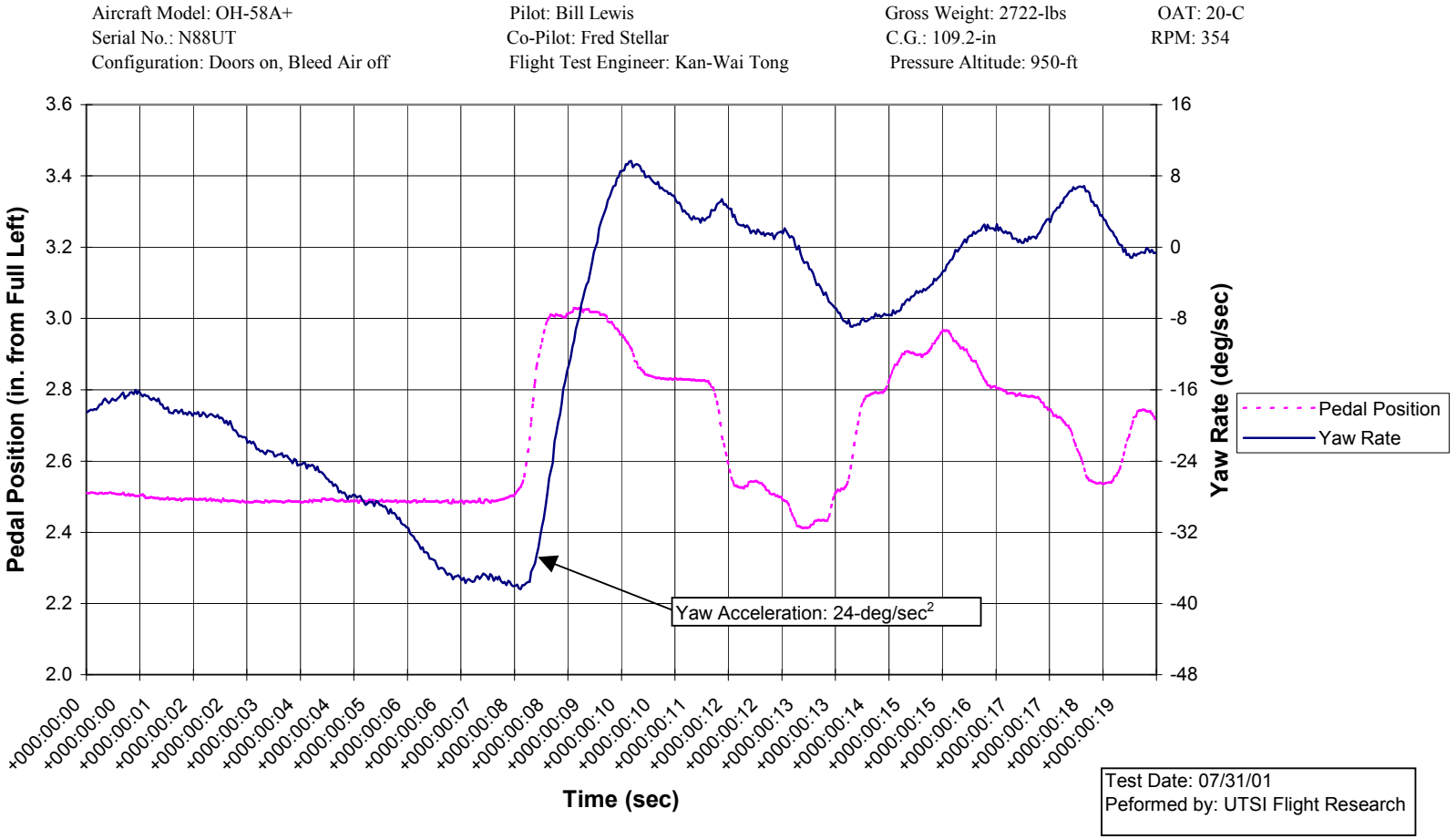

Figure D.17. Yaw Rate (18-deg/sec Left, 73% Engine Torque)

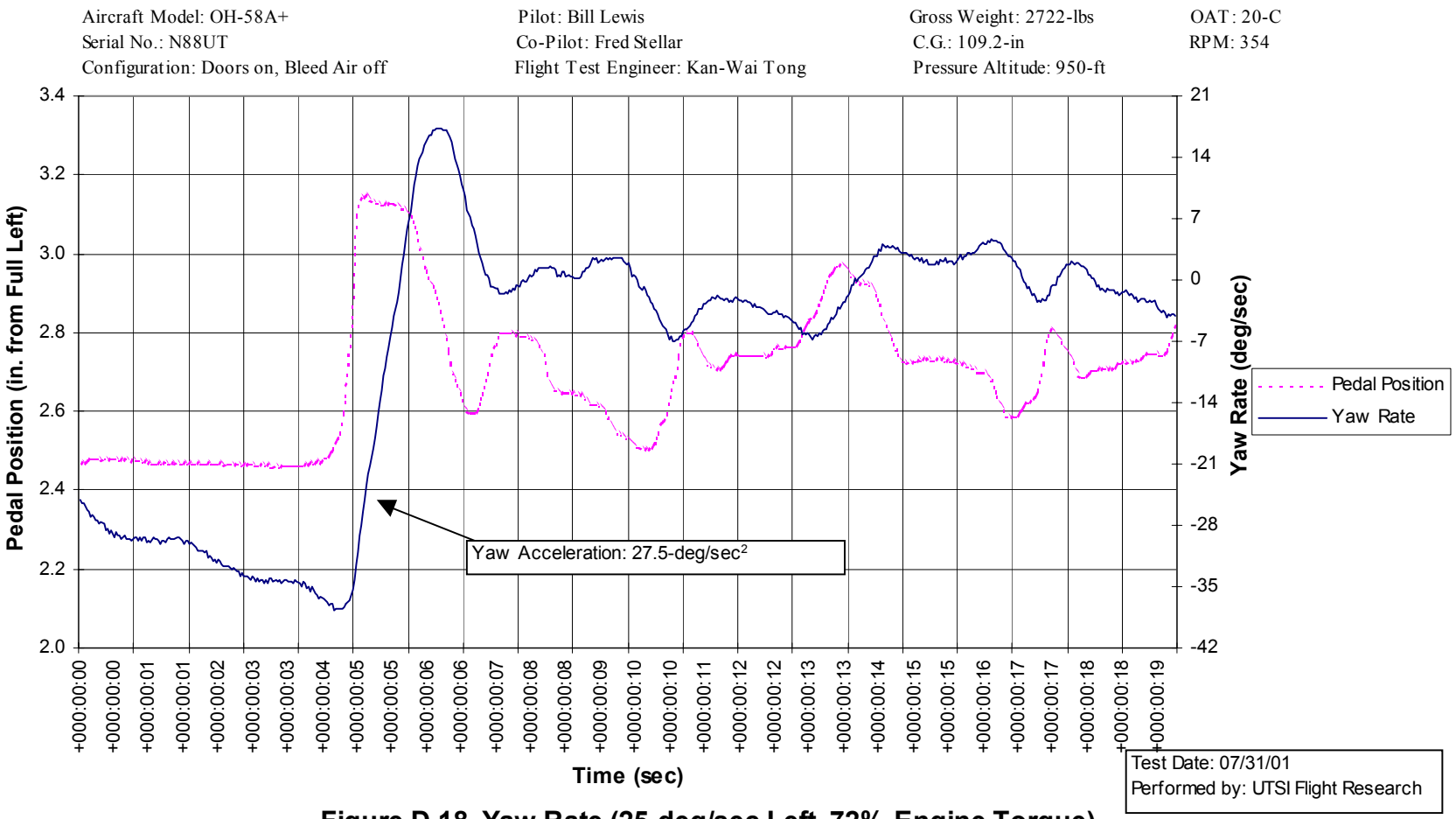

Figure D.18. Yaw Rate (25-deg/sec Left, 72% Engine Torque)

Aircraft Model: OH-58A+
Serial No.: N88UT
Configuration: Doors on, Bleed Air off

Pilot: Bill Lewis
Co-Pilot: Fred Stellar
Flight Test Engineer: Kan-Wai Tong

Gross Weight: 2722-lbs
C.G.: 109.2-in
Pressure Altitude: 950-ft

OAT: 20-C
RPM: 354

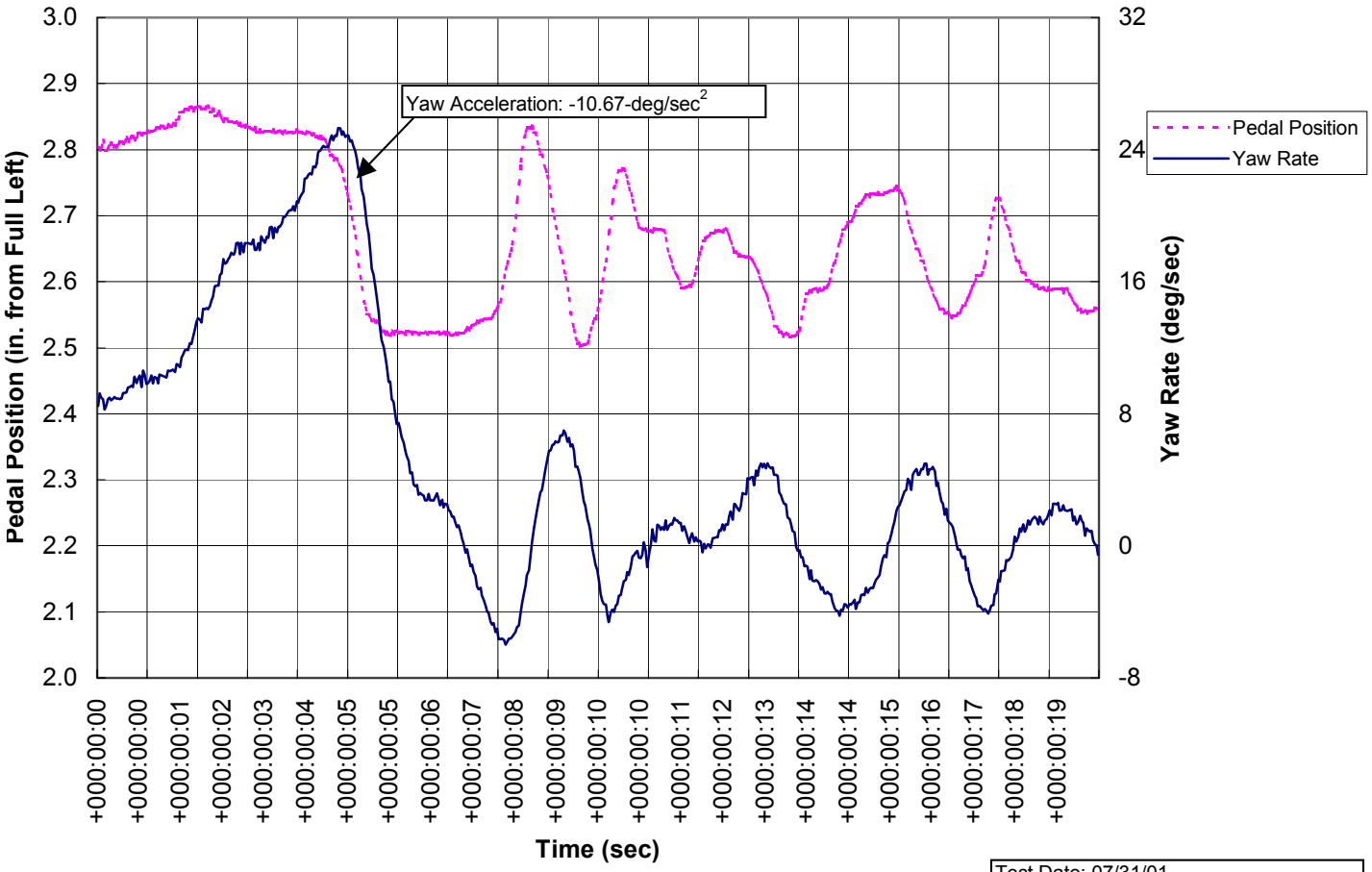

Test Date: 07/31/01
Performed by: UTSI Flight Research

Figure D.19. Yaw Rate (25-deg/sec Right, 74% Engine Torque)

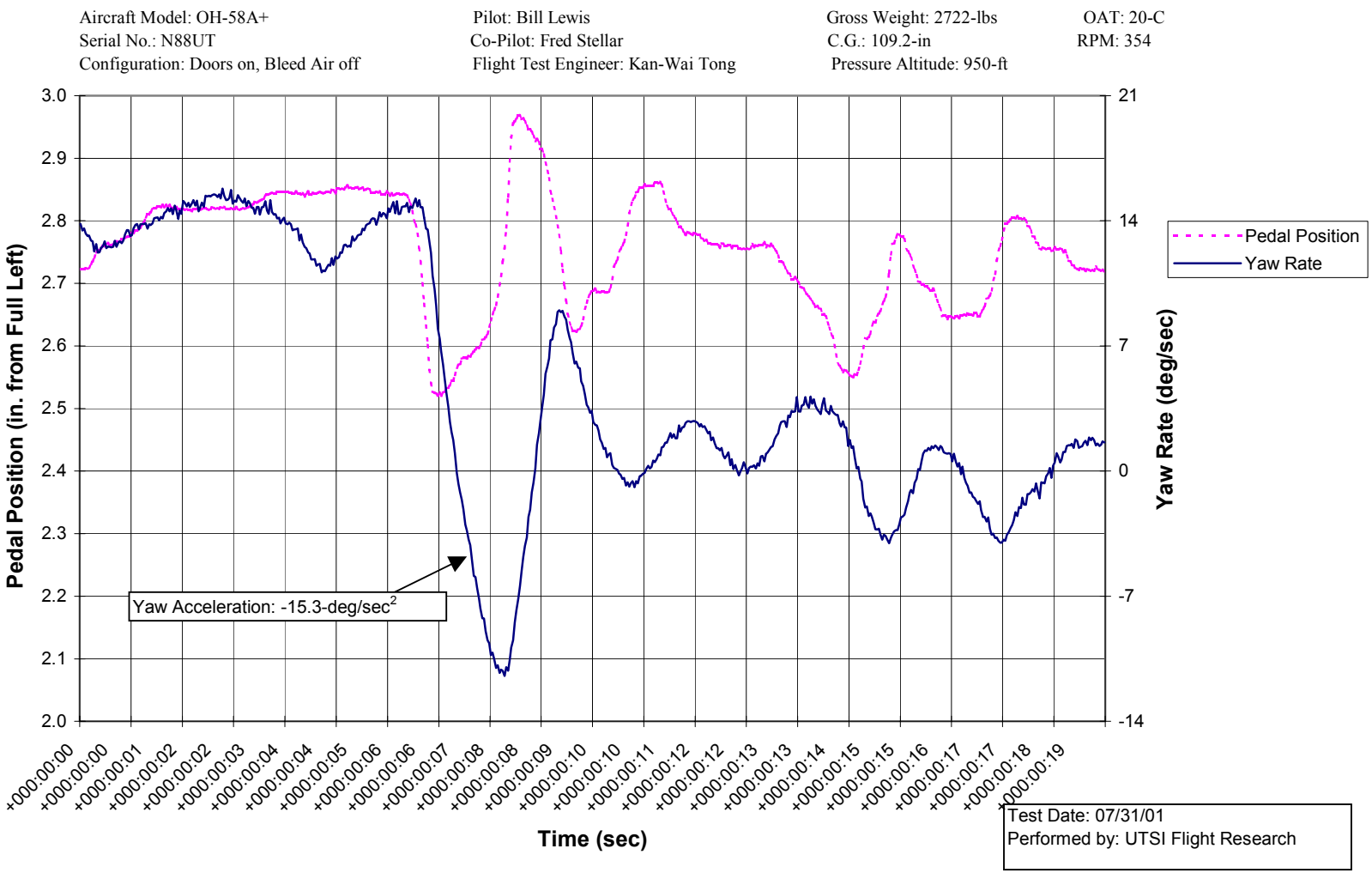

Figure D.20. Yaw Rate (15-deg/sec Right, 72% Engine Torque)

Aircraft Model: OH-58A+ | Pilot: Bill Lewis | Gross Weight: 2722-lbs | OAT: 20-C
Serial No.: N88UT | Co-Pilot: Fred Stellar | C.G.: 109.2-in | RPM: 354
Configuration: Doors on, Bleed Air off | Flight Test Engineer: Kan-Wai Tong | Pressure Altitude: 950-ft

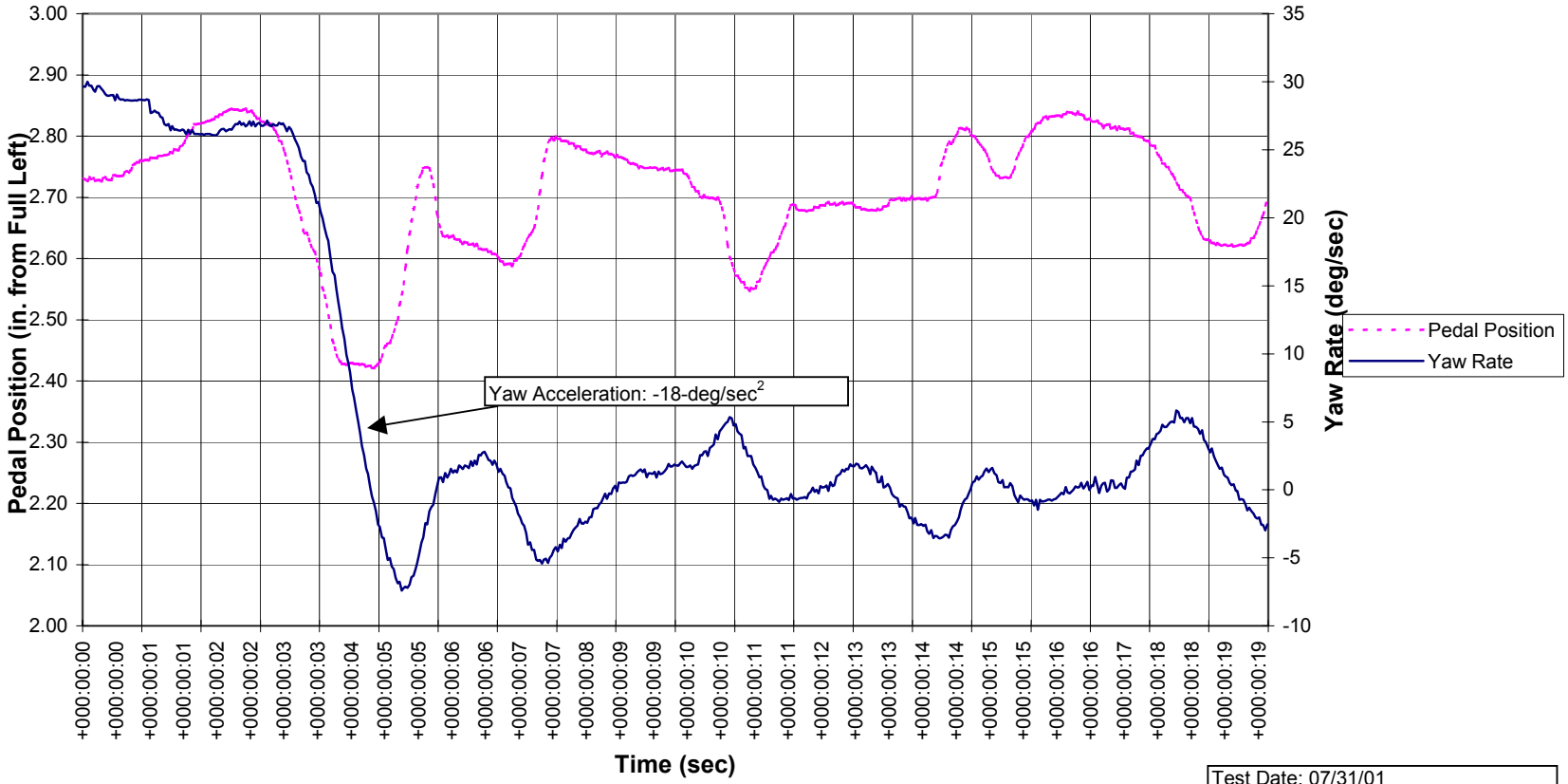

Test Date: 07/31/01
Performed by: UTSI Flight Research

Figure D.21. Yaw Rate (30-deg/sec Right, 72% Engine Torque)

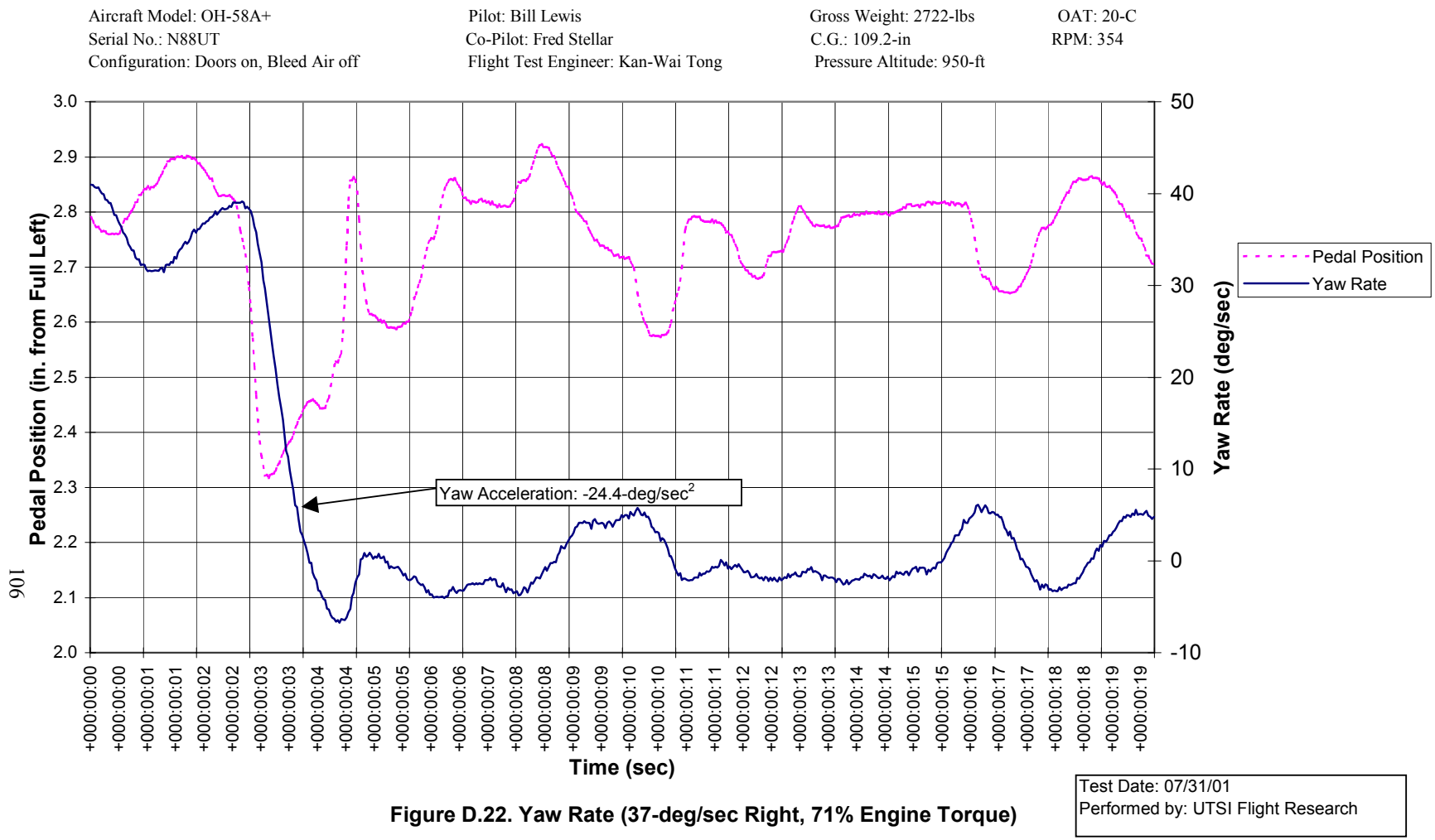

Figure D.22. Yaw Rate (37-deg/sec Right, 71% Engine Torque)

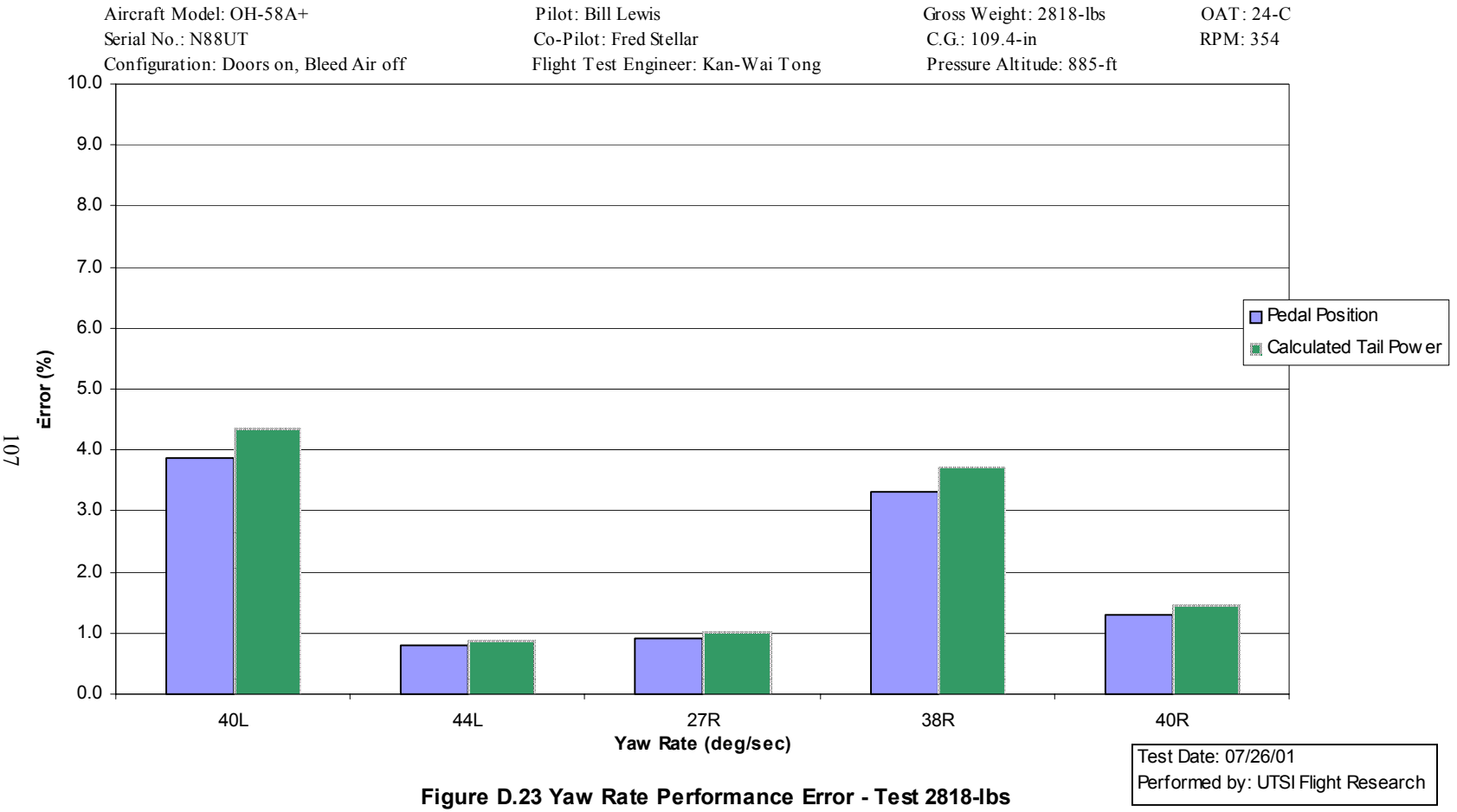

Figure D.23 Yaw Rate Performance Error - Test 2818-lbs

Aircraft Model: OH-58A+ | Pilot: Bill Lewis | Gross Weight: 2722-lbs | OAT: 20-C
Serial No.: N88UT | Co-Pilot: Fred Stellar | C.G.: 109.2-in | RPM: 354
Configuration: Doors on, Bleed Air off | Flight Test Engineer: Kan-Wai Tong | Pressure Altitude: 950-ft

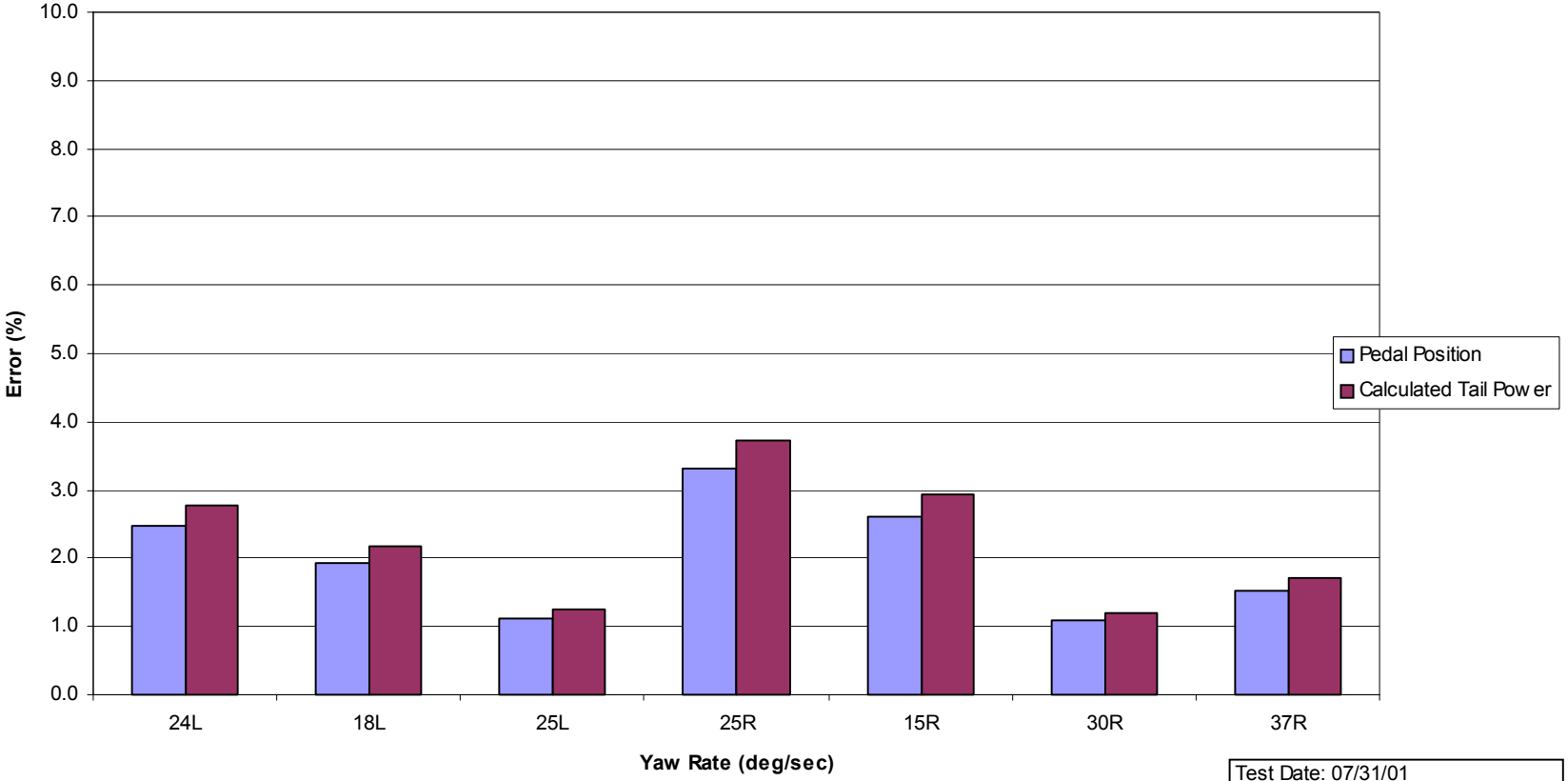

Figure D.24. Yaw Rate Performance Error - Test 2722-lbs

Aircraft Model: OH-58A+ | Pilot: Bill Lewis | Gross Weight: 2816-lbs | OAT: 24-C
Serial No.: N88UT | Co-Pilot: Fred Stellar | C.G.: 109.4-in | RPM: 354
Configuration: Doors on, Bleed Air off | Flight Test Engineer: Kan-Wai Tong | Pressure Altitude: 885-ft

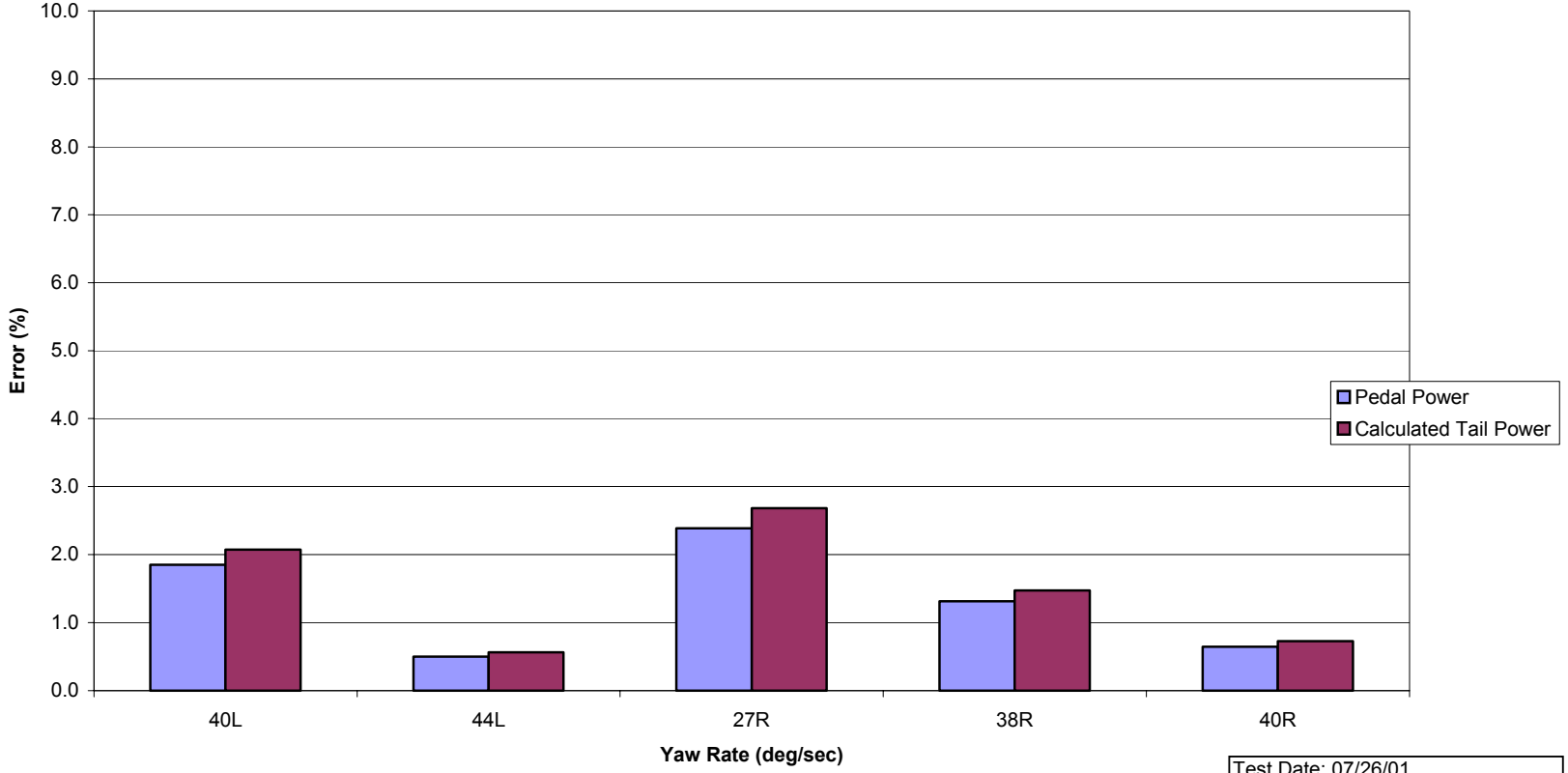

Test Date: 07/26/01
Performed by: UTSI Flight Research

Figure D.25. Deceleration Recovery Performance Error - Test 2816-lbs

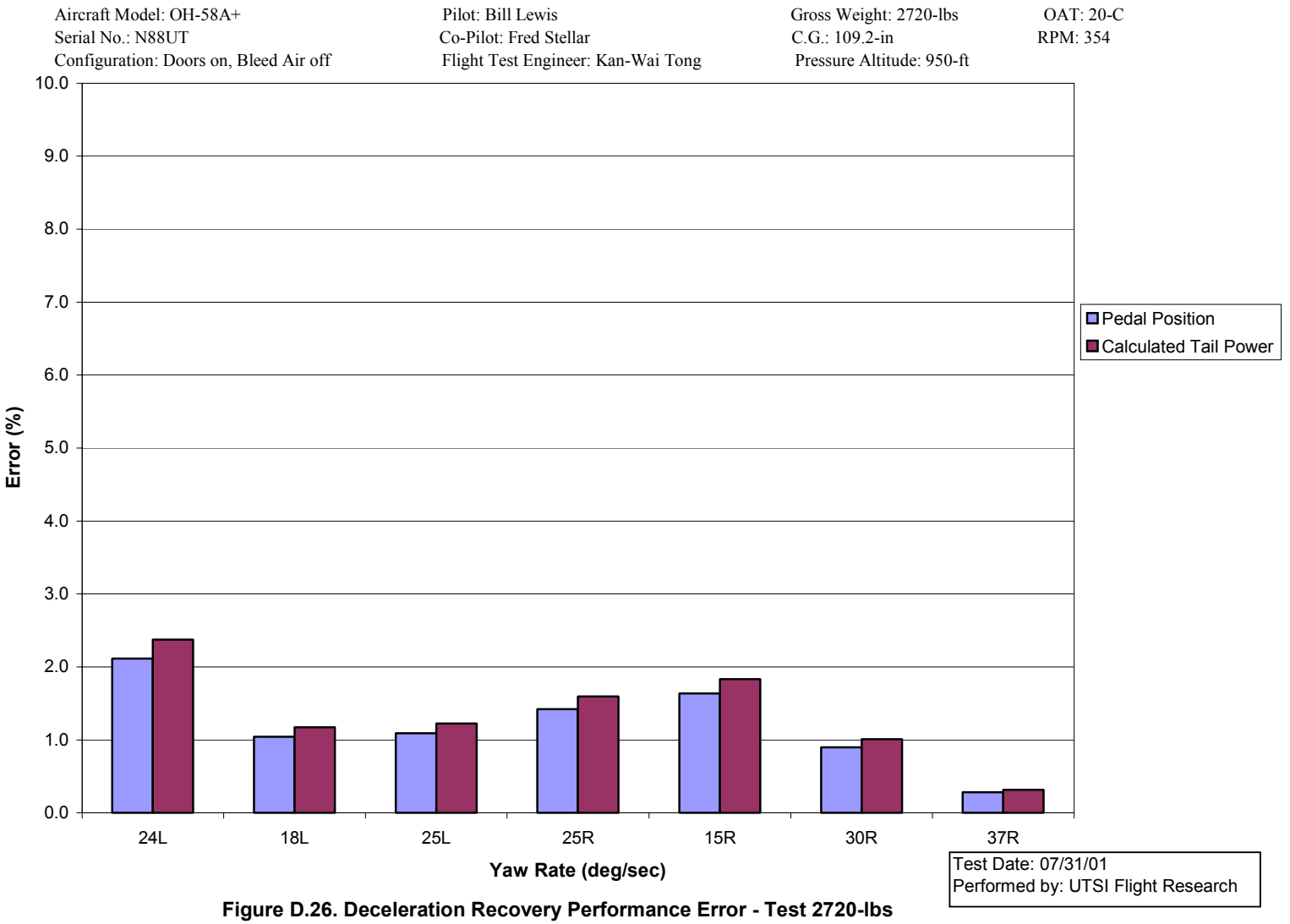

Figure D.26. Deceleration Recovery Performance Error - Test 2720-lbs

Aircraft Model: OH-58A+
Serial No.: N88UT
Configuration: Doors on, Bleed Air off

Pilot: Bill Lewis
Co-Pilot: Fred Stellar
Flight Test Engineer: Kan-Wai Tong

Gross Weight: 2830-lbs
C.G.: 109.4-in
Pressure Altitude: 880-ft

OAT: 24-C
RPM: 354

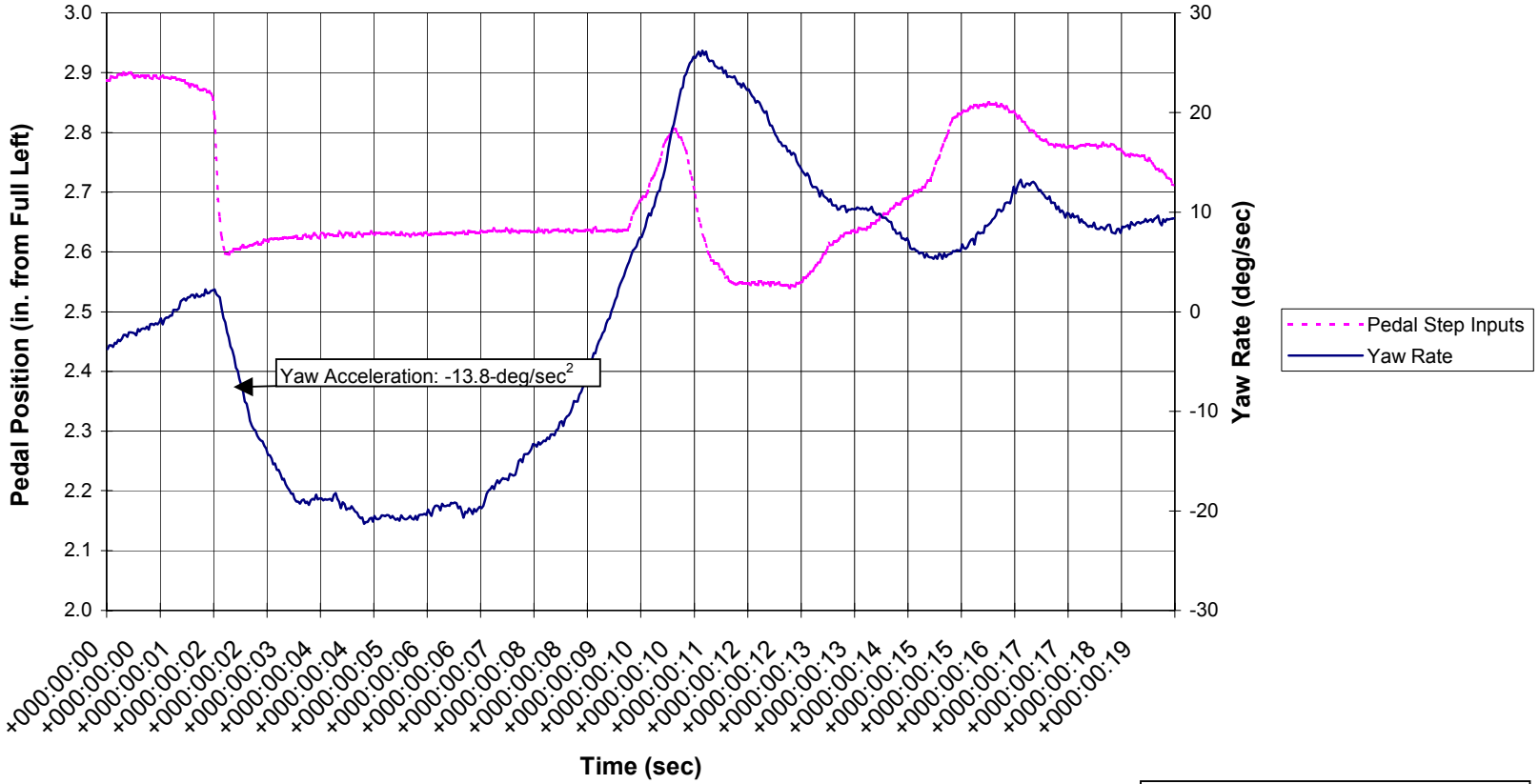

Figure D.27. Step Input (0.25-in Left, 72% Engine Torque)

Test Date: 07/26/01
Performed by: UTSI Flight Research

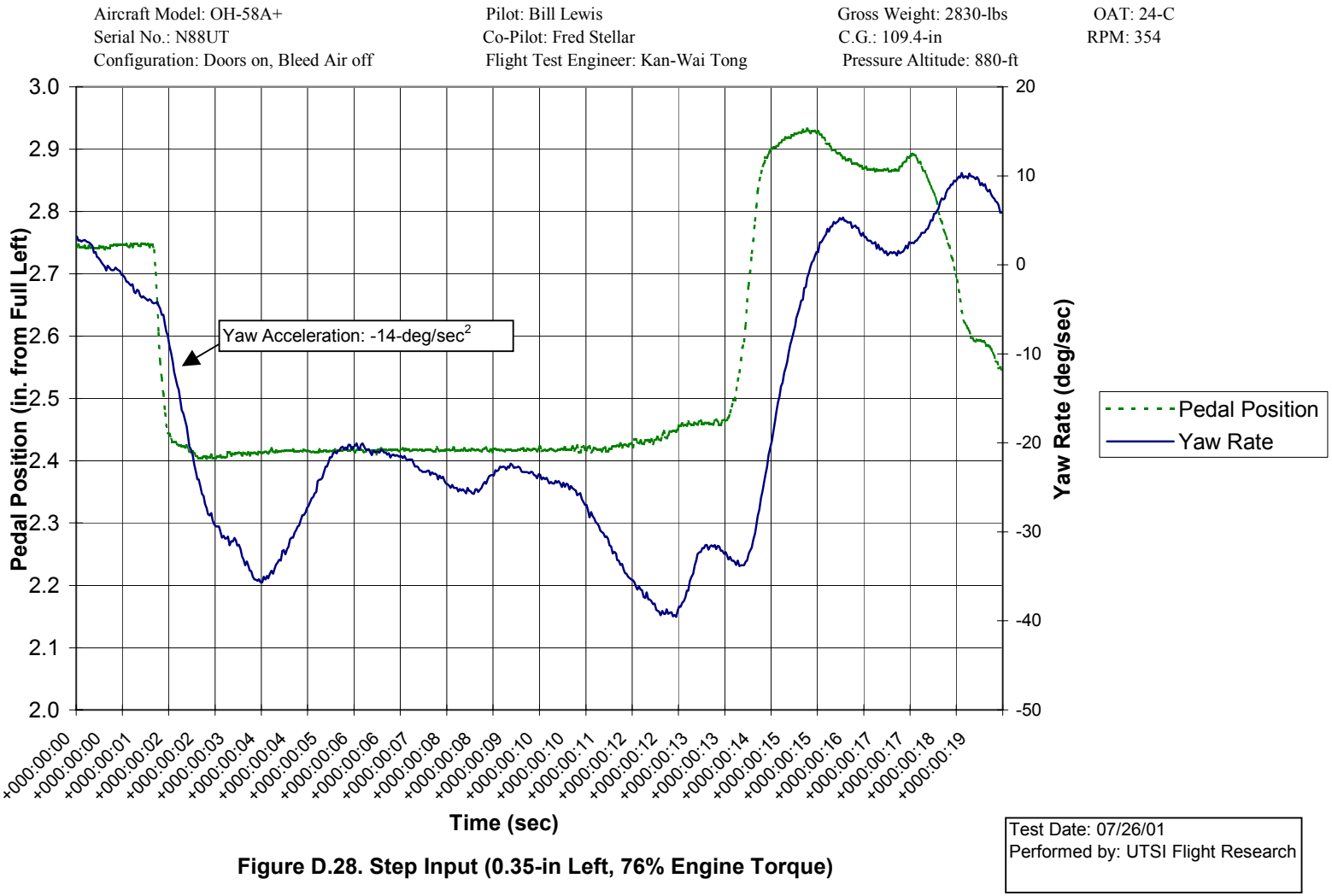

Figure D.28. Step Input (0.35-in Left, 76% Engine Torque)

Aircraft Model: OH-58A+ | Pilot: Bill Lewis | Gross Weight: 2830-lbs | OAT: 24-C
Serial No.: N88UT | Co-Pilot: Fred Stellar | C.G.: 109.4-in | RPM: 354
Configuration: Doors on, Bleed Air off | Flight Test Engineer: Kan-Wai Tong | Pressure Altitude: 880-ft

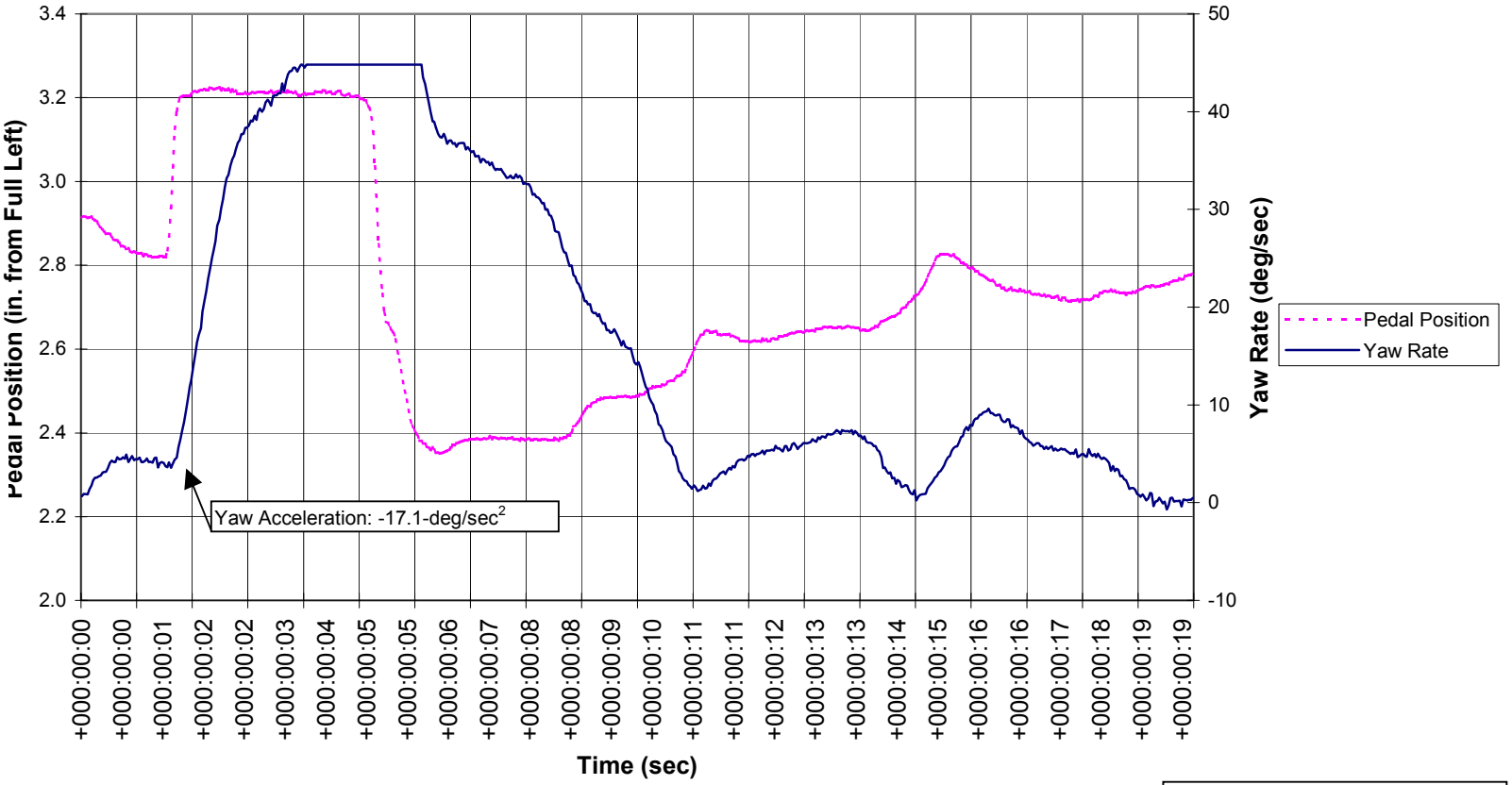

Figure D.29. Step Input (0.25-in Right, 74% Engine Torque)

Test Date: 07/26/01
Performed by: UTSI Flight Research

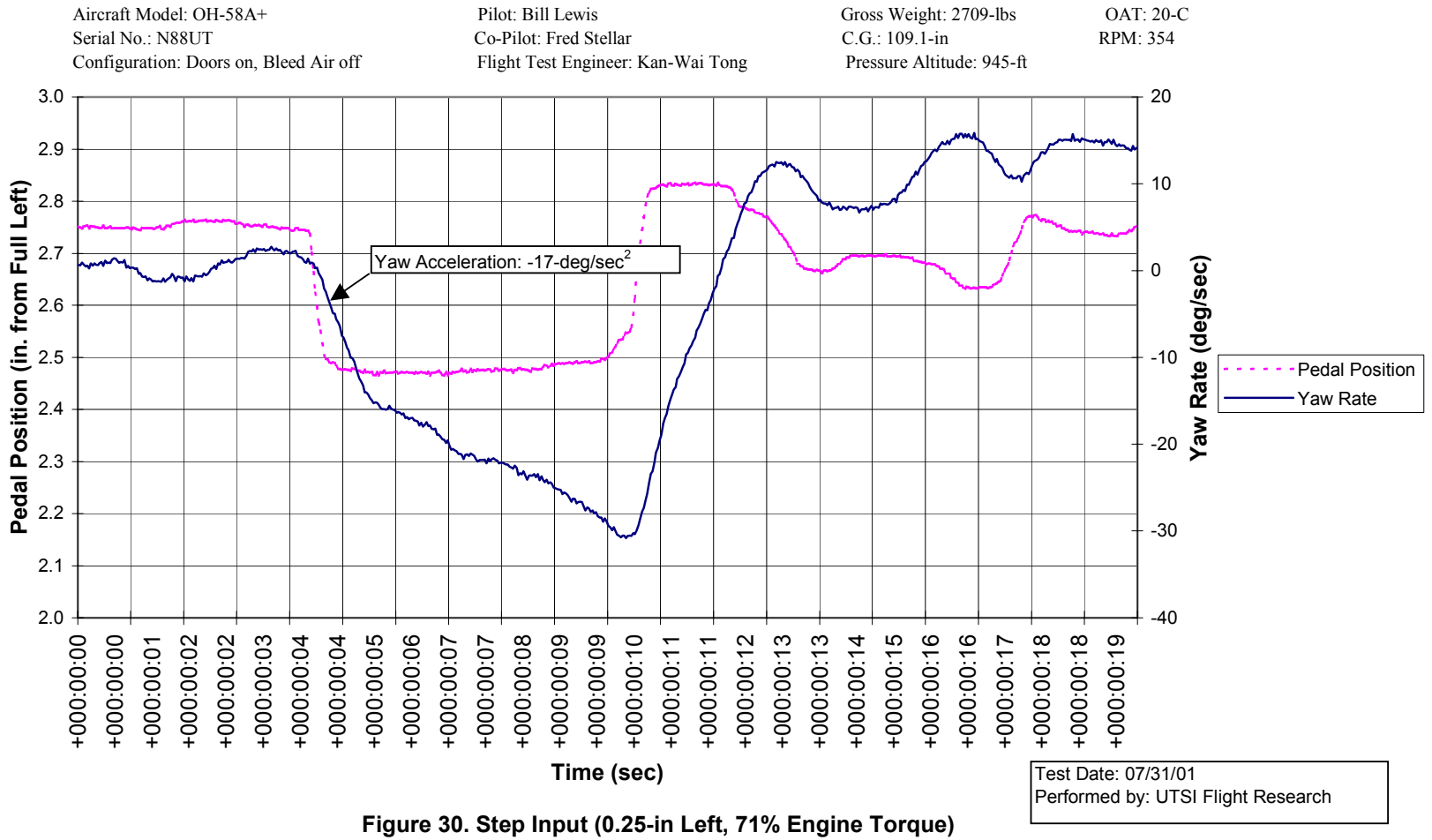

Figure 30. Step Input (0.25-in Left, 71% Engine Torque)

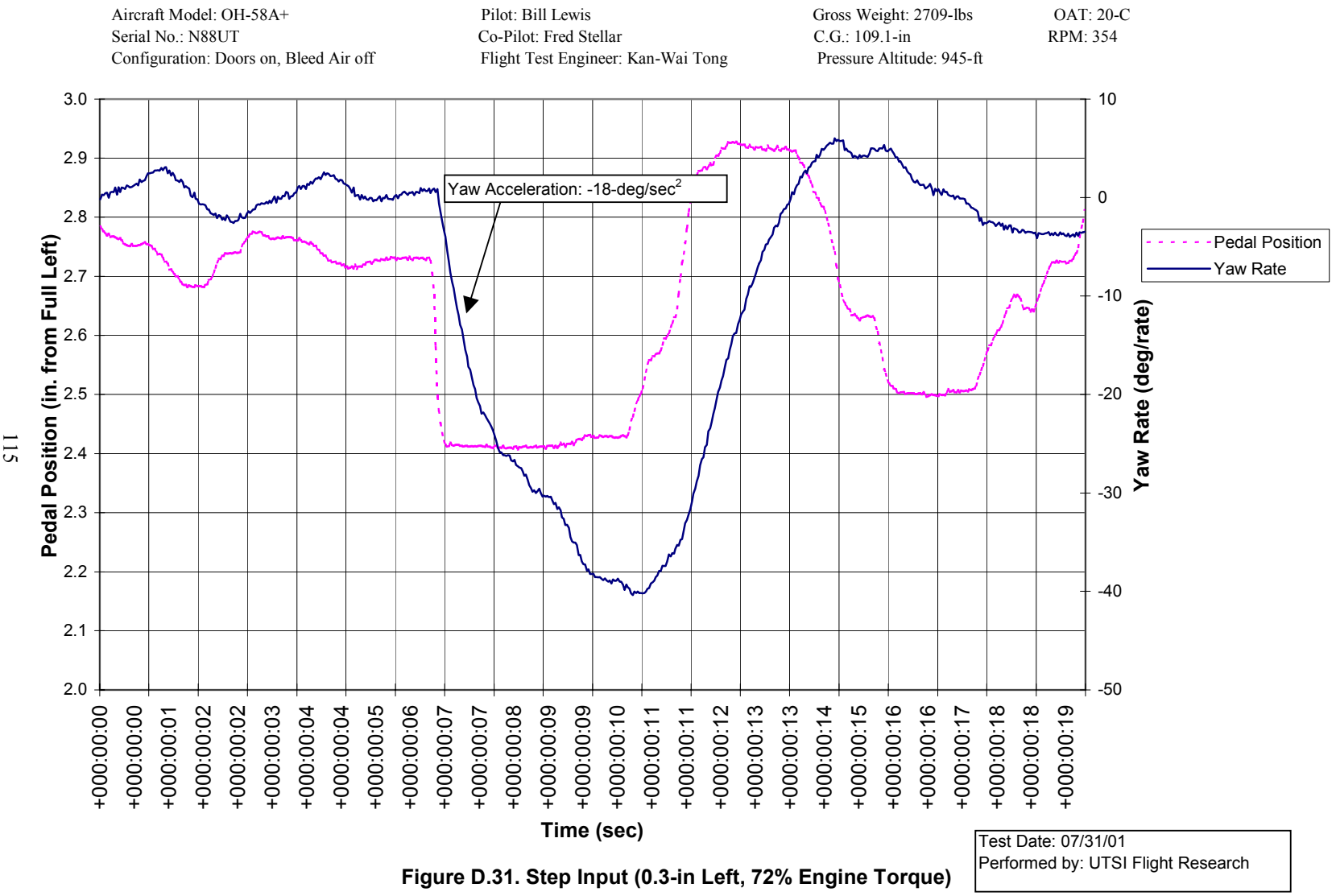

Figure D.31. Step Input (0.3-in Left, 72% Engine Torque)

Aircraft Model: OH-58A+ | Pilot: Bill Lewis | Gross Weight: 2725-lbs | OAT: 24-C
Serial No.: N88UT | Co-Pilot: Fred Stellar | C.G.: 109.4-in | RPM: 354
Configuration: Doors on, Bleed Air off | Flight Test Engineer: Kan-Wai Tong | Pressure Altitude: 891-ft

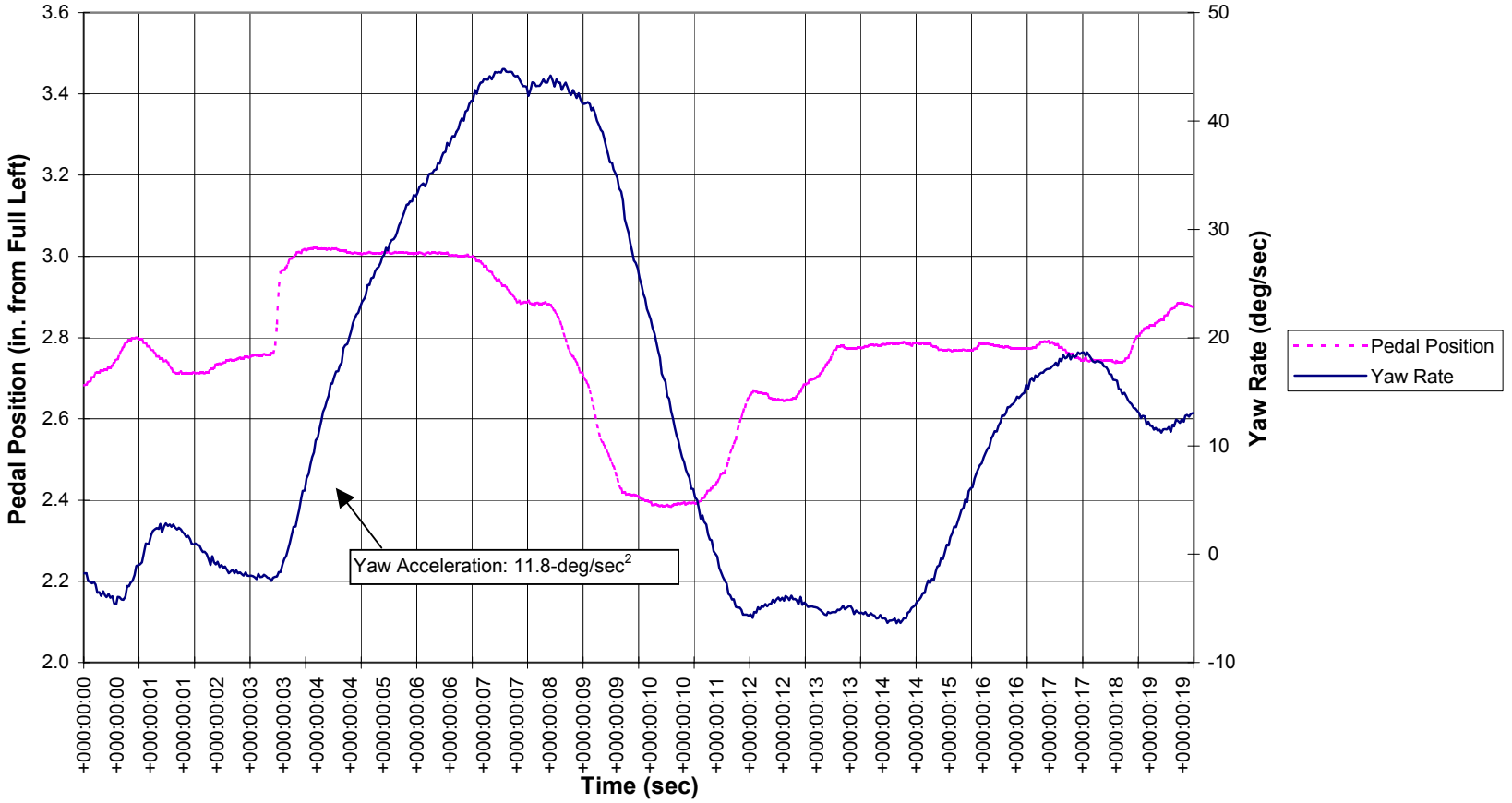

Figure D.32. Step Input (0.25-in Right, 71% Engine Torque)

Test Date: 07/31/01
Performed by: UTSI Flight Research

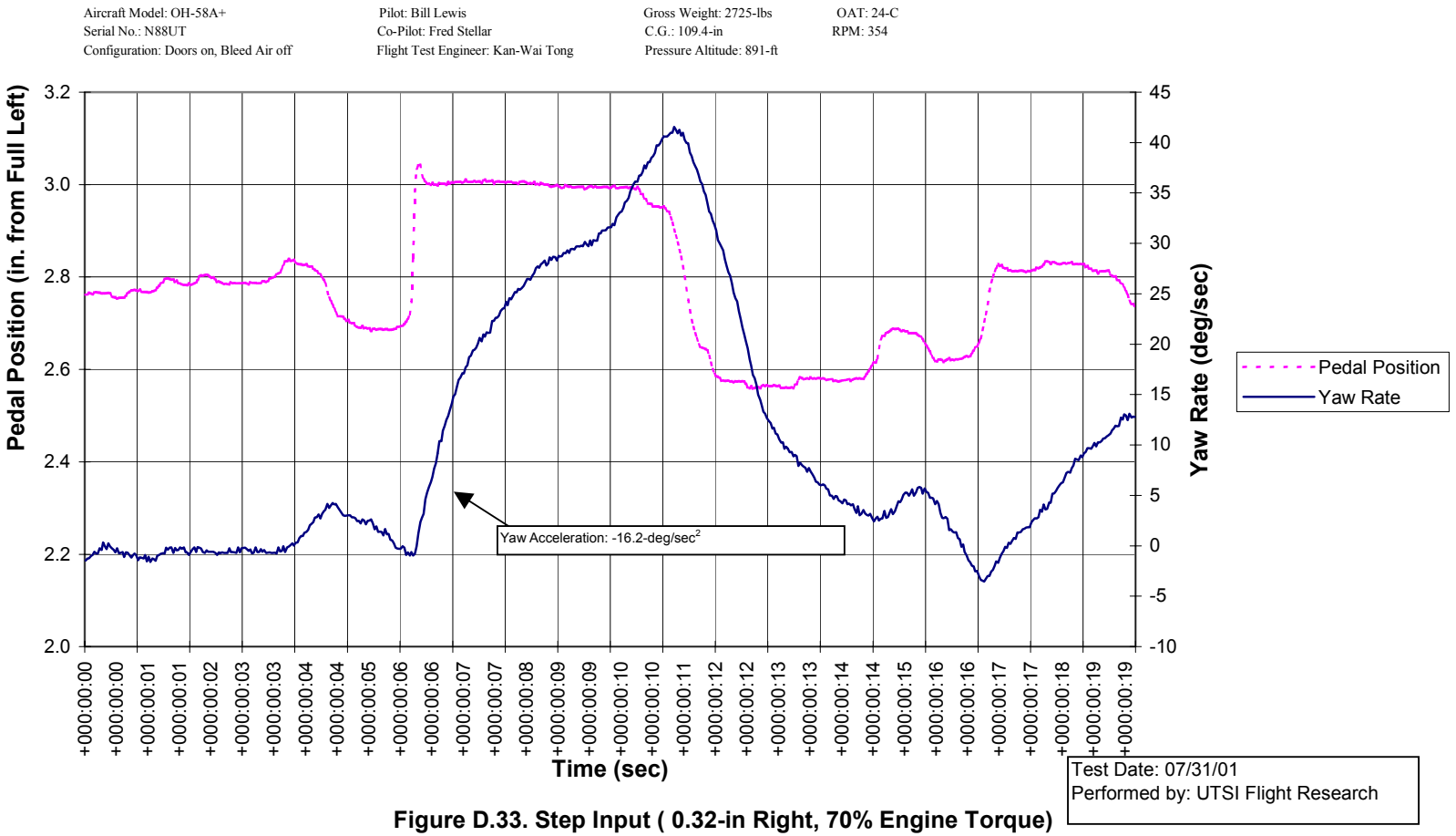

Figure D.33. Step Input (0.32-in Right, 70% Engine Torque)

Aircraft Model: OH-58A+ | Pilot: Bill Lewis | Gross Weight: 2830-lbs | OAT: 24-C
Serial No.: N88UT | Co-Pilot: Fred Stellar | C.G.: 109.4-in | RPM: 354
Configuration: Doors on, Bleed Air off | Flight Test Engineer: Kan-Wai Tong | Pressure Altitude: 880-ft | Engine Torque: 74- 76-%

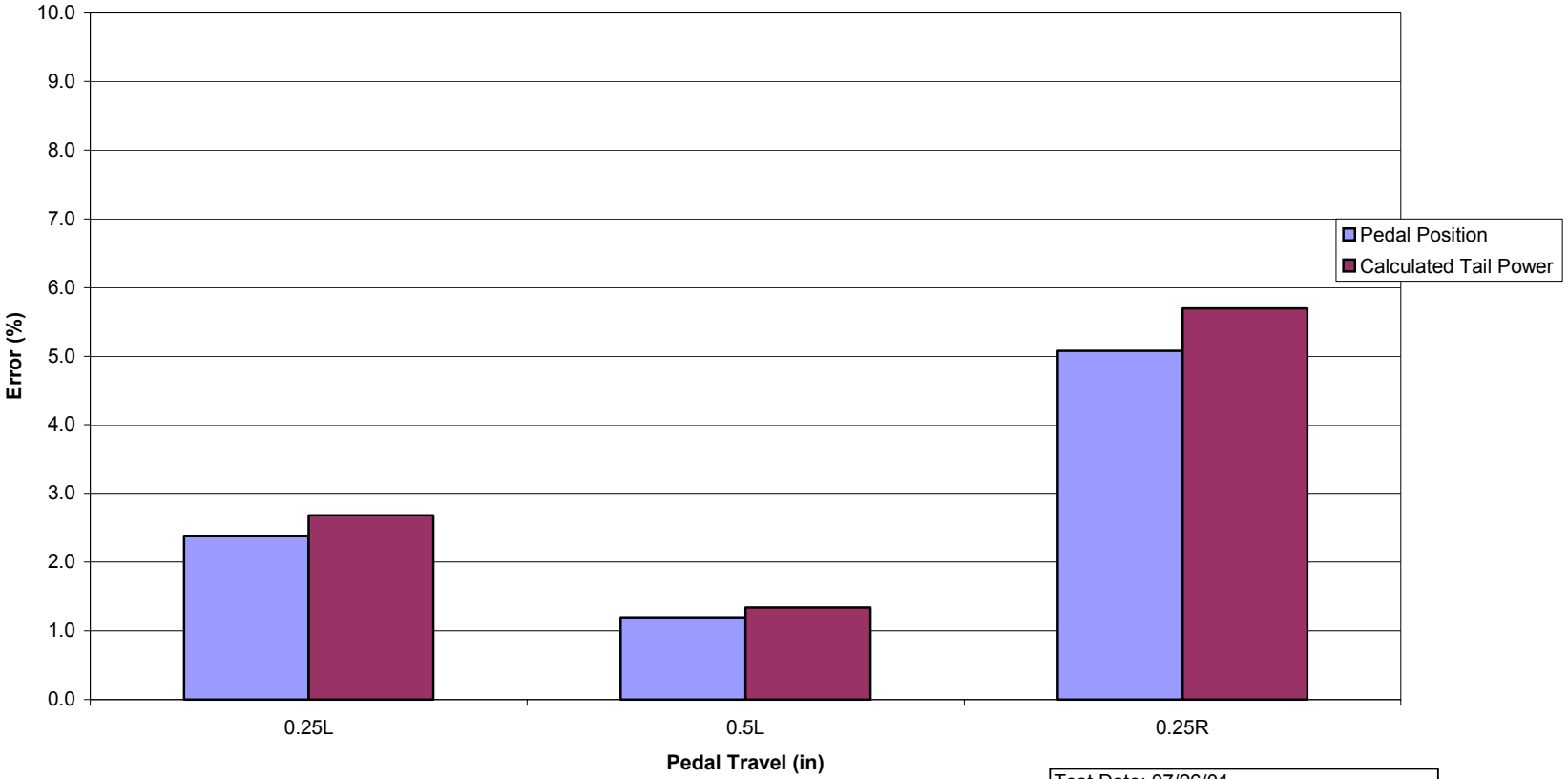

Figure D.34. Step Input Error - Test 74-76%

Aircraft Model: OH-58A+ | Pilot: Bill Lewis | Gross Weight: 2709-lbs | OAT: 20-C
Serial No.: N88UT | Co-Pilot: Fred Stellar | C.G.: 109.1-in | RPM: 354
Configuration: Doors on, Bleed Air off | Flight Test Engineer: Kan-Wai Tong | Pressure Altitude: 945-ft | Engine Torque: 70 to 72-%

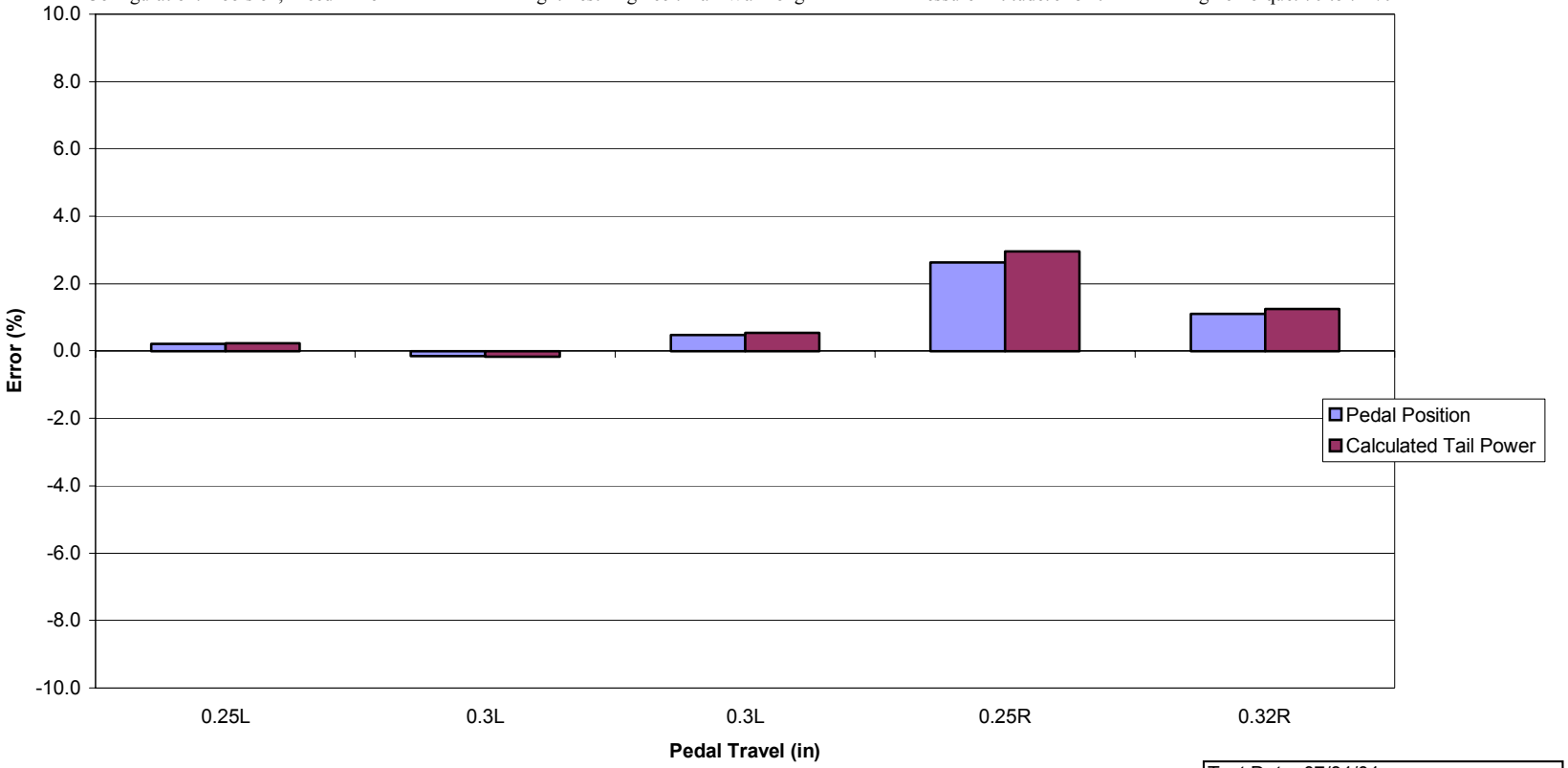

Test Date: 07/31/01
Performed by: UTSI Flight Research

Figure D.35. Step Input Error - Test 70-72%

Aircraft Model: OH-58A+ | Pilot: Bill Lewis | Gross Weight: 3020 & 2797-lbs | OAT: 24 & 20-C
Serial No.: N88UT | Co-Pilot: Fred Stellar | C.G.: 110.0 & 109.4-in | RPM: 354
Configuration: Doors on, Bleed Air off | Flight Test Engineer: Kan-Wai Tong | Pressure Altitude: 900-ft

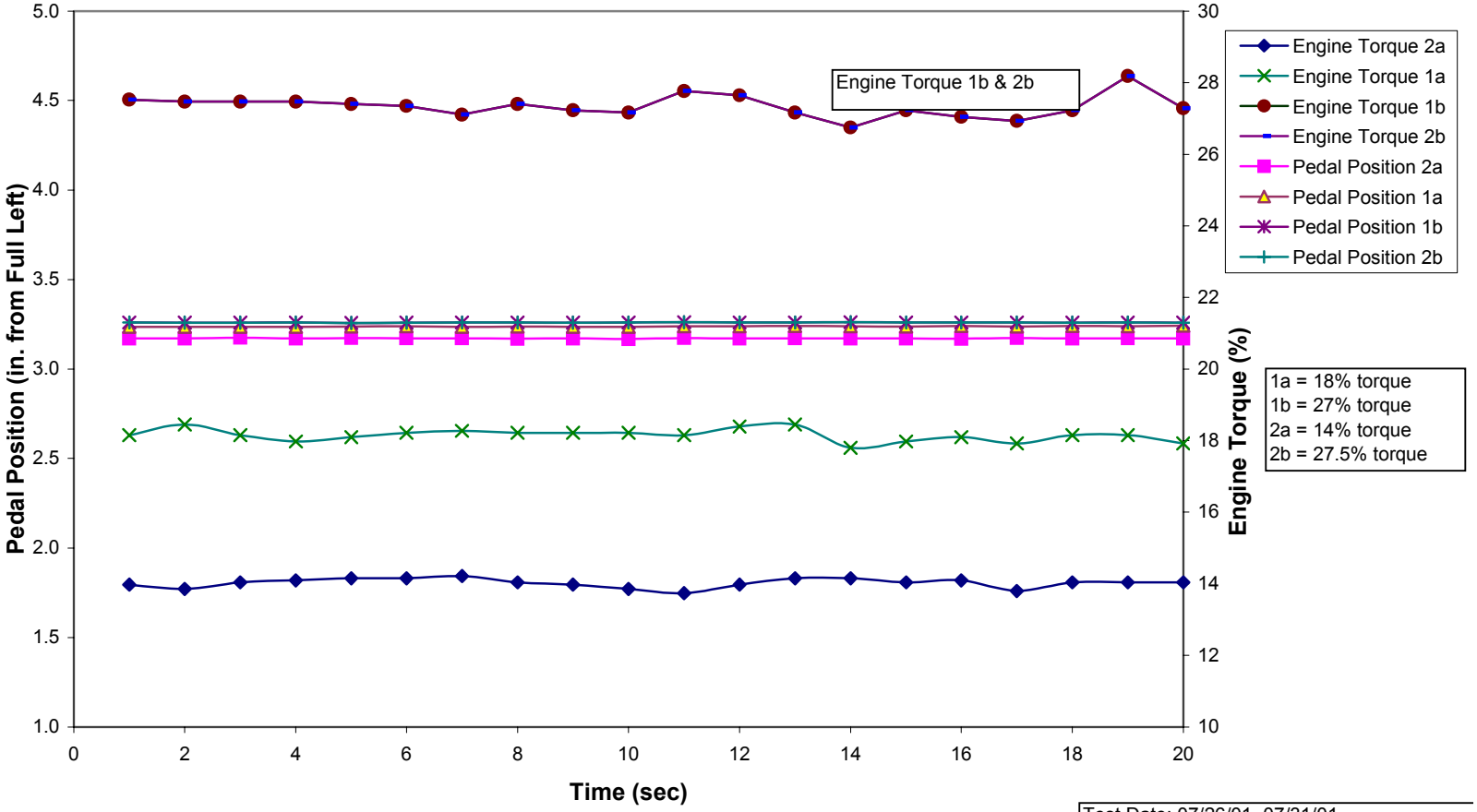

Figure D.36. Ground Operations

Test Date: 07/26/01, 07/31/01
Performed by: UTSI Flight Research

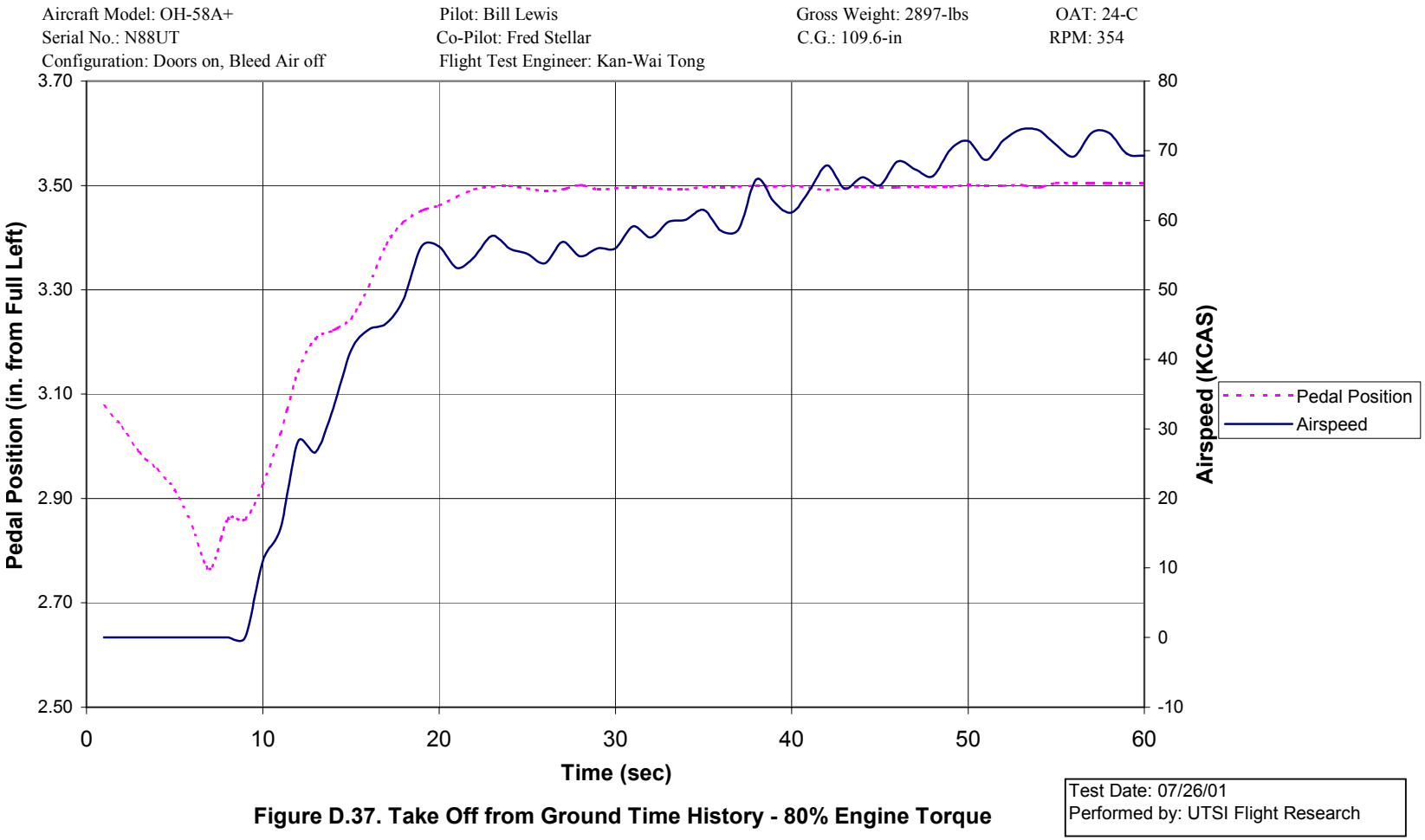

Figure D.37. Take Off from Ground Time History - 80% Engine Torque

Aircraft Model: OH-58A+
Serial No.: N88UT
Configuration: Doors on, Bleed Air off

Pilot: Bill Lewis
Co-Pilot: Fred Stellar
Flight Test Engineer: Kan-Wai Tong

Gross Weight: 2725 to 3020-lbs
C.G.: 103.4 to 109.4-in
Pressure Altitude: 900-ft

OAT: 20 to 24-C
RPM: 354

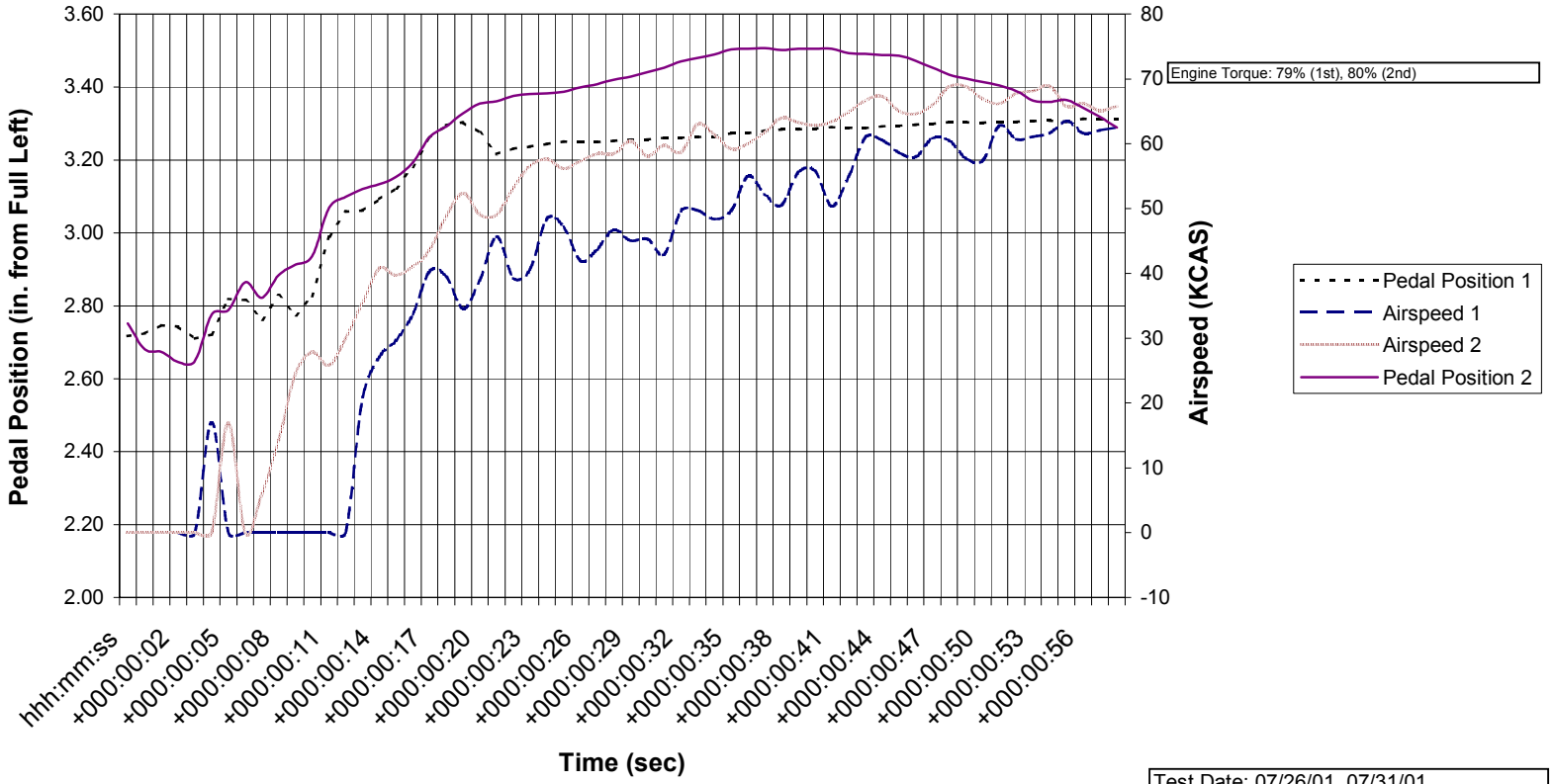

Figure D.38. Climb Performance Time History - (75% to 80% Engine Torque)

Test Date: 07/26/01, 07/31/01
Performed by: UTSI Flight Research

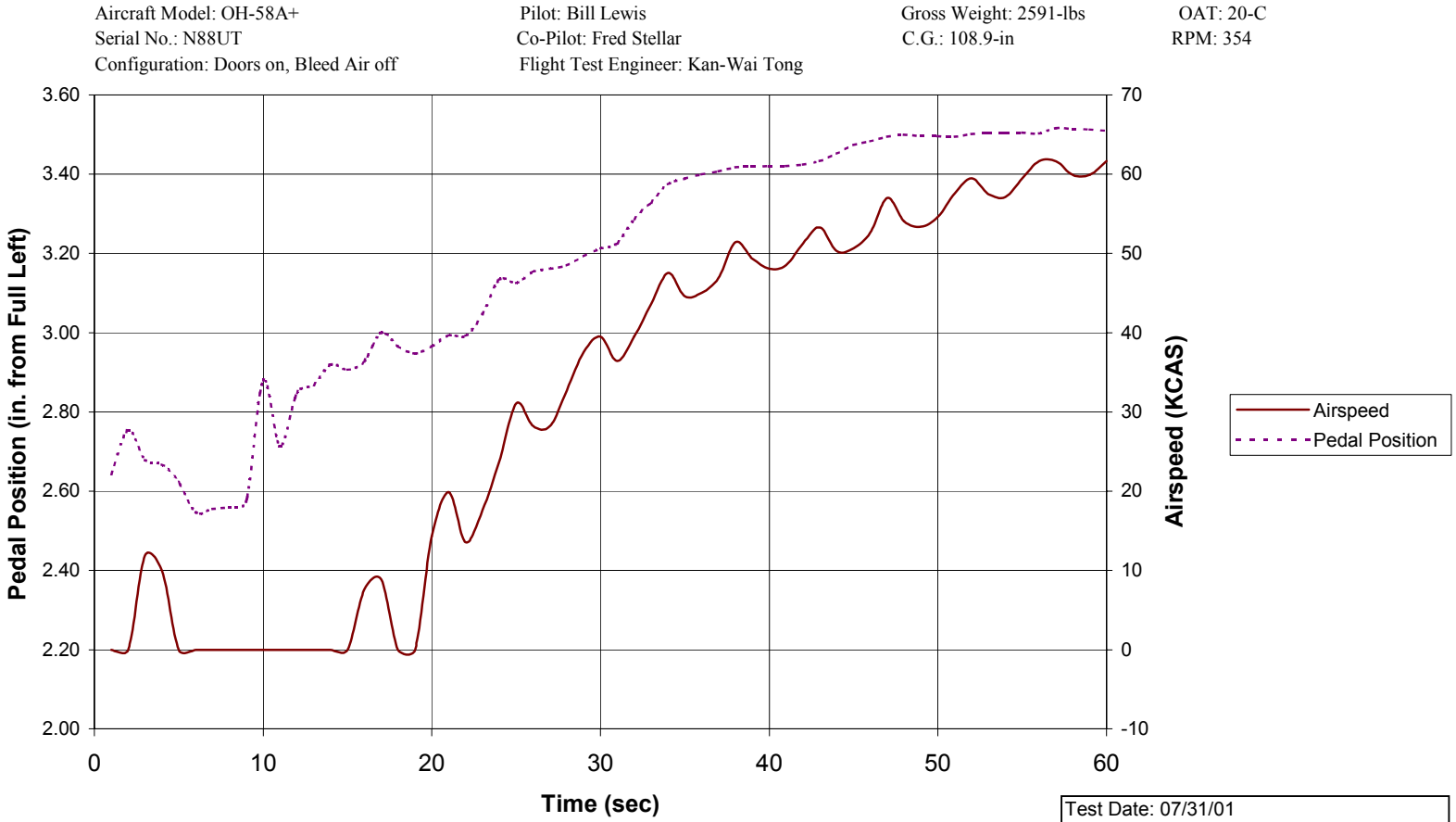

Figure D.39. Climb Performance Time History - (73% Engine Torque)

Aircraft Model: OH-58A+
Serial No.: N88UT
Configuration: Doors on, Bleed Air off

Pilot: Bill Lewis
Co-Pilot: Fred Stellar
Flight Test Engineer: Kan-Wai Tong

Gross Weight: 2897 to 2591-lbs
C.G.: 109.6 to 108.9-in

OAT: 20 to 24-C
RPM: 354

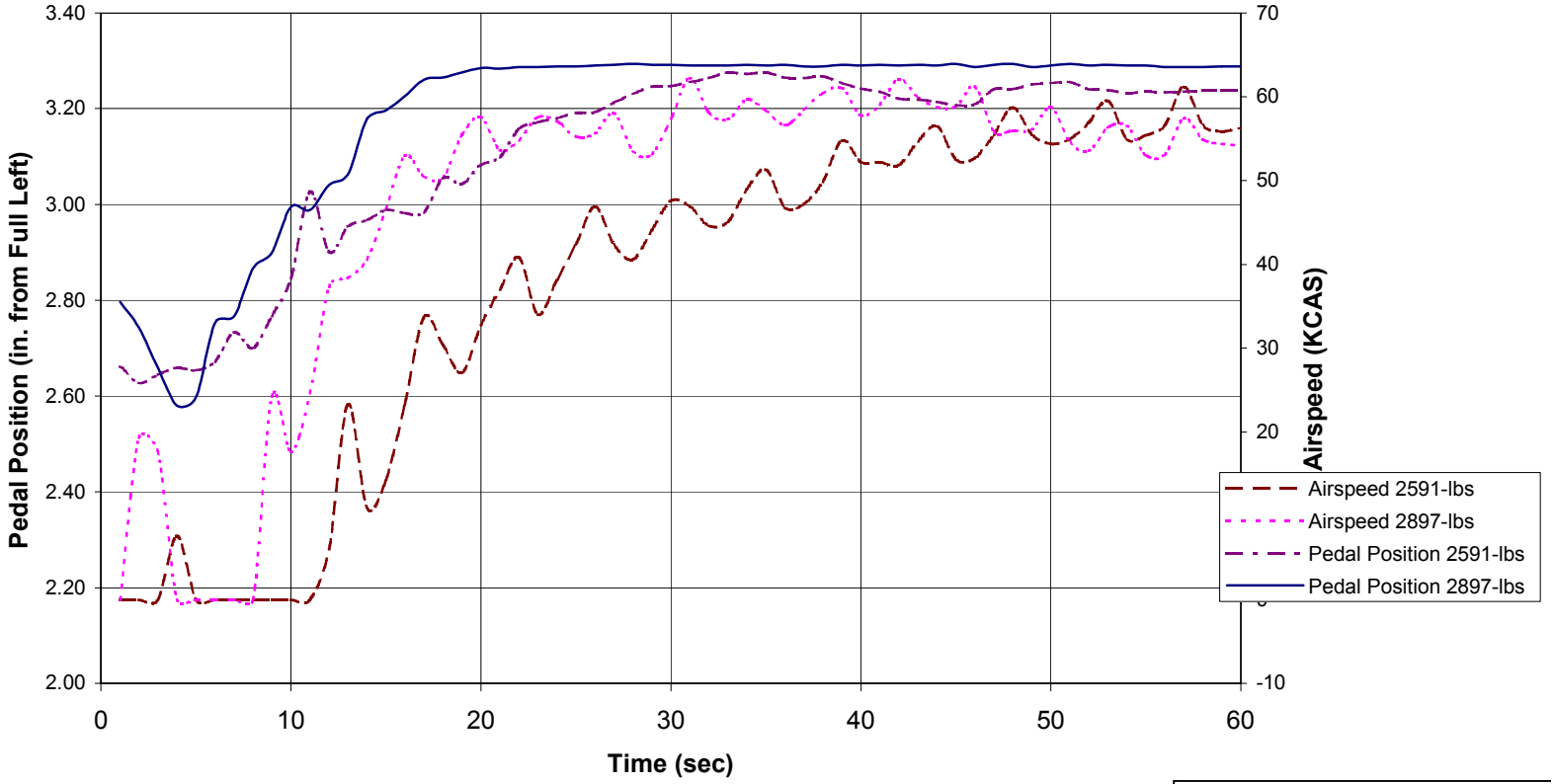

Figure D.40. Climb Performance Time History - (86% Engine Torque)

Test Date: 07/26/01, 07/31/01
Performed by: UTSI Flight Research

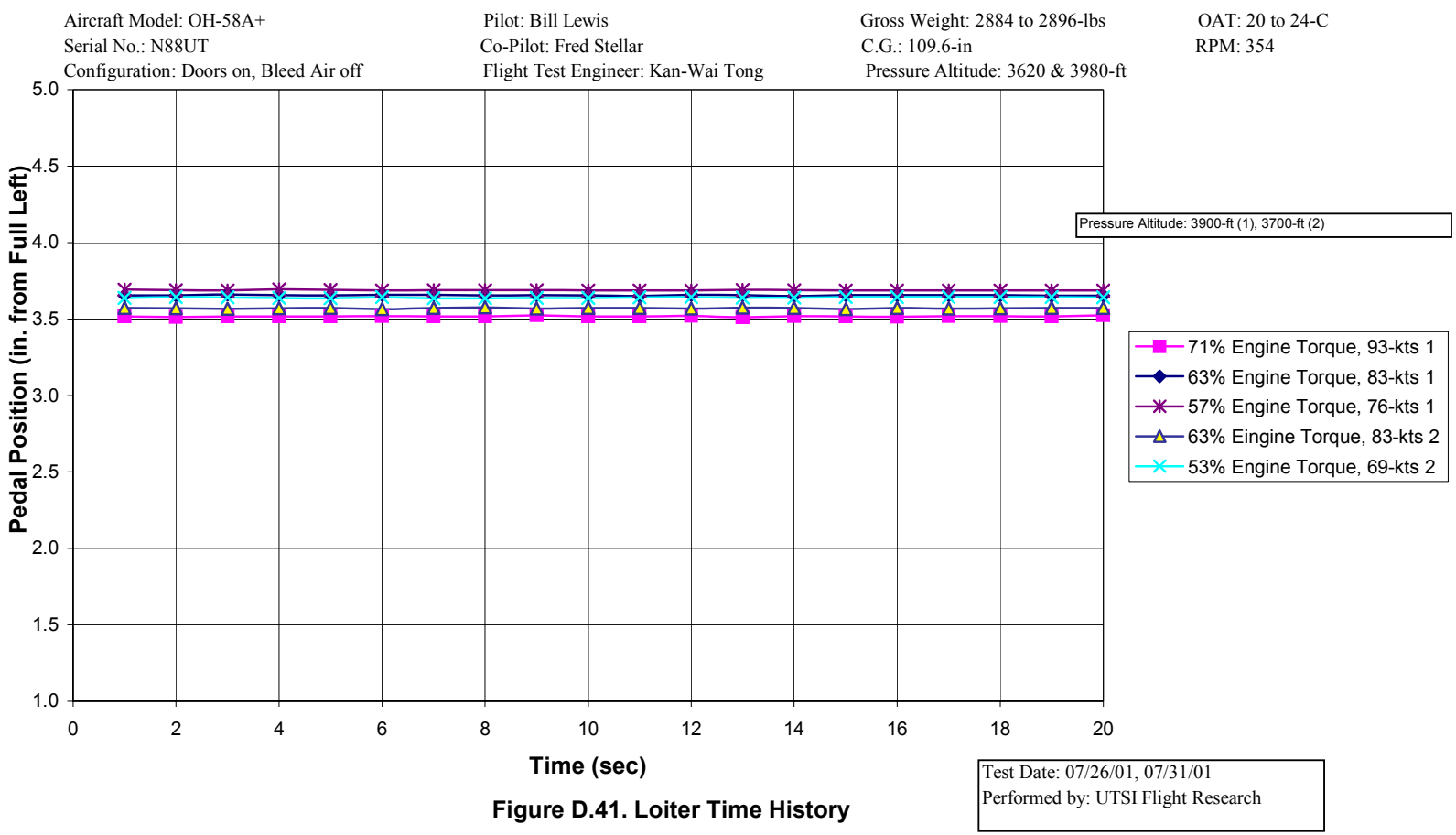

Figure D.41. Loiter Time History

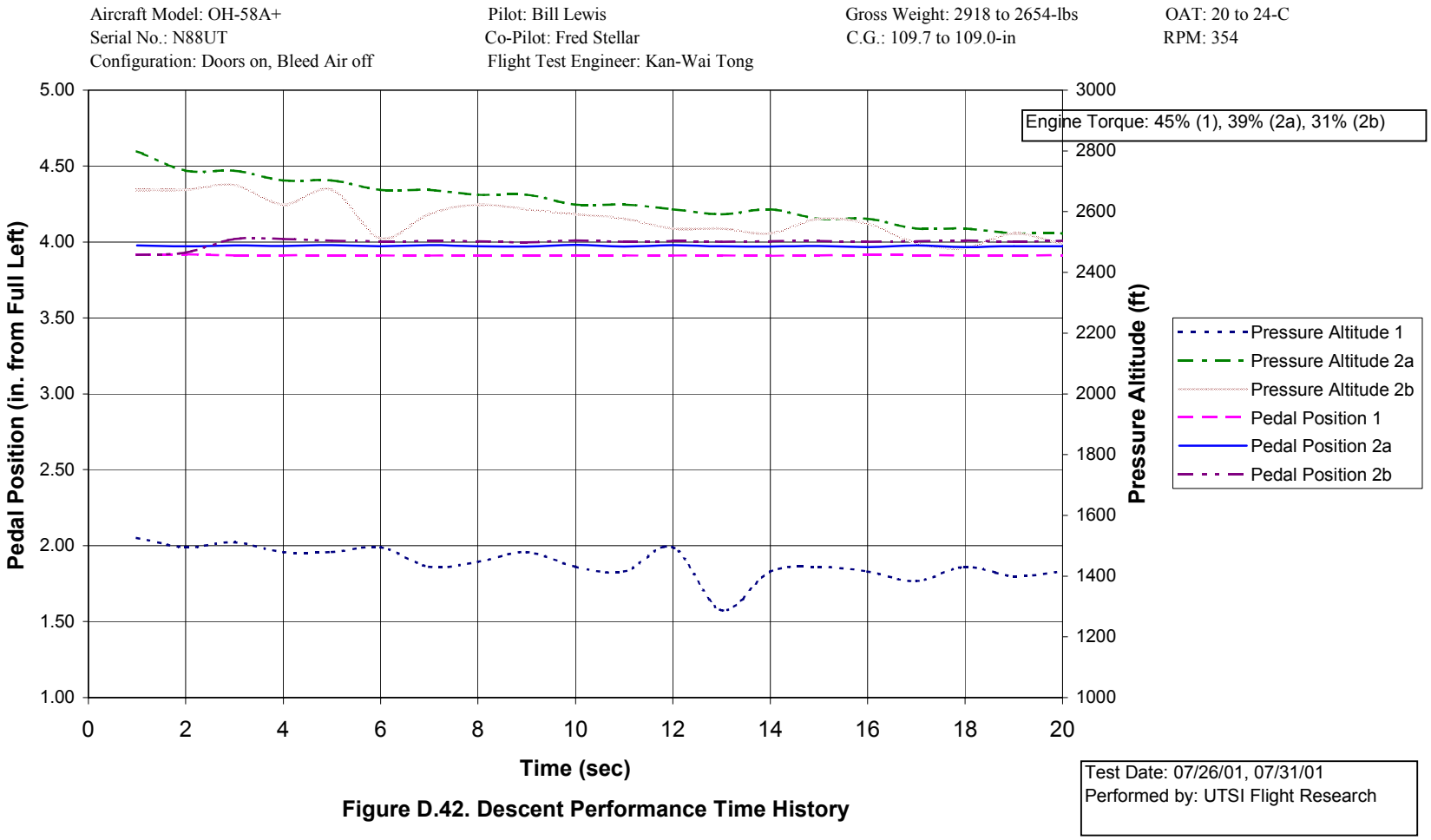

Figure D.42. Descent Performance Time History

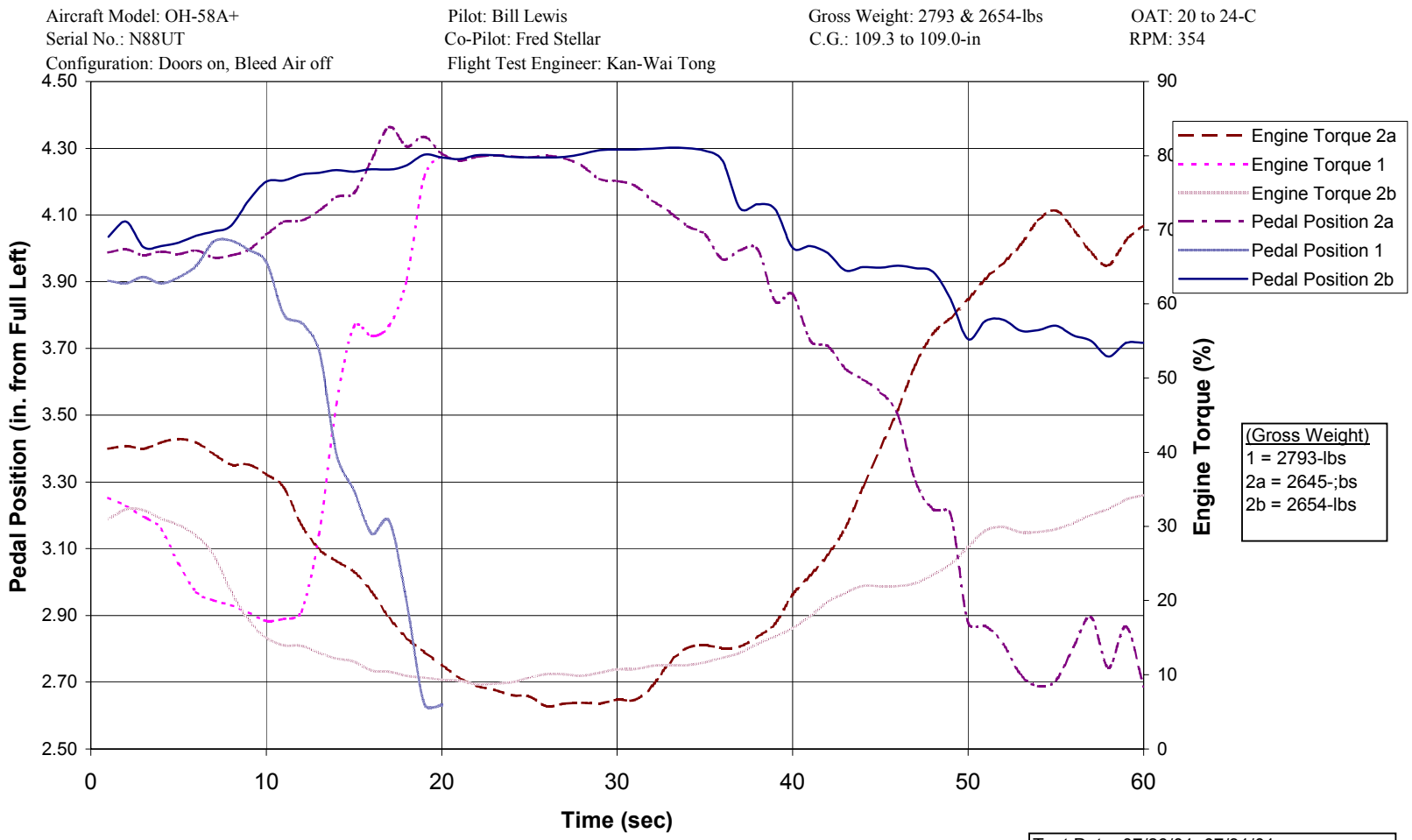

Figure D.43 Approach & Landing Time History

APPENDIX E

SAMPLE CALCULATION

Nomenclature:

a	Tail Rotor Blade Lift Curve Slope (1/rad)
b	Number of Tail Rotor Blades
c	Tail Rotor Blade Cord
c_d	Drag Coefficient
e	Hinge Offset (m, ft)
h_D	Density Altitude (m, ft)
l_T	Tail Rotor Moment Arm (m, ft)
r	Yaw Rate of the Tail Section (deg/sec)
A_b	Tail Rotor Blade Area (m^2, ft^2)
A	Tail Rotor Disc Area (m^2, ft^2)
B	Tail Rotor Tip Loss Factor
C_{LF}	Vertical Fin Thrust Coefficient
C_P	Coefficient of Power
C_{TM}	Main Rotor Thrust Coefficient
C_T	Tail Rotor Thrust Coefficient
F_D	Density Correction Factor
F	Tail Rotor-Fin Blockage Factor
IE	Tail Rotor Inertial Effect (m-kN, ft-lbf)
I_{ZZ}	Moment of Inertia (m^4, ft^4)
K_{BG}	Bevel Gear Loss Coefficient
L_F	Vertical Fin Lift (kN, lbf)
P_M	Main Rotor Horsepower
P	Tail Rotor Horsepower
$P_{T/Total}$	Tail/Total Horsepower (%)
$P_{T/M}$	Tail/Main Rotor Horsepower (%)
P_i	Tail Induced Power (hp)
P_o	Tail Profile Power (hp)
P_{fnB}	Vertical Fin Blockage Power (hp)
P_G	Gear Box Power Loss (hp)
Q_M	Main Rotor Torque (m-kN, ft-lbf)
R	Tail Rotor Radius (m, ft)
Re	Reynolds number
R_M	Main Rotor Radius (m, ft)
s	Distance from Fin to Rotor (m, ft)

S_{fn}	Fin Area (m^2, ft^2)
S_v	Vertical Fin Blockage Area (m^2, ft^2)
T	Tail Rotor Thrust (kN, lbf)
T_{IE}	
T_{fn}	Vertical Fin Thrust (kN, lbf)
V_F	Forward Flight Velocity (m/s, ft/s)
V_i	Tail Induced Velocity (m/s, ft/s)
V_o	Tail Inflow Velocity (m/s, ft/s)
V_v	Total Kinematic Velocity (m/s, ft/s)
ρ_{SL}	Air Sea Level Density (km/m^3, $slug/ft^3$)
ρ_D	Air Altitude Density (km/m^3, $slug/ft^3$)
α_a	Angular Acceleration (deg/sec^2)
θ	Tail Rotor Blade Angle (deg)
Ω_M	Main Rotor Speed (rad/s)
Ω	Tail Rotor Speed (rad/s)
μ	Tip Speed Ratio
σ_M	Main Rotor Solidity
σ	Tail Rotor Solidity
β	Side Slip Angle (deg)
θ_{iF}	Vertical Fin Angle of Incidence (deg)
ϕ_i	Inflow Angle (rad)
η	Mechanical Efficiency

Variables Input: (OH-58A+)

change

not change

	Hover	FWD	Units
Q_{Total}	100	20	-%
Ω	100	100	-%
$P_{T/Total}$	10.40	17.73	-%
b	2	2	
c	0.439	0.439	-ft
c_d	0.017	0.017	@7-deg AA
h_D	0	0	-ft
r	0	60	-deg/sec
P_{rated}	317.0	317.0	-hp
P_A	317.0	63.4	-hp
l_T	20.125	20.125	-ft
s	1.625	1.625	-ft
I_{ZZ}	17553	17553	-in-lb-sec^2
K_{BG}	0.0025	0.0025	
R_M	17.7	17.7	-ft
R	2.58	2.58	-ft
Re	1.97E+06	1.97E+06	
S_{fn}	10	10	-ft^2
S_v	8	8	-ft^2
V_F	0	100	-kts
V_L	0	0.00	-kts

(- right, + left)

Errors	
0.00	1.33

Ped Pos		
1.949	5.452	-in

(from Full Left)

Left Pedal Right Pedal

(NACA 0012)

(+ = nose right, - = nose left)

(Ref. Bell Data I-7) 17553

15100

viscosity 0.00016

(F value in Hover Gain-loss needs to be changed if varied)

Variables Input: (OH-58A+)

ρ_{SL}	0.002377	0.002377	(slug/ft^3)
ρ_D	0.002377	0.002377	(slug/ft^3)
Ω_M	37.07	37.07	(rad/s)
Ω	275.4	275.4	(rad/s)
θ_{iF}	7	7	-deg
β	0	0	-deg
α	0	0	-deg/sec^2

(β must be between -20 to +20, with 4 increment, except -2,-6, 2 & 6, otherwise, please look up the N/q from the attached yaw moment chart)

Center Center

(- = nose right, + = nose left)

Hovering Power Gain/Losses:

1 Tip Losses Factor (B):

$B = 1 - (2 * C_T)^{0.5} / b$

$B = 1 - (2 * 0.008343)^{0.5} / 2$

$B = 0.94$

2 Inertia Effects (IE):

$N = I_{ZZ} * \alpha = l_T * T_{IE}$

$T_{IE} = I_{ZZ} * \alpha / l_T$

$T_{IE} = 17553 * 0 / 20.125$

$T_{IE} = 0.0\text{-lbf}$

3 Vertical Fin Blockage Correction (F):

$s/R = 1.625 / 2.58$ $\quad S_v/A = 8 / 20.91$

$s/R = 0.630$ $\quad S_v/A = 0.3826$

$F = 1.07$ (Ref. 3.5, p.36)

4 Gear Box Loss (P_G):

$P_G = 0.0025*(P_{rated} + P_{actual})$ (Ref. 3.1, p. 277)

$P_G = 0.0025*(317 + 32.98)$

$P_G = 0.8749\text{-hp}$

$\eta = 1-(P_G / P_A)$

$\eta = 1-(0.8749 / 317.00)$

$\eta = 0.9972$

5 Fuselage Moment Contribution (N)

α =	**1-deg**
(Chart)	**Run 82**

N/q = error $\quad N/q = -46$ $\quad \beta$ Nosecenter = 0- deg

$N/q = -46\text{-ft}^3$

$V_N = [V_F^2 + V_v^2]^{0.5}$

$V_N = [0^2 + 0.00^2]^{0.5}$

$V_N = 0.00\text{-ft/sec}$

$q = 0.5 * \rho_D * V_N^2$

$q = 0.5 * 0.002377 * 0.00^2$

$q = 0.00\text{-lb/ft}^2$

$N = N / q * q$

$N = -46 * 0.00$

$N = 0.00\text{-ft-lb}$

$T_{fn} = N / l_T$

$T_{fn} = 0.00 / 20.125$

$T_{fn} = 0.00\text{-lb}$

6Rotor Solidity:

σ_R=	b	*	c	/(	π	*	R	)
σ_R=	2	*	0.439	/(	π	*	2.58	)
σ_R=	0.1083							

7Inflow Effects:

V_v=	r	*	l_T	+	V_L
V_v=	0	*	20.125	+	0
V_v=	0.00-ft/sec				

$B*V_v/v_o$=	0.94*	0.00	/	49.06
$B*V_v/v_o$=	0.00			

$B*V_i/v_o$ =	1.19			(Chart)	
V_i =	1.19	*	v_o	/	B
V_i =	1.19	*	49.06	/	0.94
V_i =	62.41-ft/sec				

Hover:

$$\mathbf{P} = (\mathbf{P_i} * \mathbf{F} + \mathbf{P_o}) / \boldsymbol{\eta}$$

1 $P = P_{T/Total} * P_{Total} / 100$
$P = 10.40 * 317.0 / 100$
$P = 32.98$ -hp

2 $P_M = P_A - P$
$P_M = 317.0 - 32.98$
$P_M = 284.0$-hp

3 $Q_M = P_M * 550 / \Omega_M$
$Q_M = 284.0 * 550 / 37.07$
$Q_M = 4214$-ft-lbf

4 $T = Q_M / l_T + T_{fn} + T_{IE}$
$T = 4213.9 / 20.125 + 0.00 + 0.00$
$T = 209.4$-lbf

5 $C_T = T / [\rho_D * (\Omega * R)^2 * (\pi * R^2)]$ (Ref. 3.2, p. 29)
$C_T = 209.4 / [0.002377 * (275.4 * 2.58)^2 * (\pi * 2.58^2)]$
$C_T = 0.008343$

6 $A_M = \pi * R_M^2$
$A_M = \pi * 17.7^2$
$A_M = 984.2$-ft^2

7 $C_P = P_A * 550 / [\rho_D * A_M * (\Omega_M * R_M)^3]$
$C_P = 317.0 * 550 / [0.002377 * 984.2 * (37.1 * 17.7)^3]$
$C_P = 0.0002638$

8 $A = \pi * R^2$
$A = \pi * 2.58^2$
$A = 20.91$-ft^2

9 $v_o = [T / (2 * \rho_D * A * B^2)]^{0.5}$
$v_o = [209.4 / (2 * 0.002377 * 20.91 * 0.94^2)]^{0.5}$
$v_o = 49.06$-ft/s

Induced + Inflow Effect
$V_i = 62.41$-ft/s

10 $P_i = T * V_i / 550$
$P_i = 209.4 * 62.41 / 550$
$P_i = 23.76$-hp

11 $\sigma_R = b * c / (\pi * R)$
$\sigma_R = 2 * 0.439 / (\pi * 2.58)$
$\sigma_R = 0.1083$

12 $P_o = [\rho_D * A * (\Omega * R)^3 * 0.125 * \sigma_R * c_d] / 550$

$P_o = [0.002377 * 20.91 * (275.4 * 2.58)^3 * 0.125 * 0.1083 * 0.02] / 550$

$P_o = 7.464\text{-hp}$

13 $\mathbf{P = (P_i * F + P_o) / \eta}$

$\mathbf{P = (23.76 * 1.07 + 7.464) / 0.9972}$

$\mathbf{P = 32.98\text{-hp}}$

14 $P_{ME} = P_A - P$

$P_{ME} = 317.0 - 32.98$

$P_{ME} = 284.0\text{-hp}$

15 **Error = $\mathbf{P_{ME} - P_M}$** (Use Goal Seek to set Error to 0 by changing the %)

Error = $\mathbf{284.0 - 284.0}$

Error = $\mathbf{0.00}$-hp

16 $P_{T/M} = P / P_{ME} * 100$

$P_{T/M} = 33.0 / 284.0 * 100$

$P_{T/M} = 11.6\%$

17 $U^2 = (\Omega * R)^2 + V_i^2$

$U^2 = (275.4 * 2.58)^2 + 62.41^2$

$U^2 = 508799\text{-ft}^2/\text{sec}^2$

18 $C_L = 2 * T / (\rho_D * U^2 * A)$

$C_L = 2 * 209.4 / (0.002377 * 508799 * 20.91)$

$C_L = 0.01656$

19 $C_L = a * (\theta - \phi_i)$

19a $\phi_i = ATAN [V_i / (\Omega * R)]$

$\phi_i = ATAN [62.41 / (275.4 * 2.58)]$

$\phi_i = 0.08761\text{-rad}$

19b $\theta = \phi_i + (C_L / a)$

$\theta = 0.08761 + (0.016558 / 0.1025)$

$\theta = 0.2492\text{-rad}$

19c $\theta = 14.28\text{-deg}$

20 ped pos = 1.949Left Pedal

Forward Power Gain/Losses:

1Tip Losses Factor (B):

$B = 1 - (2 * C_T)^{0.5} / b$

$B = 1 - (2 * 0.001599)^{0.5} / 2$

$B = 0.97$

2Inertia Effects (IE):

$N = I_{ZZ} * \alpha = l_T * T_{IE}$

$T_{IE} = I_{ZZ} * \alpha / l_T$

$T_{IE} = 17553 * 0 / 20.125$

$T_{IE} = 0.0\text{-lbf}$

3Vertical Fin Blockage Factor (F):

$s_{fin}/R = 1.625 / 2.58$ $S_{fin}'/A = 8 / 20.91$

$s_{fin}/R = 0.6298$ $S_{fin}'/A = 0.3826$

$F = 1.07$ (Ref. 3.5, p.36)

4Gear Box Loss (P_G):

$P_G = 0.0025*(P_{rated} + P_{actual})$ (Ref. 3.1, p. 277)

$P_G = 0.0025*(317 + 11.24)$

$P_G = 0.8206\text{-hp}$

$\eta = 1-(P_G / P_A)$

$\eta = 1-(0.8206 / 63.40)$

$\eta = 0.9871$

5Fuselage Moment Contribution (N)

α = 1-deg
(Chart) Run 82

N/q = error $N/q = -46$ β NoseCenter = 0- deg

$N/q = -46\text{-ft}^3$

$V_N = [V_F^2 + V_v^2]^{0.5}$

$V_N = [100^2 + 21.07^2]^{0.5}$

$V_N = 170.09\text{-ft/sec}$

$q = 0.5* \rho_D * V_N^2$

$q = 0.5* 0.002377 * 170.1^2$

$q = 34.38\text{-lb/ft}^2$

$N = N / q * q$

$N = -46 * 34.38$

$N = -1581.7\text{-ft-lb}$

$T_{fin} = N / l_T$

$T_{fin} = -1581.7 / 20.125$

$T_{fin} = -78.59\text{-lb}$

6Rotor Solidity:

σ_R = b * c /(π * R)

σ_R = 2 * 0.439 /(π * 2.58)

σ_R = 0.1083

7Inflow Effects:

V_v = r * l_T + V_L

V_v = 60 * 20.125 + 0.00

V_v = 21.07-ft/sec

$B*V_v/v_o$ = 0.97* 21.07 / 20.68

$B*V_v/v_o$ = 0.99

$B*V_H/v_o$ = 7.9

$B*V_i/v_o$ = 0.22 (Chart)

V_i = 0.22 * v_o / B

V_i = 0.22 * 20.68 / 0.97

V_i = 4.68-ft/s

Forward Flight:

	P	=(	**P_i**	*	**F**	+	**P_o**	) /	**η**					
1	P	=	$P_{T/A}$	*	P_A	/	100							
	P	=	17.73	*	63.4	/	100							
	P	=	11.24											
2	P_M	=	P_A	-	P									
	P_M	=	63.4	-	11.24									
	P_M	=	52.2	-hp										
3	Q_M	=	P_M	*	550	/	Ω_M							
	Q_M	=	52.2	*	550	/	37.07							
	Q_M	=	774-ft-lbf											
4	T	=	Q_M	/	l_T	+	T_{fn}	+	T_{IE}					
	T	=	774	/	20.125	+	-78.59	+	0.00					
	T	=	-40.1-lbf											
5	C_T	=	T	/ [	ρ_D	* (	Ω	*	R	)^2	* (	π	*	R ^{2})]
	C_T	=	-40.1	/ [	0.002377	* (	275.4	*	2.58	)^2	* (	π	*	2.58 ^{2})]
	C_T	=	0.001599											
6	A_M	=	π	*	R_M^2									
	A_M	=	π	*	17.7^2									
	A_M	=	984.2-ft^2											
7	C_P	=	P_A	*	550	/ [	ρ_D	*	A_M	* (	Ω_M	*	$R_M)^3$]	
	C_P	=	63.4	*	550	/ [	0.002377	*	984.2	* (	37.1	*	18)^3]	
	C_P	=	0.0000528											
8	A	=	π	*	R^2									
	A	=	π	*	2.58^2									
	A	=	20.91	-ft^2										
9	v_o	=[	T	/(	2	*	ρ_D	*	A	*	$B^2)]^{0.5}$			
	v_o	=[	40.1	/(	2	*	0.002377	*	20.91	*	$0.97^2)]^{0.5}$			
	v_o	=	20.68-ft/s											
10	$B*V_H/v_o$	=	0.97	*	100.00	/	20.68				(Chart)			
	$B*V_H/v_o$	=	7.9											
11	$B*V_v/v_o$	=	0.97	*	21.075	/	20.68							
	$B*V_v/v_o$	=	1.0											

Induced + Inflow Effect

12	V_i	=	4.68-ft/s											
13	P_i	=	T	*	V_i	/	550							
	P_i	=	40.1	*	4.68	/	550							
	P_i	=	0.34-hp											

14 $\mu = V_F / (\Omega * R)$

$\mu = 100 / (275.4 * 2.58)$

$\mu = 0.2375$

15 $\sigma_R = b * c / (\pi * R)$

$\sigma_R = 2 * 0.439 / (\pi * 2.58)$

$\sigma_R = 0.1083$

16 $P_o = [\rho_D * A * (\Omega * R)^3 * 0.125 * \sigma_R * c_d * (1 + 4.7 * \mu^2)] / 550$

$P_o = [0.002377 * 20.91 * (275.4 * 2.58)^3 * 0.125 * 0.1083 * 0.02 * (1 + 4.7 * 0.238^2)] / 550$

$P_o = 9.422$ -hp

17 **$P = (P_i * F + P_o) / \eta$**

$P = (0.34 * 1.07 + 9.422) / 0.9871$

$P = 9.92$-hp

18 $P_{ME} = P_A - P$

$P_{ME} = 63.40 - 9.92$

$P_{ME} = 53.5$-hp

19 **$Error = P_{ME} - P_M$** (Use Goal Seek to set Error to 0 by changing the %)

$Error = 53.5 - 52.2$

Error= 1.33-hp

20 $P_{T/M} = P / P_{ME} * 100$

$P_{T/M} = 9.9 / 53.5 * 100$

$P_{T/M} = 18.5$-%

21 $U^2 = (\Omega * R)^2 + V_i^2$

$U^2 = (275.4 * 2.58)^2 + 4.68^2$

$U^2 = 504925$-ft^2/sec^2

22 $C_L = 2 * T / (\rho_D * U^2 * A)$

$C_L = 2 * -40.1 / (0.002377 * 504925 * 20.91)$

$C_L = -0.00320$

23 $C_L = a * (\theta - \phi_i)$

23a $\phi_i = ATAN[V_i / (\Omega * R)]$

$\phi_i = ATAN[4.68 / (275.4 * 2.58)]$

$\phi_i = 0.00659$-rad

23b $\theta = \phi_i + (C_L / a)$

$\theta = 0.00659 + (-0.003199 / 0.1025)$

$\theta = -0.0246$-rad

23c $\theta = -1.41$-deg

24 ped pos = 5.452Right Pedal

Summary of Results: **(OH-58A+)**

	Hover	FWD	
Q_{Total}	100	20	-%
Ω	100	100	-%
V_F	0	100	-kts
P_M	284.0	52.2	-hp
T	209.4	-40.1	-lbf
T_{IE}	0.0	0.0	-lbf
T_{fn}	0.0	-78.6	-lbf
P_i	23.8	0.34	-hp
P_o	7.46	9.42	-hp
P_G	0.8749	0.8206	-hp
F	1.07	1.07	
P	32.98	9.92	-hp
P_A	317.00	63.40	-hp
$P_{T/A}$	**10.40**	**17.73**	-%
Error	0.00	1.33	-hp
$P_{T/M}$	11.61	18.54	-%
C_P	0.0002638	0.0000528	
C_T	0.0083	0.00160	
C_L	0.01656	-0.00320	
θ	14.28	-1.41	-deg
Ped Pos	1.949	5.452	-in Left Pedal Right Pedal

Results of Different Regimes:

Yaw Accelerations

	Test 1	40L	44L	27R	38R	40R
Flight Test		2.61	2.44	2.62	2.70	2.59
Model		2.35	2.39	2.56	2.48	2.50
Difference (in)		0.26	0.05	0.06	0.22	0.09
Difference (ped - %)		3.88	0.79	0.90	3.33	1.30
Difference (tail - %)		4.36	0.89	1.02	3.74	1.46

	Test 2	24L	18L	25L	25R	15R	30R	37R
Flight Test		2.57	2.51	2.48	2.81	2.82	2.7	2.78
Model		2.40	2.38	2.40	2.59	2.65	2.65	2.68
Difference (in)		0.17	0.13	0.08	0.22	0.17	0.07	0.10
Difference (ped - %)		2.47	1.94	1.12	3.31	2.61	1.08	1.52
Difference (tail - %)		2.77	2.18	1.26	3.72	2.93	1.21	1.70

Step

	Test 1	0.25L	0.5L	0.25R
Flight Test		2.6	2.4	3.2
Model		2.44	2.32	2.86
Difference (in)		0.16	0.08	0.34
Difference (ped - %)		2.39	1.19	5.07

Deceleration Recovery

	Test 1	40L	44L	27R	38R	40R
Flight Test		3.11	3.18	2.54	2.35	2.30
Model		2.99	3.15	2.38	2.26	2.26
Difference (in)		0.12	0.03	0.16	0.09	0.04
Difference (ped - %)		1.85	0.50	2.39	1.32	0.65
Difference (tail - %)		2.08	0.56	2.68	1.48	0.73

	Test 2	24L	18L	25L	25R	15R
Flight Test		3.02	3.01	3.15	2.52	2.52
Model		2.88	2.94	3.08	2.42	2.41
Difference (in)		0.14	0.07	0.07	0.10	0.11
Difference (ped - %)		2.12	1.04	1.09	1.42	1.63
Difference (tail - %)		2.38	1.17	1.23	1.60	1.83

Step

	Test 2	0.25L	0.3L	0.3L	0.25R	0.32R
Flight Test		2.47	2.41	2.41	3.01	3.00
Model		2.46	2.42	2.38	2.83	2.93
Difference (in)		0.01	-0.01	0.03	0.18	0.07
Difference (ped - %)		0.21	-0.15	0.48	2.63	1.10

APPENDIX F

MISCELLANEOUS FIGURES

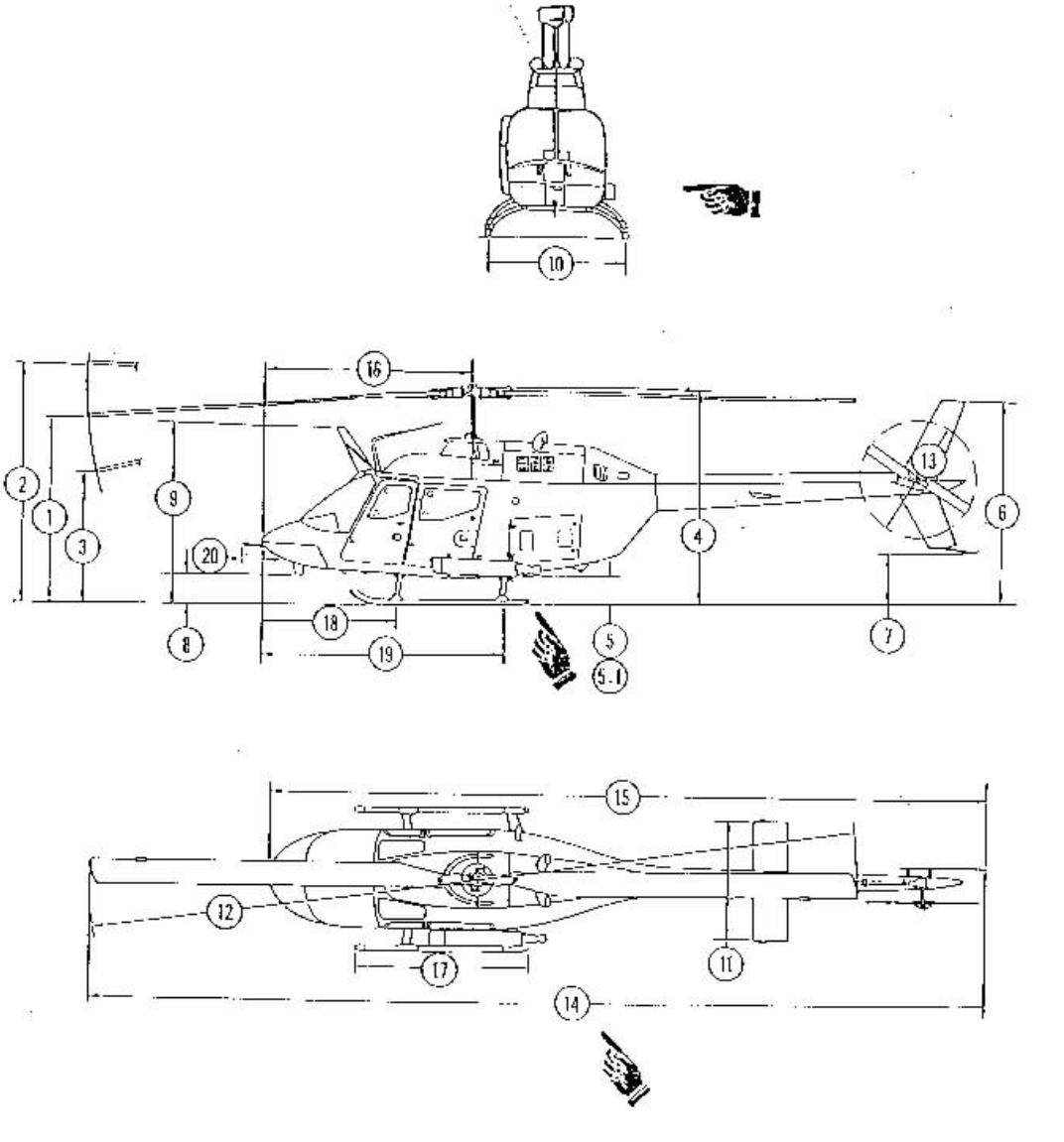

Figure F.1. Principal Dimensions (Sheet 1 of 2)

	HEIGHT	STANDARD SKID GEAR	HIGH SKID GEAR	FLOAT GEAR A
1.	Forward Tip of Main Rotor (Static Position) to Ground with Droop	9 ft. 6.0 in.	10 ft. 0.0 in.	9 ft. 7.9 in.
2.	Forward Tip of Main Rotor to Ground (Tie-down)	12 ft. 0.0 in.	12 ft. 6.0 in.	12 ft. 1.9 in.
3.	Forward Tip of Main Rotor to Ground (Forward Down)	6 ft. 8.0 in.	7 ft. 2.0 in.	6 ft. 10 in.
4.	Ground to Top of Main Rotor Reservoirs	9 ft. 7.0 in.	10 ft. 9.0 in.	10 ft. 5.4 in.
5.	Bottom of Cabin	13.0 in.	27.0 in.	28 in.
5.1.	Bottom of ATAS Launcher CS	13.0 in.	27.0 in.	N/A
6.	Top of Vertical Stabilizer	8 ft. 1.5 in.	10 ft. 1.5 in.	11 ft. 1.0 in.
7.	Tail Skid to Ground	1 ft. 4.4 in.	3 ft. 4.4 in.	4 ft. 4.0 in.
8.	Lower Cutter to Ground	12.0 in.	2 ft. 2.0 in.	2 ft. 3.0 in.
9.	Upper Cutter to Ground	7 ft. 9.5 in.	9 ft. 9.5 in.	9 ft 10.5 in.
	WIDTH			
10.	Skid Gear	6 ft. 5.4 in.	7 ft. 3.0 in.	11 ft. 6.1 in.
11.	Horizontal Stabilizer	6 ft. 5.2 in.	No change	No change
	DIAMETERS			
12.	Main Rotor	35 ft. 4.0 in.	No change	No change
13.	Tail Rotor	5 ft. 2.0 in.	No change	No change
	LENGTH			
14.	Overall (Main Rotor Fore and Aft) to Aft End of Tail Skid	40 ft. 11.8 in.	No change	No change
15.	Nose of Cabin to Aft End of Tail Skid	32 ft. 2.0 in.	No change	No change
16.	Nose of Cabin to Center Line of Main Rotor	8 ft. 10.1 in.	No change	No change
17.	Skid Gear	8 ft. 1.3 in.	10 ft. 4.2 in.	19 ft. 5.0 in.
18.	Nose of Cabin to Center Line of Forward Cross Tube	6 ft. 0.0 in.	5 ft. 9.4 in.	5 ft. 11.7 in.
19.	Nose of Cabin to Center Line of Aft Cross Tube	10 ft. 9.0 in.	10 ft. 6.3 in.	10 ft. 8.7 in.
20.	Pitot Tube	6.8 in.	No change	No change

*Check antennas that may protrude lower.

206900-509-2A

Figure F.1. Principal Dimensions (Sheet 2 of 2)

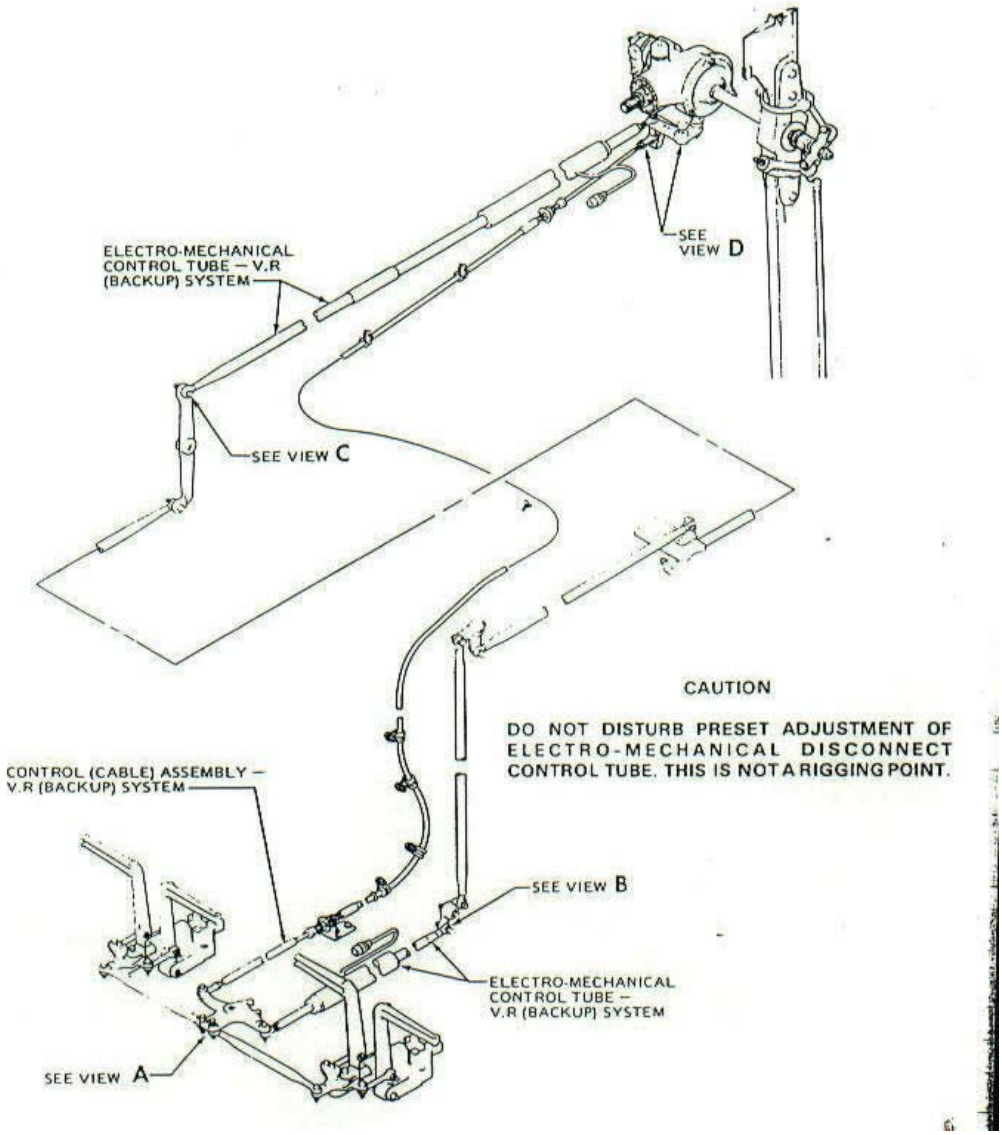

Figure F.2. Tail Rotor Control Systems

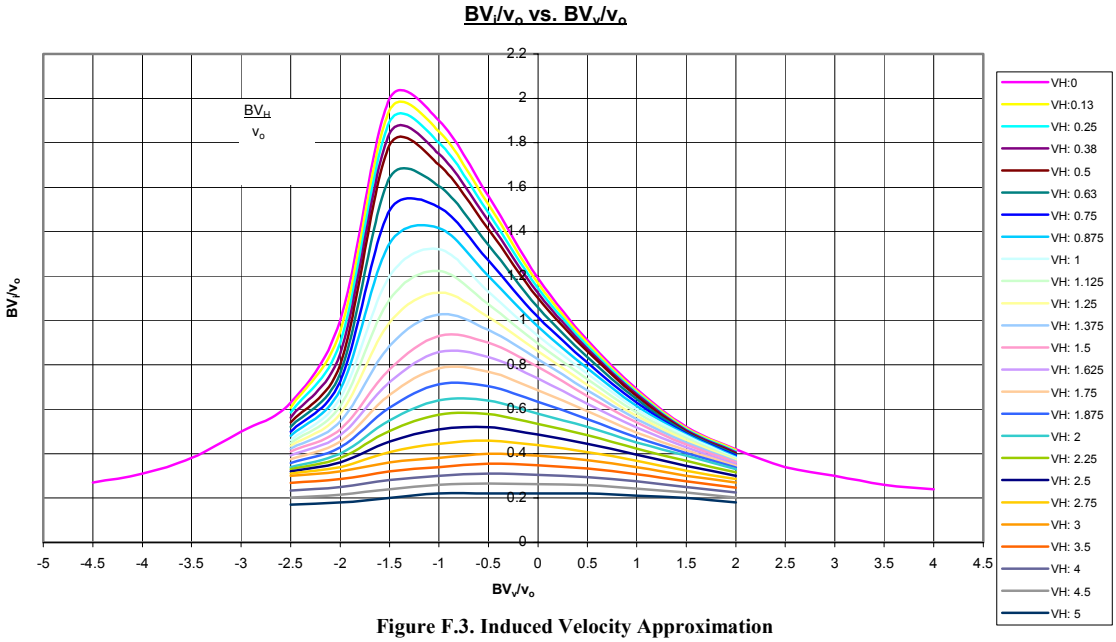

Figure F.3. Induced Velocity Approximation

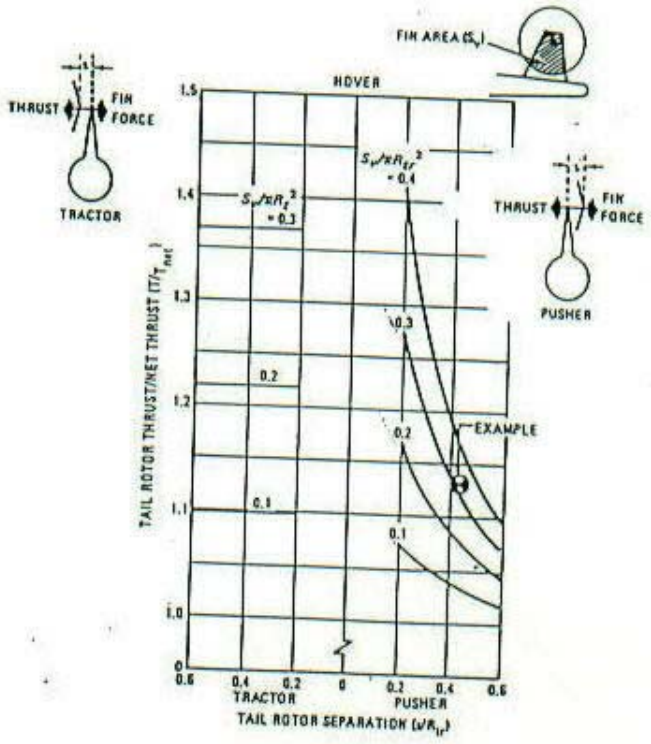

Figure F.4. Vertical Tail Blockage Correction

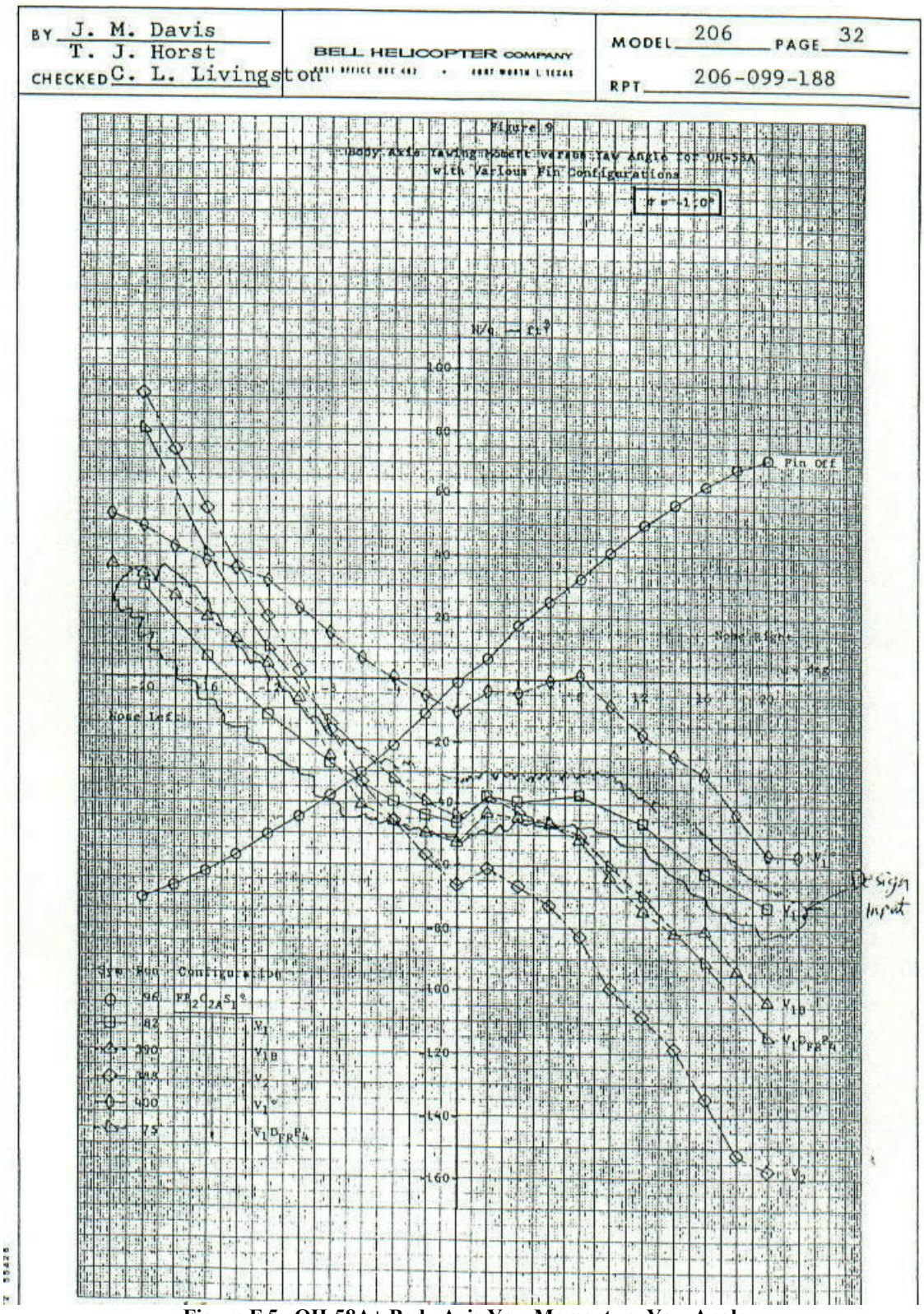

Figure F.5. OH-58A+ Body Axis Yaw Moment vs. Yaw Angle

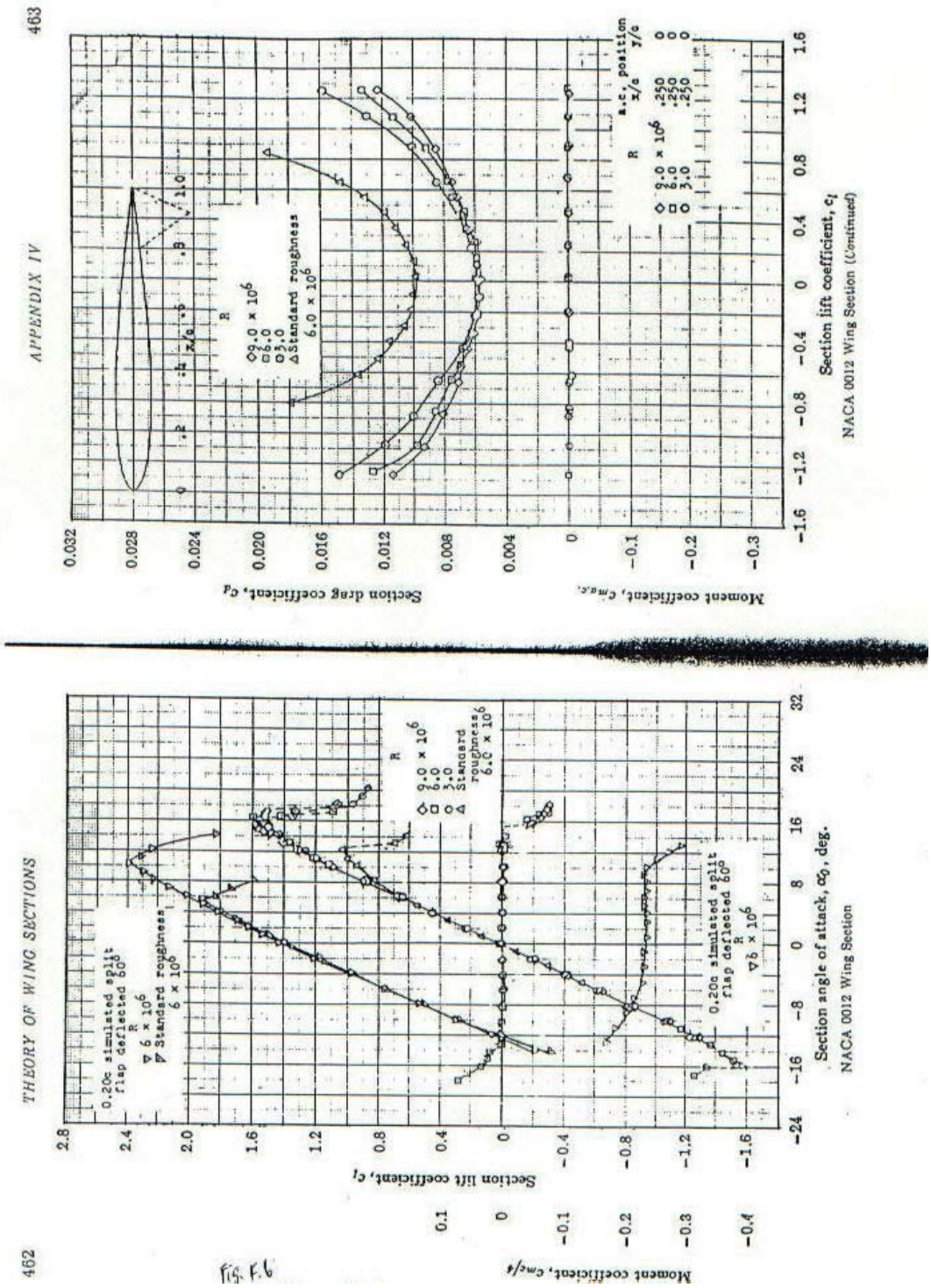

Figure F.6. NACA 0012 (OH-58A+) Wing Section

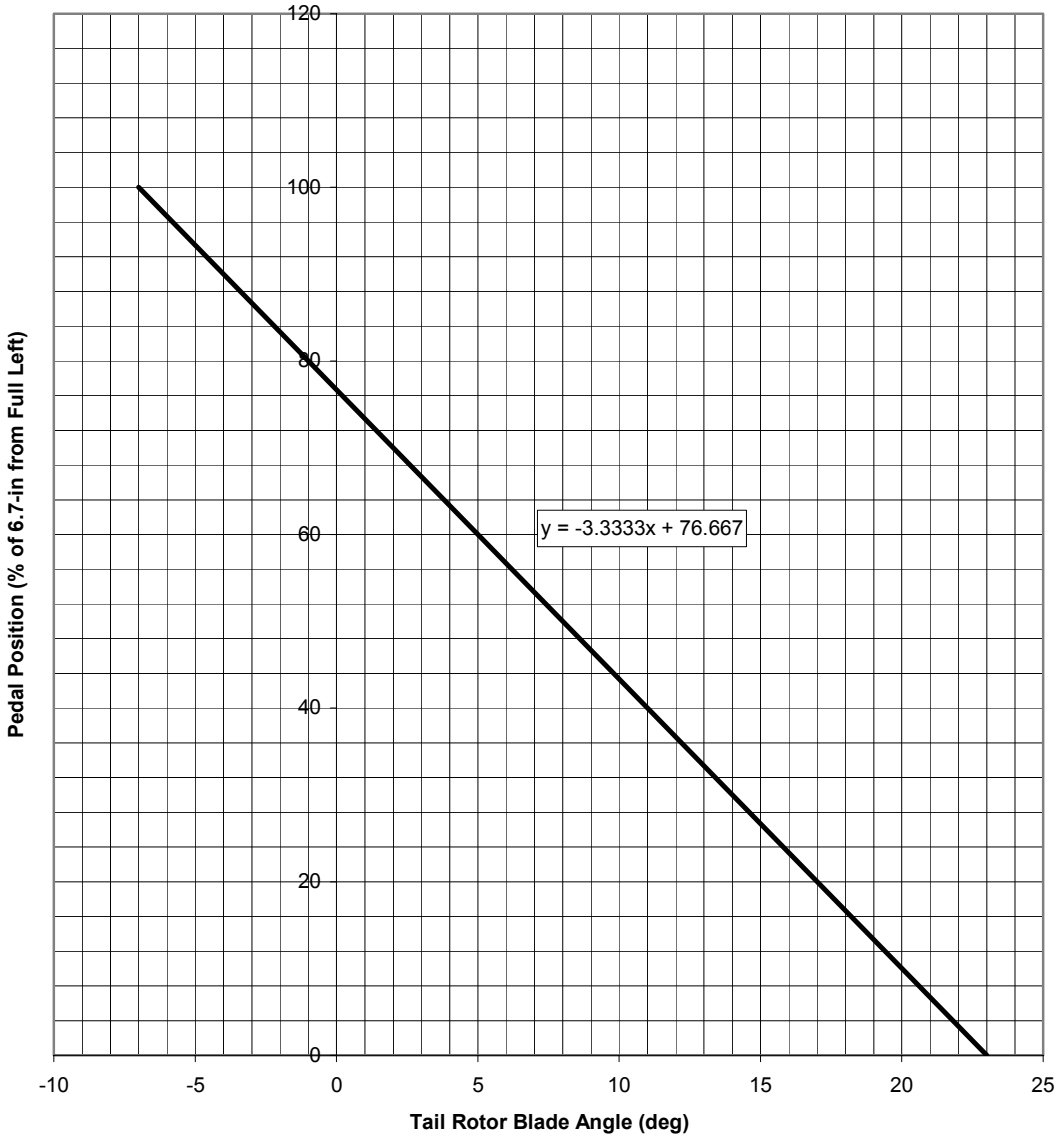

Fig. F.7. Pedal Position vs Tail Rotor Collective Blade Angle

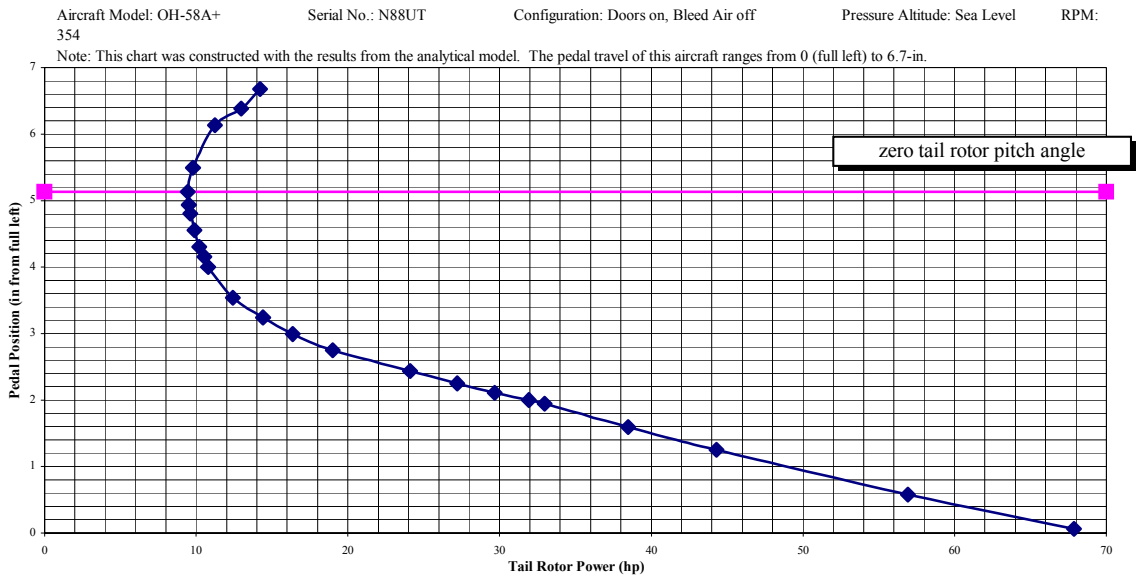

Figure F.8. Pedal Position vs. Calculated Tail Rotor Power

VITA

Mr. Kan-Wai Tong was born and raised in Hong Kong. In 1993, he immigrated to New York City and continued his education at High School in Humanities. Following the completion of high school in 1994, Mr. Tong entered the State University of New York Maritime College and studied for a Bachelor degree in Marine Engineering. Upon graduation, he was given a mechanical engineering position at Three Mile Island Nuclear Generating Station. Then, Mr. Tong discovered an opportunity at the University of Tennessee Space Institute (UTSI). Mr. Tong decided to give up his job and get involved in aviation industries. During his time at UTSI, he was active in various student clubs. He was the president of the Boat Club and treasurer of the Aero Club. Before he completed his master degree in Aviation Systems, he obtained a private pilot license. After graduation, Mr. Tong would look for an aviation related job.